Aalto University
School of Electrical
Engineering

Analyzing the characteristic radio variability of AGNs on up to 40 years of 37 GHz data from the Metsähovi Radio Observatory

Sofia Suutarinen

School of Electrical Engineering

Thesis submitted for examination for the degree of Master of Science in Technology.
Espoo, 22.02.2021

Supervisor

Prof. Anne Lähteenmäki

Advisor

Docent Merja Tornikoski

Author Sofia Suutarinen

Title of thesis Analyzing the characteristic radio variability of AGNs on up to 40 years of 37 GHz data from the Metsähovi Radio Observatory

Programme
Master's Programme in Electronics and Nanotechnology

Major Space Science and Technology

Thesis supervisor Professor Anne Lähteenmäki

Thesis advisor(s) Docent Merja Tornikoski

Date 22.02.2021 **Number of pages** 74 + 6 **Language** English

Abstract
Active galactic nuclei (AGNs) are exceptionally bright compact sources located at the centers of some galaxies. The supermassive black hole at the center of the AGN drives the variability of the source causing visible changes in the observed light curve over different frequencies. This variability is a common subject of studies.

The amount of data in AGN radio analyses is often limited to relatively short monitoring periods of e.g., 5 years. However, it has been shown that longer monitoring periods are usually needed in order to identify variability timescales from the data. Identifying such characteristic timescales could help in understanding the underlying processes governing AGN variability and they could potentially be linked to physical conditions in the analyzed sources.

The aim of this thesis was to characterize AGN variability timescales from uniquely long radio AGN data from the Metsähovi Radio Observatory 37 GHz monitoring sample and specifically to identify how the results are dependent on the monitoring period length. Especially of interest was to see, if a simple power law is sufficient in characterizing the underlying noise process of AGNs in radio frequencies. The used methods included the periodogram, Lomb-Scargle periodogram, structure function, and discrete correlation function.

The results showed that the monitoring period length has a significant role on the estimated power spectrum of the sources. In many cases, the simple power law seemed inadequate in describing the noise process of the sources for long-term data. In contrast, shorter monitoring segments of 5 years were more often in apparent agreement with the null hypothesis. For many sources, the poor fits in long-term data appeared to be caused by the power spectrum experiencing a flattening of the slope after a characteristic timescale. The results also indicated that for some sources even 30-40 years of monitoring may not be enough to reveal a characteristic timescale.

Keywords Active Galactic Nuclei, AGN, active galaxy, characteristic variability

Tekijä Sofia Suutarinen

Työn nimi Aktiivisten galaksiytimien radiomuuttuvuuden karakterisointi Metsähovin radio-observatorion 37 GHz:n otoksesta 40 vuoden ajalta

Koulutusohjelma
Elektroniikan ja nanotekniikan maisteriohjelma

Pääaine Avaruustiede ja -tekniikka

Vastuuopettaja/valvoja Professori Anne Lähteenmäki

Työn ohjaaja(t) Dosentti Merja Tornikoski

Päivämäärä 22.02.2021 **Sivumäärä** 74 + 6 **Kieli** Englanti

Tiivistelmä

Aktiiviset galaksiytimet ovat huomattavan kirkkaita kompakteja kohteita joidenkin galaksien keskustoissa. Keskustan supermassiivinen musta aukko toimii moottorina kohteen muuttuvuudelle aiheuttaen näkyviä muutoksia havaitussa valokäyrässä vaihtelevilla taajuuksilla. Tämä muuttuvuus on yleinen tutkimusten kohde.

Aktiivisten galaksiytimien tutkimuksessa käytettävä data on usein rajoittunut suhteellisen lyhyisiin havaintojaksoihin, pituudeltaan esimerkiksi 5 vuotta. On kuitenkin näytetty, että ominaisaikaskaalojen määrittäminen radiotaajuuksilla vaatii usein pidempiä havaintojaksoja. Tällaisten ominaisaikaskaalojen löytäminen auttaisi ymmärtämään aktiivisten galaksiytimien muuttuvutta säteleviä prosesseja ja ne voitaisiin mahdollisesti yhdistää analysoitavien kohteiden fysikaalisiin olosuhteisiin.

Tämän työn tavoite oli karakterisoida aktiivisten galaksiytimien aikaskaaloja ainutlaatuisen pitkästä radiodatasta Metsähovin radio-observation 37 GHz:n havainto-otoksesta ja erityisesti identifioida, miten tulokset riippuvat havaintojakson pituudesta. Erityisesti oli kiinnostavaa nähdä, onko yksinkertainen potenssilaki riittävä karakterisoimaan aktiivisten galaksiytimien taustaprosesseja radiotaajuuksilla. Käytettyihin metodeihin kuuluivat periodogrammi, Lomb-Scargle periodogrammi, rakennefunktio, sekä diskreetti korrelaatiofunktio.

Tulokset osoittivat, että havaintojakson pituudella on merkittävä vaikutus kohteiden arvioituihin tehospektreihin. Useassa tapauksessa yksinkertainen potenssilaki ei näyttänyt riittävän kuvaamaan kohteen kohinaprosessia pitkän havaintojakson datassa. Sen sijaan useammalle kohteelle yksinkertainen potenssilaki oli riittävä kuvaamaan 5 vuoden havaintojakson tehospektriä. Potenssilain huono sopivuus pitkän havaintojakson datassa näytti johtuvan tehospektrin kulmakertoimen tasoittumisesta ominaisaikaskaalan jälkeen. Tulokset myös indikoivat, että joillakin kohteilla edes 30-40 vuotta monitorointia ei välttämättä riitä ominaisaikaskaalan havaitsemiseen.

Avainsanat Aktiivinen galaksiydin, aktiivinen galaksi, AGN, ominaisaikaskaala

Contents

Preface

First and foremost, I would like to thank my advisor Merja Tornikoski for giving me a great topic that started my journey into the exciting lives of AGNs. I especially want to thank her for our weekly Zoom conversations where I was able to get valuable input for my ideas as well as some much needed contact with the outside world during these peculiar times. I would also like to thank my supervisor Anne Lähteenmäki as well as my manager Joni Tammi in Metsähovi Radio Observatory for initially hiring me for a summer position. I also want to thank Talvikki Hovatta for our Zoom conversations discussing my analyses and Venkatessh Ramakrishnan for answering my burning questions.

I would also like to thank some close people in my life. My family, who have always supported and believed in me. My friends, who have been there for me even if it has mostly been through messages and voice calls due to the pandemic. I am also more than grateful for our weekly gaming sessions, although writing this thesis significantly reduced my 'online time'. Last, I want to thank Tino. Despite my having to work late hours and weekends trying to understand *everything*, he has been more than understanding and he has helped me feel confident even when I have been overwhelmed.

Espoo, 22.02.2021
Sofia Suutarinen

'Ad astra'

Symbols and abbreviations

Symbols

α	Slope of structure function
A	Normalization of periodogram
β	Slope of Power Spectral Density estimate
$D^1(\tau)$	First-order structure function
f	Frequency
M	Bin size
N	Number of data points
μ	Mean
p	p-value
p_o	Confidence level for FAP
$P(f)$	Periodogram
$\overline{P_{sim}(f)}$	Mean of simulated power spectra
$\Delta\overline{P_{sim}(f)}$	RMS error of simulated power spectra about the mean
σ	Standard deviation
σ^2	Variance
S_v	Flux density
$S(\omega_i)$	Power law spectrum at Fourier frequency ω_i
T_{samp}	Sampling interval
$\Delta\tau$	Global lag
$\Delta\tau_{ij}$	Pairwise lag
VI	Variability index
ω	Angular frequency
χ_{dist}	Chi-Square distribution
z_o	False Alarm Probability

Operators

$\frac{d}{dA}$	Derivative with respect to variable A
Σ_k	Sum over index k

Abbreviations

AGN	Active Galactic Nucleus
BLO	BL Lacertae object

DCF	Discrete correlation function
ECDF	Empirical cumulative distribution function
FAP	False Alarm Probability
GAL	Radio galaxy
HPQ	High-polarization Quasar
IAAFT	Improved amplitude adjusted Fourier transform
LPQ	Low-polarization Quasar
LS periodogram	Lomb-Scargle periodogram
PSD	Power Spectral Density
QPO	Quasi-periodic oscillation
RMS	Root mean square
SF	Structure function
SMBH	Supermassive black hole
PSREP	Power Spectral Response

1 Introduction

Active galactic nuclei (AGNs) are exceptionally bright compact sources located at the centers of some galaxies. The nuclei host supermassive black holes (SMBHs), 10^6 – 10^9 times the mass of the Sun, which cause extreme events in the vicinity of these black holes. In some AGNs, plasma jets shooting from the nuclei can extend to distances of thousands of parsecs, thus demonstrating the tendency of AGNs to be the sources of extreme physical events. AGNs can be observed with a multitude of instruments, including radio telescopes, which allow monitoring of radio flux density caused by accelerating relativistic particles in AGN magnetic fields.

Although AGNs are continuously studied in the whole electromagnetic spectrum, many aspects including the exact mechanism generating the collimated jets are still under debate. All AGNs with jets are sources of strong synchrotron radiation meaning they are well observable in the radio band. The consensus is that most of the observed radio variability is the result of physical events occurring within the jets. The origin of AGNs is unknown, though it has been suggested that they could result from the merging of galaxies.

While AGN variability has been studied over the years, the amount of data is often very limited. In principle, data for analysis often consists of short few-year surveys, which especially for slowly varying radio sources is insufficient for proper analysis (Hovatta et al., 2007). The Metsähovi Radio Observatory is one of the few observatories, that have consistently observed radio flux densities of different AGNs for up to 40 years. Such data gives many new possibilities for data analysis allowing to understand AGN behavior across different monitoring periods.

Often studied phenomena in AGN flux density curves are the presence of characteristic timescales (e.g., Hovatta et al., 2007). Periodicity in a flux density curve would be seen as a recurring intensification of the flux density, called flaring. Quasiperiodicity is a less strict version of periodicity, where a periodic component is visible but occurs in unpredictable intervals. Another type of characteristic timescale would be associated with the Power Spectral Density (PSD) of the source, which describes how the power of a source is distributed over different frequencies. Studying these characteristic timescales is very important because currently there is little information on the long-term behavior of AGNs, and for statistical studies it is vital to understand if the behavior changes during long monitoring periods. Finding a characteristic timescale in the source power spectrum could possibly be linked to physical conditions such as the SMBH mass (e.g., Papadakis 2004).

Unfortunately, AGN data is not unproblematic for typical timeseries analysis. The studies aiming at the identification of periodic or quasiperiodic behavior often use Fourier analysis methods, which may have been modified for irregularly sampled data. These methods include the periodogram for regularly sampled data (Schuster, 1897), the Lomb-Scargle (LS) periodogram for irregularly sampled data (Scargle, 1982; Lomb, 1976), the structure function (SF) (Simonetti et al., 1985) and the

discrete correlation function (DCF) (Edelson & Krolik, 1988). Due to the nature of the data, the results from these methods are often noisy and may include artefacts (e.g., Emmanoulopoulos, 2010; VanderPlas, 2018). Finding the best-fit method is not a straightforward issue to solve, since neither the methods modified for irregular sampling nor interpolating the data to mimic regular sampling are without significant drawbacks. It is crucial that the methods are chosen based on the type of analysis being conducted. In addition, the shortcomings of the methods need to be clearly identified and their contributions to the result errors must be properly analyzed.

Another problem arises from the initial statistical assumptions made on the data. Monte Carlo simulations are commonly used to give confidence levels for the analysis results; however, the initial assumptions may not hold causing the results to be unreliable. For instance, assuming the underlying noise process to follow a certain functional relationship may give inaccurate results. Therefore, it is important to analyze long-term data and to identify if the underlying process can be modelled accurately enough with the used initial assumptions.

The aim of this thesis is to characterize AGN variability timescales from uniquely long radio AGN data and specifically to identify how the results are dependent on the monitoring period length. This aim is achieved by using the periodogram, LS periodogram, structure function, and DCF on the data and the results will be compared both between different monitoring period lengths as well as between the methods. Especially of interest is to see if a simple power law noise process is sufficient in characterizing the underlying noise process of AGNs in radio.

The scope of this thesis is limited to single frequency analysis because Metsähovi data is at the present time mostly observed in the 37 GHz frequency. Although 22-GHz frequency data has been used in earlier studies (e.g., Hovatta et al., 2007), this frequency has been excluded, since the main objective of this thesis is to analyze uniquely long monitoring periods in the radio domain.

The rest of this thesis is divided into four chapters. Chapter 2 presents some basic information on AGNs relevant to this thesis as well as reviews literature on AGN variability. Chapter 3 describes the used data sample and presents the analysis methods. The shortcomings of the methods are also discussed. Chapter 4 presents and discusses the results. Since this thesis uses several methods for identifying the same or similar properties in the data, the results are compared and evaluated for significance. Chapter 5 summarizes the contribution of this thesis and suggests future directions for AGN variability studies in the radio domain.

2 Literature review

2.1 AGNs

Active Galactic Nuclei (AGNs) are compact sources, whose observed emission over some frequency domains is significantly higher than the expected emission from the nuclei of typical galaxies. The AGN region size varies, but it can be in the vicinity of the size of the Solar System. The galaxies containing an AGN are called active galaxies.

The supermassive black holes of AGNs are surrounded by rapidly rotating gas. This gas, known as the accretion disk, is where the black hole draws its energy from. The rotating hot matter releases enormous amounts of energy as the gas accretes closer to the black hole.

2.1.1 AGN data

The data gathered by the Metsähovi Radio Observatory is flux density data. The differential flux density S_v is the energy flowing through area dA in time dt differentiated over the observing frequency (Böttcher & Reimer, 2012).

$$S_v = \frac{d^3E}{dAdtdv} \tag{1}$$

The used flux density unit is Jy (Jansky), where

$$1\,Jy = 10^{-26}\,W\,m^{-2}Hz^{-1}. \tag{2}$$

AGNs are monitored with both ground- and space-based telescopes throughout the electromagnetic spectrum. Their variability and overall behavior can be analyzed with flux density data, which shows how the luminosity of a source changes over time. Different statistical methods are used to understand the underlying processes, and comparing observations across different frequencies allows understanding the physical conditions governing the AGN variability. In this thesis only 37 GHz data from the Metsähovi Radio Observatory was used; however, the results will be important in characterizing the radio variability of AGNs and understanding the effects seen in long-term data.

Length of the observing period

The term long monitoring period will be used in this thesis frequently. There is no exact definition for what a long monitoring period is, and it depends on the observed frequency. On some frequency domains, such as X-ray -frequencies, observations only last for e.g., $N * 10^4$ seconds ($N \sim few$) and it is expected that a monitoring period of minimum 10^5 seconds or more is required to adequately sample the whole variability of the source (Vaughan et al., 2003). This means that e.g., two days of observations might be considered a long observing period. However, AGNs in the radio domain are generally expected to have slow variability in which case variations at an interval of up to many years are expected. Hovatta et al. (2007) show that even 10 years of monitoring may not be enough to reveal the true variability of a source. Their analyses showed that many of the sources observed in radio extending to 25 years of monitoring still did not exhibit any characteristic timescales for their variability. If the analysis aim is to search for periodicities or quasiperiodicities, it is expected that the repeating interval can be seen several times in the entire monitoring period. This further increases the required length for the observed data.

With this definition in mind, there is currently no known definite monitoring period length which can be said to be long enough to show the characteristic variability behavior of an AGN in radio. In this thesis, the timeseries lengths were assessed for whether they seemed to be adequately long to reveal the characteristic variability of AGNs in radio.

2.1.2 AGN variability

AGNs are typically classified based on their variability properties. Variability in this context means the magnitude of the variation of the flux density S_v. A source which exhibits large variations between its minimum and maximum flux density state is called a highly variable source. In contrast, a weakly variable source will not have a significant difference between its minimum and maximum flux density. There are different ways to measure the variability of a source. Naturally, visual inspection shows the overall behavior of an AGN well; however, the variability may be measured via different indices. An often used simple variability index (e.g., Aller et al., 1991) calculates the difference between the minimum and maximum state of the flux density of a source as

$$VI = \frac{S_{max} - S_{min}}{S_{max} + S_{min}}. \quad (3)$$

Thus, depending on the used definition, a highly variable source may only have one large deviation from its mean flux density; it gives no guarantees on the temporal occurrence of the variation.

There are different theories as to why some AGNs are variable and some are not. It is common to see a source, which is highly variable in some frequency range, but remains more stable in other frequencies. Generally, the emission on different frequencies may be of different origin or type. The emission on radio frequencies is only caused by synchrotron radiation whereas optical emission may be a combination of synchrotron and thermal radiation. The location of the emission site may also be different, and it is a common subject of studies to analyze the variability of sources across frequencies to see if there are correlations. Raiteri et al. (2017) explain that for instance a large contribution from the accretion disk thermal emission may cause the light curve observed in the optical frequencies to have a low variability amplitude. Near-infrared observations may in such a case show larger variability amplitudes due to the more erratic synchrotron radiation.

Some AGNs are associated with a one- or double-sided jet, which is a highly energetic outflow of charged particles extending to distances of megaparsecs or more (Böttcher et al., 2012). The jets contain moving 'knots' which are locations of extreme brightness. First proposed my Marscher & Gear (1983), rapid increases in the source flux density are thought to be caused by propagating shocks in the jets of AGNs. A disturbance in the accretion disk surrounding the central SMBH would cause a shock to be formed and its propagation through the jet would be seen in the observed flux density data.

The variability may also be explained by changes in the jet orientation. Raiteri et al. (2017) report that the variability of the source CTA 102 is best explained by the orientation changes of its jet. Doppler-boosting is an effect, where the relativistic motion of particles in the jet cause the observed luminosity to be higher in the direction of particle movement. The changes in the orientation of the jet would change its relative Doppler factors causing the apparent luminosity changes (Raiteri et al., 2017).

One hypothesis is that some of the variability may be caused by a tilted accretion disk. Chatterjee et al. (2020) show that a misalignment between the accretion disk and black hole spin axis may cause some of the observed variability e.g., in the form of quasi-periodic oscillations (QPOs).

Flaring

When a source exhibits significant increases in its flux density compared to nearby observations, it is called flaring. Individual spikes in the magnitudes are called flares. Figure 1 shows the flux density curve of the source OQ530, which has a large flare between ~2014-2018.

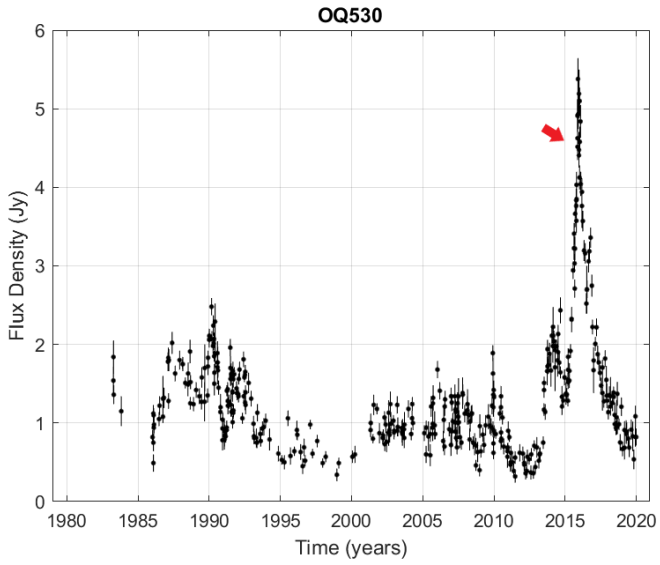

Figure 1: The flux density curve of OQ530. The red arrow points to a large flare. The smaller flux density increases are also considered as flaring of the source.

Typically, flares have been identified through visual inspection as there is no established standard procedure for defining their start and end times. An aid to this issue could come from characterizing the flares and finding flare types. The types could then be analyzed and possibly linked to the different underlying processes. Unfortunately, because the behavior of sources can vary quite significantly, it is difficult to define any universal parameters for the slopes of flares.

While visual identification of flaring and periodicity is a decent albeit subjective way of analyzing time-series data, it has its caveats. Press (1978) notes that even pure noise processes without any underlying features can appear as if they had some clear changes in their flux densities in some structured way. There have also been notions (e.g., Mandelbrot & Wallis, 1969) that the eye tends to overinterpret variations in the data even if they are not statistically significant. For instance, according to Press (1978) the eye seems to efficiently remove linear trends making the most apparent pseudo-period one-third the length of the entire data sample. This subjective bias is something to be considered when analyzing data visually.

2.1.3 AGN types

AGNs are divided into categories and sub-categories based on their observed properties. The information on the types is from Krawczynski et al. (2012) and Netzer (2013). Some of the most common AGN classes are:

Blazar

Blazars are a class, which show the most variability over short timescales as well as high polarization. They have strong continuum emission and they typically radiate over the whole electromagnetic spectrum. Their jet is assumed to point towards Earth, which would explain the observed intense and rapid variability. Blazars can further be divided into subclasses BL Lacertae objects (BLOs) and Flat-spectrum radio quasars (FSRQs).

Quasar

Quasar is an AGN, whose jet has a small angle in its pointing towards Earth as compared to Blazars. Most of the sources observed by the Metsähovi Radio Observatory are Blazars and Quasars. Because the sample includes some other source types as well, the term AGN will be used in this thesis for the sake of clarity.

Quasars can further be divided e.g., into High-Polarization Quasars (HPQs) and Low-Polarization Quasars (LPQs). An LPQ can change into an HPQ if high polarization is at some point observed from the source; however, an HPQ will always retain its classification.

Seyfert galaxy (type I and type II)

Seyfert galaxies are high-luminosity AGNs whose host galaxies are bright and thus observable. The difference between the Seyfert galaxy types comes from their optical-ultraviolet spectra, which show different types of emission lines. The differences are assumed to be caused by viewing angles.

2.1.4 AGN power spectral density

The power spectrum, or Power Spectral Density (PSD), of a source describes how its power at each temporal frequency is distributed. In astronomy, the PSD is often used to analyze the spectral properties of AGNs (e.g., Uttley et al., 2002; Max-Moerbeck et al., 2014; Ramakrishnan et al., 2015). In case of a simple power law of the form

$$P(f) \propto f^{-\beta}, \tag{4}$$

the PSD slope index β is usually assessed from the periodogram, which shows the power of the signal at each frequency. The PSD slope index is then estimated from the slope of the periodogram e.g., by fitting a straight line. Figure 2 shows a typical periodogram for a source with $\beta = 2$ generated with Matlab.

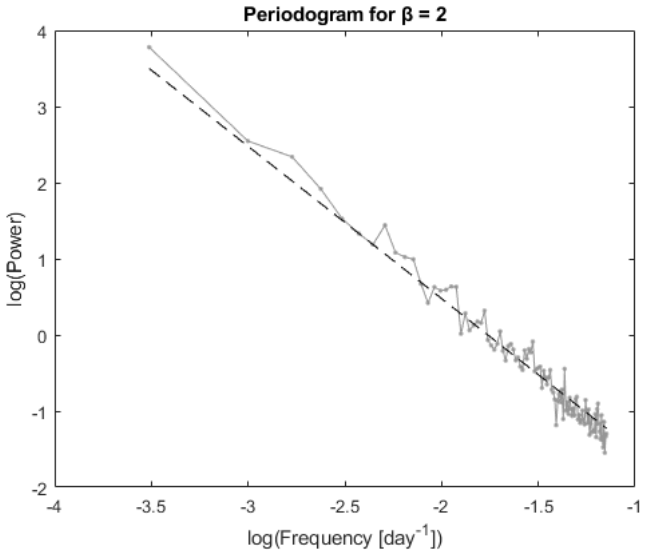

Figure 2: The plot shows the binned periodogram (grey) for a simple power law of $\beta = 2$. The black dashed line depicts the expected PSD slope.

The index β describes the frequency dependence of the analyzed data, which usually in AGN data ranges between $1 < \beta < 3$ depending on the observing frequency and source (e.g., Uttley et al., 2002). Figure 3 shows an arbitrary signal with $\beta = 1$, also called pink noise or flicker noise.

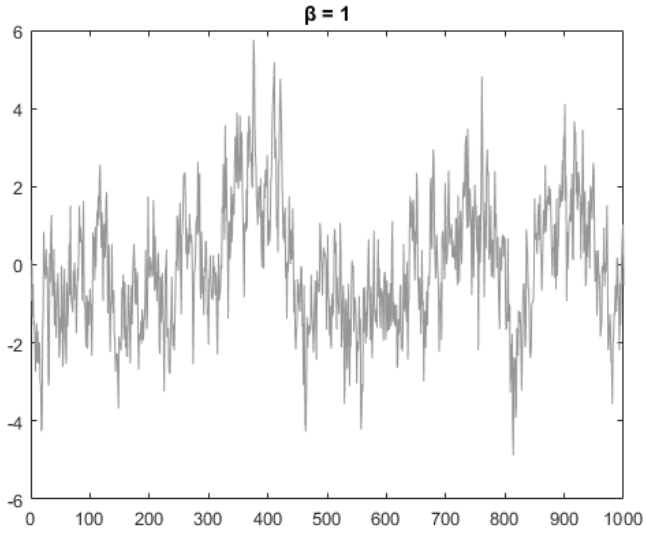

Figure 3: A pink noise signal.

If the index $\beta > 0$, then the signal is called correlated noise. White noise is uncorrelated noise with an index $\beta = 0$ meaning its power content on each frequency is independent from the other frequencies. Figure 4 shows a white noise signal.

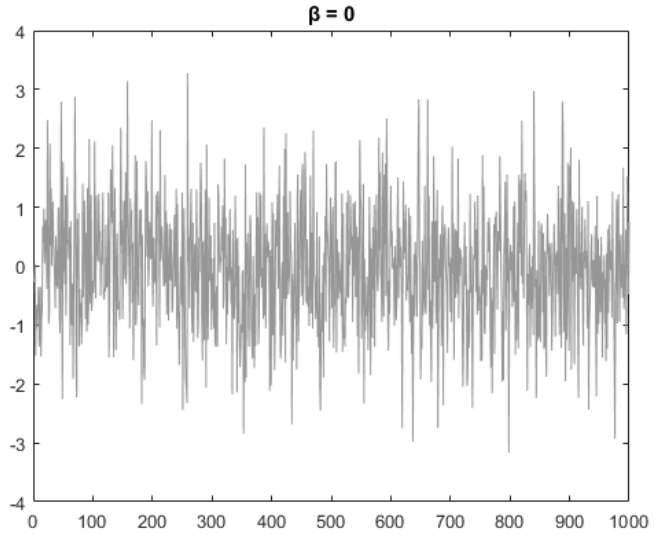

Figure 4: A white noise signal.

In the radio domain, the noise is expected to be correlated and usually close to the index $\beta = 2$, also called red noise (Max-Moerbeck et al., 2014; Park and Trippe, 2014; Ramakrishnan et al., 2015). In essence, this means its variability is over longer intervals. Figure 5 shows a red noise signal.

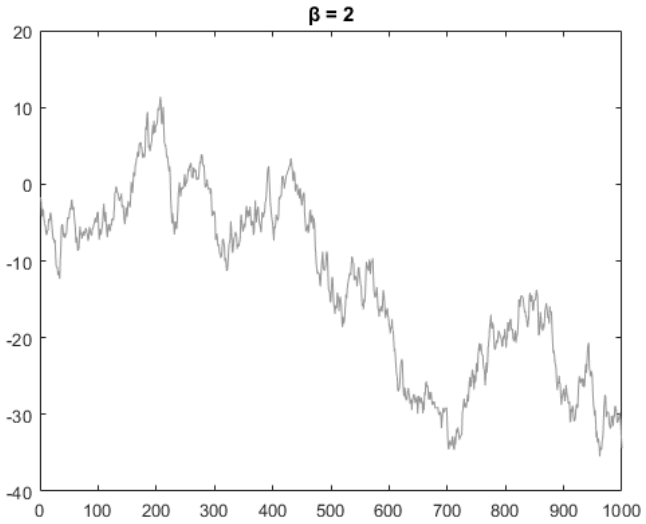

Figure 5: A red noise signal.

When looking at the different noise types, it can be seen that the steeper the spectrum, the smoother the variations. This occurs because the power of the signal is increasingly at the lower frequencies when moving to steeper indices.

The PSD slope index β is an important characteristic on the underlying noise process of the observed AGN. It is also necessary knowledge when data is simulated for e.g., confidence interval estimations. In case of an underlying power law noise process, which is not of the simple power law form, more parameters are introduced to equation (4).

2.2 AGN studies

2.2.1 Variability studies

Analyzing the variability properties of AGNs from their flux density curves is a common subject of studies (e.g., Lainela & Valtaoja, 1993; Hovatta et al., 2007; Hovatta et al., 2008; Park & Trippe, 2014) and different tools, such as the periodogram, give a fairly simple and straightforward way of investigating timeseries data through estimated power spectrums. Variability studies attempt to find characteristic timescales from the data, which would reveal information about the underlying behavior of the source. A characteristic timescale may be seen as a bend or break in the power spectrum and a periodicity as a singular spike. The studies by Lainela & Valtaoja (1993) and Hovatta et al. (2007, 2008) are somewhat rare, because they focus on large samples of data instead of analyzing the variability of individual sources.

Hovatta et al. (2007) used the structure function (SF), the discrete correlation function (DCF), and the Lomb-Scargle (LS) periodogram in their multifrequency study of AGN radio variability on 80 sources observed in the Metsähovi Radio Observatory spanning a maximum of 25 years. The studied sample was large, which they motivated to be important in order to understand the statistical nature of AGN radio behavior. The study discovered that smaller flux density variations occur in the studied sources on short timescales of 1-2 years; however, larger outbursts happen on average only once in every 6 years. There were no indications of significant differences in the timescales between source classes.

It was concluded in the paper that many of the observed sources had changed their behavior during the observation period. Hovatta et al. (2007) discussed that only very long-term monitoring of radio AGNs can reveal the maxima and minima of the flux densities of most sources. It was also noted that typically the highest flux densities during flares are observed in the 22 GHz and 37 GHz frequencies as compared to other radio frequencies.

Hovatta et al. (2008) studied the radio flare characteristics of a slightly smaller sample of 55 sources. The conclusions were that flares last on average 2.5 years at the 22 and 37 GHz frequencies and slightly longer at lower frequencies: the durations vary from 0.3 years to 13.2 years. The study added, that considering the findings by Hovatta et al. (2007), which concluded, that on average the source flares occur every

4-6 years, monitoring campaigns lasting at least 5-7 years would be needed to observe a source in both its quiet and flaring state while also observing the whole flare evolution. Clearly, studying periodicities and quasiperiodicities would then require a very long monitoring program.

Park & Trippe (2014) used the DCF and PSD analysis as well as the LS periodogram to characterize the radio variability of four Blazars in three radio frequency bands. Their sample was small but included data spanning at least 30 years from the 26m UMRAO database. Additionally, the sampling of the data was faster than monthly and consisted of violent flux variability with a minimum flux of 2 Jy.

Their analysis found no evidence of periodicities or quasiperiodicities in the data. The conclusion was that the four sources were in agreement with the underlying noise process being of the power-law noise type with a slope index $\beta = 2$.

2.2.2 Criticism on variability analyses

Vaughan et al. (2016) demonstrate the issues in analyzing short-term irregularly sampled data for periodicities and quasiperiodicities. They note that often reports of periodic or quasi-periodic behavior of AGNs are based on data, which presents only a few cycles of the claimed period. Additionally, these reports fail to consider the red-noise properties of the underlying process, which can produce seemingly periodic random fluctuations over a short interval.

Vaughan et al. (2016) tested their hypothesis on a reported detection of optical periodic modulations of the quasar PG 1302-102 by Graham et al. (2015). The used data was irregularly sampled with clear seasons and periodically clustered observations. The idea was to compare the results from fitting a sinusoid and a stochastic model to the data, in this case the damped random walk (DRW) model. In the DRW model the PSD slope has the value $\beta = 0$ below a certain frequency after which the slope smoothly bends to an index $\beta = 2$. Vaughan et al. (2016) concluded that their results showed a strong preference of the DRW model over the sinusoidal model.

Vaughan et al. (2016) also tested, how often a simple stochastic model might produce nearly sinusoidal light curves. They used the sampling pattern of the original PG 1302-103 data with three different processes: A Gaussian noise process with a steep, bending power law power spectrum, a DRW model, and a sinusoidal process. The results were that in such data it is likely to find so called 'phantom periodicities' caused by a stochastic red-noise process. These 'periodicities' tend to have a period extending to near the longest allowed period i.e., 1.5-2.5 cycles over the available data.

It was also pointed out, that if measurement errors are greatly overestimated, the simulations will be unrealistic. In such a case, the simulations will be too noisy (i.e.,

they will have too much white noise) and the probability of producing the expected strong and smooth modulations will be reduced. In a test case using more accurate errors, they reported a significant drop of phantom periodicities.

2.2.3 Characteristic timescales in relation to data stationarity

A profound issue with regard to using different methods and assumptions is the statistical nature of the underlying process of which the data, in this case flux density data, is one manifestation. Most statistical methods, e.g., the defining of the PSD, assume that the underlying physical process is stationary. Whether the data actually conforms to these assumptions is not always considered.

Stationarity means that a process retains its statistical properties over time. For instance, the mean value and variance of the timeseries remains the same regardless of the surveyed time period as long as the analyzed time windows are of equal length. Thus, stationarity also requires that the PSD of the process should not change over time. However, Vaughan et al. (2003) demonstrate that stationary processes can be the source of seemingly non-stationary timeseries. Even in the absence of errors, the mean and variance can change over time indicating that the stationarity of an underlying process cannot be evaluated directly from the statistical properties of one of its realizations.

According to Vaughan et al. (2003), for a timeseries generated by an underlying noise process with a PSD slope $\beta \geq 1$, the integrated periodogram would diverge as $f \to 0$. In this type of scenario, the timeseries would not have a well-defined mean and would have to be considered weakly non-stationary (Press & Rybicki, 1997). However, Vaughan et al. (2003) continue that this cannot be the case with any real process. It is explained that for a real process the PSD must eventually flatten because the integrated power cannot actually diverge. Weak non-stationarity would thus only be an effect caused by finite sampling, which could be overcome by longer observing periods. Currently, it is unknown at what frequency the radio PSD slopes should typically shift to flatter indices. It is also possible that some AGNs have multiple break-frequencies (Papadakis, 2004).

In the case of a break in the power spectrum, the effect may be seen as flattening of the slope index when fitting a simple power law. Uttley et al. (2002) attempted to fit such a power law without a break to their X-ray data. The best-fit values were low indices $\beta = 1.4 - 1.8$. Upon fitting a high-frequency break model, their results shifted to a much steeper slope above the frequency break varying between $\beta = 2.0$ and $\beta = 2.4$ depending on the source. These fits demonstrate how the chosen power spectral model may alter the results in a significant way; in the case of long-term data the slope value may shift to a flatter index compared to analyses with data from shorter monitoring periods.

A break in the power spectrum has been hypothesized to be caused by a real physical characteristic timescale related to e.g., the mass of the black hole (Markowitz et al. 2003; Papadakis 2004). Finding characteristic timescales in radio AGNs would therefore open new possibilities for understanding AGN physics and allow comparing the results to data from other frequencies.

3 Data and methods

3.1 Data

Metsähovi Radio Observatory

The Metsähovi Radio Observatory is an astronomical radio observatory located in Kirkkonummi, Finland. Its main instrument is a 13.7-metre Cassegrain radio telescope. The telescope is used to gather data from over 1000 AGNs in both 22- and 37-GHz frequencies.

The observatory started its operation in 1974 with the first AGN observations taking place in 1979. The observed data is unique as few radio observatories have consistently observed the same sources for over 40 years. This type of long-term data allows unprecedented analyses to be conducted.

3.1.1 Sample

The sample used in this thesis consists of AGN data gathered by the Metsähovi radio telescope at 37 GHz frequency. The sample was chosen such that the sources exhibit reasonable variability over a long monitoring period. To aid in the choosing of the sample, the whole Metsähovi database was reviewed. Different criteria, such as the number of data points, were chosen as parameters for a database-query script written in the previous summer as part of summer work. The light curves for the resulting sources were then plotted with Matlab and reviewed visually for their variability properties and suitability for the sample.

Based on the light curves, it was initially decided that the maximum flux density would have to be at least 1 Jy and the number of data points over 20. To ensure that the analysis only consists of long observing periods, the data points would have to be spread over a time period of minimum 10 years. These requirements ensured the possibility of conducting at least some of the planned analyses. With these requirements set, the initial number of sources was 170.

The number of sources eventually narrowed down to 123 due to the fact that accurate simulations required the PSDs of all sources to be estimated. While more data points would have been better, a lower limit of N = 100 was set. After visual examination, a few sources were cut from the sample because their data-point distribution was too inconsistent to represent the true light curve well enough.

The sample in this thesis includes all of the sources used in the analyses by Hovatta et al. (2007), as well as new sources, which had insufficient amount of data in 2007. The used sample of 123 sources is listed in Appendix A including some other relevant information such as the number of data points and first and last observations.

The average monitoring period counting the difference between the last and first observation for each source is 31 years. This is an exceptionally long overall monitoring period for such a large well-sampled data set. 85 sources in the sample have been monitored for a minimum of 30 years and 40 sources for a minimum of 35 years. 13 of the sources have been observed for approximately 40 years.

The AGN types in the sample are: 18 HPQs, 22 LPQs, 38 QSOs, 35 BLOs, 10 GALs. Those Quasars, which had their LPQ or HPQ classification in Hovatta et al. (2007) were marked as such and the rest as QSOs.

Figure 6 shows the maximum and average fluxes of all the sources in the Metsähovi 37 GHz sample. The sources used in this thesis are additionally circled in orange.

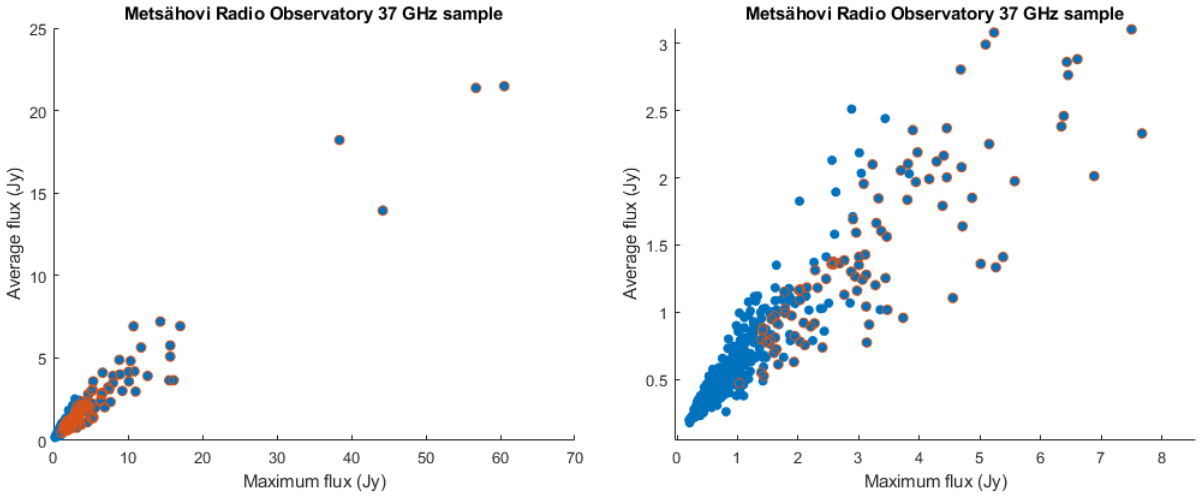

Figure 6: The left plot shows the entire Metsähovi Radio Observatory 37 GHz sample with the maximum and avarage fluxes of all sources plotted. The data points with orange circles are the sources in the sample of this thesis. The left plot is zoomed in to show the lower flux sources in more detail.

3.2 Methods

The presented methods were written as Matlab code for the purposes of this thesis. While some code would have been available online or possibly upon request from researchers in the field, writing them ensured a better understanding of how the methods work. Exceptions were the Lomb-Scargle periodogram and the generalized Lomb-Scargle periodogram, former having an intrinsic Matlab function ('plomb') and the latter a script written by Zechmeister (2018). A Mathematica notebook for the Monte Carlo simulations included in Emmanoulopoulos et al. (2013) was used as an aid when writing the Matlab code for the light curve simulations. While the DCF and structure function were both relatively simple to implement based on

theoretical papers, the Monte Carlo simulations proved to be unexpectedly time-consuming to implement and to test. Particularly difficult was to reproduce the results from other papers (e.g., Ramakrishnan et al., 2015). The choice of bin size, interpolation type, normalization, and adding of noise among other things have all some effect on the results. For the sake of reproducibility, all parameter choices have been stated and methods used in this thesis are described as thoroughly as possible.

3.2.1 PSD estimation and Monte Carlo simulations

To be able to estimate the source PSD slopes and to assign confidence limits for the analysis results, algorithms by Timmer & König (1995, hereafter TK95) and Emmanoulopoulos et al. (2013, hereafter EMM13) were used to generate artificial light curves matching the statistical properties of the observed data. A modification of the power spectral response (PSRESP) method by Uttley et al. (2002) was used to find the best-fitting PSD and to estimate the PSD slopes for the sources. These same methods were used by e.g., Ramakrishnan et al. (2015) for the determination of radio- and gamma-ray PSD slopes, though their PSD estimation procedure used the EMM13 algorithm.

The EMM13 procedure consists of a combination of two different methods: a method for the simulation of Gaussian distributed light curves (TK95) and the improved amplitude adjusted Fourier transform (IAAFT) by Schreiber & Schmitz (1996). The TK95 method is commonly used in astronomy (e.g., Uttley, 2002; Max-Moerbeck et al., 2014) to produce simulated light curves; however, it is only suitable for the production of Gaussian distributed data. Max-Moerbeck et al. (2014) discuss the possible issue in having used the TK95 method in assigning confidence levels for their DCF analysis, though they argue that for their radio data sample it should not be a significant issue. The confidence levels in the analysis of this thesis were generated with the EMM13 algorithm, because the analyzed sample is large and some of the sources show behavior which may not be consistent with Gaussianity. For this reason, the second part, the IAAFT method, is included in the EMM13 procedure to ensure that the simulated data has the same probability distribution function (PDF) as the original source data. Because the observed PDF is used, even if the data were Gaussian distributed, the method would give the correct result.

TK95

TK95 is a method used to generate Gaussian-distributed data with the power law of choice. It randomizes both the phase and amplitude of the generated data. The procedure is such that for each Fourier frequency two random Gaussian-distributed numbers are generated and multiplied by

$$\sqrt{\frac{1}{2}S(\omega_i)}, \tag{5}$$

where $S(\omega_i)$ is the chosen power law spectrum at Fourier frequency ω_i. The negative Fourier components are chosen by taking the conjugative $f*(\omega_i)$ of the positive frequencies. The result is then inverse Fourier transformed in order to obtain a simulated light curve.

IAAFT

The IAAFT method by Schreiber & Schmitz (1996) is a surrogate method, where the original source data is shuffled, spectral- and amplitude-adjusted with the correct PSD and PDF, and then iterated over until both the PSD and the PDF match the original data. The difference in the EMM13 method is that in place of the shuffled original data, a pseudo-random data set generated from the estimated PDF is used. In addition, instead of the original data, the spectral adjustment phase uses the amplitudes taken from the TK95 simulated light curves.

PDF estimation

EMM13 suggests estimating the PDF of the observed data from either fitting a probability density function to the histogrammed observed data, directly using a piecewise-constant representation of the PDF, or using the empirical cumulative distribution function (ECDF) from which random numbers can be directly generated. In this thesis, the last approach was chosen as it did not require any parameter choices made. Similarly to Ramakrishnan et al. (2015), to test the equality of the PDFs, a two-sample Kolmogorov-Smirnov test was used.

PSD estimation

The periodogram is an estimator for the PSD (Priestley, 1981; Bloomfield, 2000; Vaughan, 2003). It can be calculated as

$$P(f_j) = A\left\{\sum_{i=1}^{N} x_i \cos\left(2\pi f_j t_i\right)\right\}^2 + \left\{\sum_{i=1}^{N} x_i \sin\left(2\pi f_j t_i\right)\right\}^2, \tag{6}$$

where A is the normalization factor. The normalization used in this thesis is

$$A = \frac{2T_{samp}}{N\mu^2} \quad (7)$$

in accordance with Van der Klis (1997). Here T_{samp} is the sampling interval, N the length of the timeseries, and μ the mean of the data. This normalization results in the integrated periodogram giving the fractional variance of the data (Vaughan et al., 2003).

Because the EMM13 algorithm is computationally far more expensive than the TK95 method, the TK95 method was used for the PSD slope estimation and then the EMM13 method for the generation of the simulated light curves based on the best-fitting slope value. Initially, slope fitting was attempted with the EMM13 algorithm, but it proved difficult and the slopes seemed to be underestimated regardless of the adjustments made to the algorithm. The higher complexity of the algorithm also caused the varying of different parameters, such as bin size, to be very time-consuming. After some testing, it was also clear that the IAAFT portion of the EMM13 algorithm introduced some unexpected noise to the PSD estimates. The difficulties are explained in detail at the end of this subsection.

With the EMM13 method, reaching convergence in the simulations was another factor affecting the computing time especially since the sample consisted of many sources with dense sampling and long observing periods. According to EMM13 reaching convergence is not always necessary, because even at a lower iteration step the PSD parameters should be quite accurate with only slightly higher scatter. For this reason, the iteration cycle was chosen to stop at iteration step 100. To test the accuracy of non-converged results, the simulations were run twice for some sources in order to see if the variation was too high. With N = 500 and convergence maximum iteration number i = 100, tests showed an acceptable maximum variation of |0.1| when run three times for a random sub-sample of 10 sources.

Spectral distortions

Spectral distortions, namely red-noise leak and aliasing were considered in the simulations. Red-noise leak is caused by the observed finite signal: The Fourier transform of the signal is calculated within a discrete-sized window, although the probed signal, in reality, goes from $-\infty$ *to* ∞. The signal is thus multiplied with a window or convolved in the frequency domain. The window causes side-lobes in the resulting Fourier transform, which are seen as spectral leakage.

Aliasing is another spectral distortion effect, and it is caused by discrete sampling of a continuous signal. Nyquist frequency is the frequency above which the higher order frequencies of the signal start to fold back to lower frequencies and these frequencies will look as if they were true low frequency components.

Spectral distortions were added similarly to e.g., Uttley et al. (2002). The effect of red-noise leak was mimicked by simulating a long light curve 1000 times the length of the original timeseries. Aliasing was included by generating a light-curve with high-frequency components of $0.1 * day$ and then by re-sampling the TK95 data by taking a sample once per day. Instead of individually simulating long light curves, a much more efficient way of simulating one long light curve was chosen. The entire long light curve of size $1000 * T$ was divided into 1000 segments each representing one individual light curve. According to Uttley et al. (2002), the bulk of red-noise leak causing the spectral distortions in individual light curves is due to variations on timescales close to the length of the observed light curve. Therefore, the red-noise leak will be statistically independent between the segments.

When generating the EMM13 simulated light curves for confidence interval estimations, the EMM13 light curve was chopped to the length of the observed light curve already after the TK95 simulations as opposed to chopping only after the complete EMM13 procedure. This was suggested in EMM13 in cases where Fourier phases are not of interest.

Windowing

It was shown by Max-Moerbeck et al. (2014) that using a Hann window significantly reduces the red-noise leakage caused by finite sampling. This was also confirmed by testing the TK95 PSD fitting both with and without multiplying the light curve with the Hann window before the Fourier transform. The results showed that it was very difficult to define an upper limit to the confidence interval as the red-noise leak caused the power spectrum to flatten when going to steep indices $\beta > 2$.

Observational noise

White noise is usually added into simulated data to mimic observational noise. However, there is always the possibility of overexaggerating the noise properties causing distortions to the power spectrum. For this reason, it was tested whether noise should be added to the EMM13 simulations.

The test setup was such, that a source from the sample was chosen at random. A Gaussian distributed light curve of a chosen PSD slope value was then generated with the TK95 algorithm and the sampling of the observed source was applied to the data. No spectral distortions were added. Noise was then added to the simulated light curve with the standard deviation of the observed light curve errors. This data was then given to the EMM13 algorithm and it was tested if the method was able to find the correct underlying power spectrum. This test setup was repeated for 5 sources, whose sampling distributions and average SNR had a decent variation between them. The test was able to confirm that the EMM13 algorithm works well in finding

the true underlying power spectrum of a well-sampled source with uneven sampling. In addition, it was confirmed that observational noise may not need to be added to the EMM13 results, because the empirical cumulative distribution function is based on noisy data points.

Variance

With TK95, the variance of the simulated data needs to be matched with that of the observed data. Because the observed data points include observational errors, taking the variance of the data is strictly not the actual intrinsic variance. Although with high-SNR radio data this did not seem to make a great difference, the excess variance method by Nandra et al. (1997) was used. The variance is thus calculated as

$$\sigma_i^2 = \frac{1}{N}\sum_{k=1}^{N}[(x(k) - \bar{x})^2 - \sigma_k^2]\,. \tag{8}$$

The PSREP method

The goodness-of-fit of the simulated periodogram was measured via the χ^2_{dist}-distribution

$$\chi^2_{dist} = \sum_{f=f_{min}}^{f_{max}} \frac{\left(\overline{P_{sim}(f)} - P_{obs}(f)\right)^2}{\Delta\overline{P_{sim}(f)^2}}, \tag{9}$$

which seeks to minimize the χ^2_{dist} statistic (Uttley et al., 2002). Here $\overline{P_{sim}(f)}$ is the mean of the N simulated power spectra and $P_{obs}(f)$ the power spectrum of the observed data. $\Delta\overline{P_{sim}(f)}$ is the root-mean-square (RMS) error of the simulated power spectra about the mean.

The basic principle of the method is such that the periodograms of all simulated light curves are averaged to form $\overline{P_{sim}(f)}$. This value is then compared to both the periodogram of the observed light curve as well as all the individual periodograms of the simulated light curves. A larger χ^2_{dist} value indicates stronger evidence against the null hypothesis, which in this case is that the periodogram has an underlying noise process following the simple power law with $1 < \beta < 3$. Finding the best goodness-of-fit is then done by comparing the χ^2_{dist} -value of the periodogram of the observed light curve and the χ^2_{dist} -values of the periodograms of the simulated light curves. The fraction of simulated periodograms which have a higher χ^2_{dist}-value than

the corresponding value of the periodogram of the observed data, i.e., they are more likely to be rejected, reflects the goodness-of-fit for the given PSD-slope value. In short, the higher the number of χ^2_{dist}-values for the simulated data, which exceed the χ^2_{dist} of the observed data, the better the fit.

The PSREP method uses a modified version of the χ^2 -distribution, because the periodogram points are not normally distributed. Papadakis & Lawrence (1992) explain that according to the Central Limit theorem, if the periodograms are binned in sufficiently large bins, the powers at each binned frequency should follow a normal distribution approximately. They tested this on a smoothed periodogram and noticed that the bins have to be large, at minimum $M = 50$. However, if the periodograms are logarithmically transformed and accounted for bias by adding 0.25068 to the logarithmic powers, the bin size need not be as large. According to them, even a bin size of $M = 20$ may be enough. For this reason, bin sizes of $M = 10$ and $M = 20$ were tested for the PSD estimations and the chi-square goodness-of-fit test (Matlab function 'chi2gof') was used to see if the individual simulated periodograms followed a normal distribution at a 95% confidence level.

The results of the tests were that indeed $M = 20$ is a large enough bin size to allow normal distribution between the bin means. In this situation the χ^2 goodness-of-fit gave the same best-fit results as the χ^2_{dist} test as would be expected, though the p-values did not fall as sharply around the best fit. With $M = 10$ the results were not as consistent with some periodograms following Gaussian distribution closely and some not within the 95% confidence level. Papadakis & Lawrence (1992) note that depending on the application, the approximate Gaussianity of bin sizes such as $M = 10$ may be sufficient. Nevertheless, for the analyses in this thesis, bin size of $M = 10$ and the χ^2_{dist} goodness-of-fit were used. While $M = 20$ gave decent results, it required a large number of data points (e.g., $N \geq 200$) in each light curve. With $M = 10$, the lower limit of number of data points was set to 100.

Confidence levels

To calculate the 68.3% confidence limits for the PSD-slope values, the method presented by Uttley et al. (2002) was used. However, this method may be problematic as shown by Max-Moerbeck et al. (2014). One issue is that the method does not allow e.g., 68.3% confidence limit for fits, whose p-value is less than 0.317. For this reason, some of the PSD fits do not have a defined confidence level. While these issues can be problematic when comparing the PSD best-fit values, the estimation seemed adequate for the purposes of this thesis; The other used methods should reveal more about the goodness-of-fit through simulations and visual analysis. However, in order to retrieve more accurate confidence levels, a more complex and thus more time-consuming method should be used.

Re-cap of the PSD-fitting procedure:

1. Average the observed data to the nearest day to simplify resampling of simulated light curves.
2. Bin data to the chosen interval.
3. Interpolate empty bins with chosen interpolation method. (Subtract the mean and apply detrending)
4. Generate N > 100 light curves with the TK95 procedure with the chosen noise process with parameter values ranging between a chosen interval. Apply red-noise leakage by simulating long light curves and take aliasing into account by including frequencies 0.1*day into the simulated light curve.
5. Resample the simulated light curves to the original sampling of the observed data.
6. Match the variance and mean of the observed data and add white noise with the variance of the observational errors.
7. Bin the data in the same manner as the observed data and interpolate empty bins. (Subtract the mean and apply detrending)
8. Calculate their logarithmically binned and bias-corrected periodograms with the chosen bin size M.
9. Average the periodograms to form $\overline{P_{obs}}$.
10. Minimize the chi-distribution statistic and find the p-value from the distribution of χ_{sim}-values exceeding the minimized value.

Table 1 gives the parameter choices made in the simulations.

Table 1: Parameter choices for the PSD estimation.

T_{samp}	Number of simulations	Periodogram bin size	Interval for β	Interpolation method	Minimum number of data points	Minimum p-value
$2 * \frac{T}{N}$	1000	10	1.0: 0.1: 3.0	Linear	100	0.05

This procedure applies also to the EMM13 algorithm, except no mean and variance matching is needed and noise may not need to be added separately. Additionally, the EMM13 algorithm requires the PDF matching to be done. In this thesis, this was done with the ECDF, which requires no parameter choices made.

Issues with the EMM13 method

The EMM13 method showed some issues regarding the retainment of the correct PSD complicating the discrimination between PSD-slope values.

It was shown by Max-Moerbeck et al. (2014) that using a Hann window before calculating the periodogram of a light curve reduces red-noise leakage significantly. To examine this effect, windowing was tested for TK95 simulations with a variety of β-values for the simple power law. Indeed, the results showed that if the simulated data was not multiplied with a Hann window before the calculation of its periodogram, least-squares fitting gave almost the exact same slope for all $\beta > 2$.

While the Hann window worked well on the TK95 Gaussian-distributed data with a known PSD slope, the EMM13 algorithm had an issue with red-noise leak. When testing the algorithms, the EMM13 produced a much flatter slope than TK95 if red-noise leak was applied and Hann windowing was used before calculating the periodogram. Figure 7 shows an example of generating N = 100 simulations with red-noise leak, multiplying the evenly sampled data with a Hann window, and then calculating the periodogram and taking the average.

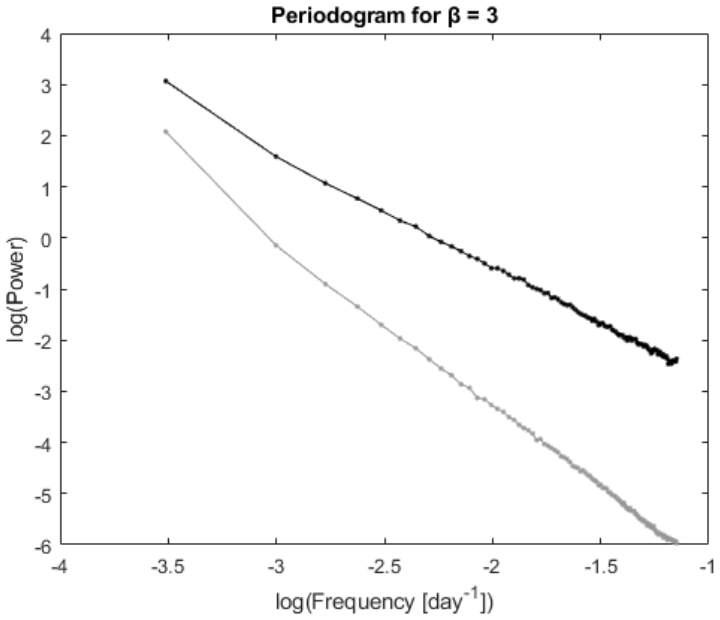

Figure 7: The binned periodogram of EMM13 simulations (black) and the binned periodogram of TK95 simulations (grey) with PSD slope $\beta = 3$. The EMM13 PSD estimate is close to $\beta = 2.2$.

It appears that windowing does not work with the EMM13 algorithm if it is done after the convergence steps. In fact, the slope remained the same regardless of whether the Hann window was used or not. The only solution seemed to be that the TK95 generated simulation be Hann windowed before the IAAFT part of the algorithm. In such situations the slope was similar to the sole TK95 result.

Upon further tests, the actual issue was found; it seemed to be caused by the chopping of the light curve before the convergence steps. While EMM13 suggests doing the chopping before the IAAFT part of the algorithm in order to save

computing time (if the Fourier phases are of no interest), this apparently causes the red-noise leak to be 'scrambled' during the iteration steps. Thus, if red-noise leak is added to the data, either the TK95 product needs to be windowed, or the entire long simulated light curve needs to be used for the iteration part after which it can be cut to the required length.

This should not have been a significant issue in the confidence levels simulations, because unevenly sampled data could not be windowed. Especially because the slopes were somewhat flat (i.e. $\beta \ll 3$), red-noise leak in general should not have been as dominant in the periodogram. Essentially, it seems that the EMM13 produced light curve (in case of red-noise leak in the TK95 product) has an underlying PSD similar to the flattened PSD caused by the red-noise leak. In future studies this assumption needs to be confirmed as it is most likely not completely accurate; in small tests there was a slight difference in the estimated slopes. For this thesis, the computational load and time from simulating 1000*T long light curves with the entire EMM13 procedure was not realistic.

3.2.2 Lomb-Scargle periodogram

The Lomb-Scargle periodogram is a Fourier-based least-squares method designed for unevenly sampled data (Lomb, 1976; Scargle, 1982). It is a modification of the classical periodogram, which only functions on evenly sampled data. The method works by fitting a model to the data at each probed frequency and then selecting the frequency, which maximizes the likelihood (VanderPlas, 2018). The LS periodogram is defined as

$$P(f_j) = \frac{1}{2}\left\{\frac{\left\{\sum_{i=1}^{N} x_i \cos\left(2\pi f_j[t_i-\tau]\right)\right\}^2}{\sum_{i=1}^{N}\cos^2(2\pi f_j[t_i-\tau])} + \frac{\left\{\sum_{i=1}^{N} x_i \sin\left(2\pi f_j[t_i-\tau]\right)\right\}^2}{\sum_{i=1}^{N}\sin^2(2\pi f_j[t_i-\tau])}\right\}, \tag{10}$$

where

$$\tan(2\omega\tau) = \frac{\sum_{i=1}^{N}\sin(2\omega\tau_i)}{\sum_{i=1}^{N}\cos(2\omega\tau_i)}. \tag{11}$$

As can be seen from equation (10), the LS periodogram does not differ from the original periodogram significantly. In fact, if the data is evenly sampled, the LS periodogram reduces to the original periodogram formulation of equation (6) (Scargle, 1982).

Because the LS periodogram requires the data to be pre-centered as it assumes the mean of the data and fitted sine wave to be equal (Zechmeister & Kürster, 2009), the generalized Lomb-Scargle periodogram (Zechmeister & Kürster, 2009) was eventually used for the analyses as suggested by VanderPlas (2018). It differs from

the original LS periodogram with an introduced offset in the estimator; this 'floating mean term' fits a full sine wave to the data. It is preferred to not have to subtract the mean from the data, because the calculated mean may be skewed from the true mean either because of uneven sampling or e.g., due to the detection threshold (in Metsähovi SNR ≥ 4). The offset term added to the sinusoidal model at each frequency is (VanderPlas 2018):

$$y_{model}(t; f) = y_o(f) + A_f \sin\left(2\pi f\left(t - \phi_f\right)\right). \quad (12)$$

Starting from the next section, the generalized LS periodogram will simply be referred to as the LS periodogram.

The analyzed frequency range was $f = 0{:}\frac{1}{4T}{:}\frac{N}{2T}$. The figures in the Results chapter are cut to start from $\frac{1}{T}$ for visual reasons as they had no apparent power visible in the $< \frac{1}{T}$ part of the spectrum.

Confidence levels

Scargle (1982) shows that determining the significance of the found timescales in the LS periodogram can be done via the false alarm probability (FAP):

$$z_o = -\ln\left[1 - (1 - p_o)^{\frac{1}{N}}\right], \quad (13)$$

where z_o is the significant power level and p_o the chosen confidence level (e.g., 0.001). For small p_o:s

$$z_o \cong \ln\left(\frac{N}{p_o}\right). \quad (14)$$

However, Scargle (1982) explicitly states that the used example data consists of a strictly sinusoidal signal and white noise; The defined false alarm probability can only be used to distinguish a periodic signal from white noise. As discussed, AGNs in the radio domain are expected to have a red noise spectrum meaning the original FAP cannot be used for peak significance determination in the LS periodogram.

In order to assign confidence levels to the LS periodograms, Monte Carlo simulations were used. Similarly to Do et al. (2009) and Park & Trippe (2014), the 3σ-confidence levels were calculated from the averaged periodogram of $N = 1000$ simulated light curves. For the simulations, the EMM13 algorithm was used.

Known issues

The Lomb-Scargle periodogram is a widely-used method in AGN variability studies. It should be well suited for astronomical data due to its ability to handle unevenly sampled timeseries data. As with other methods applied to unevenly sampled, noisy, and often presumably at best quasi-periodic data, it is not completely unproblematic.

Springford et al. (2020) discuss that Scargle (1982) is trying to detect a single periodic component from a background noise process, which would deem inconsistency and spectral leakage to be of no particular concern. Spectral leakage is however clearly a problem with the LS periodogram when analyzing e.g., astronomical data (Springford et al. 2020) and Scargle does suggest using a window function to help with the effect. Trying to identify one strictly periodic signal should keep the spectral leakage indifferent, however with AGN data there is no single periodic signal in white noise with a set frequency to be found. To complicate matters further, windowing is not possible with unevenly sampled data as shown by Moerbeck et al. (2014).

To examine the effect of uneven sampling, a sinusoid was created with the frequency corresponding to the length of the timeseries and its sampling corresponding to the sampling of the original signal. An LS periodogram was created for the sinusoid and its result was compared to an LS periodogram of an evenly sampled sinusoid with the same frequency. The evenly sampled sinusoid behaved as expected and the periodogram peak was seen at exactly the length of the timeseries. However, the unevenly sampled sinusoid behaved differently; Out of 133 sources, the sampling of 55 sources showed the periodogram peak at a frequency either lower or higher than the fundamental frequency of the sampled sinusoid. The peaks were not an integer multiple of the fundamental frequency. Repeating the analysis for a frequency $\frac{2}{T}$ increased the likelihood, that the LS periodogram would show approximately the correct period. On the other hand, further analysis with 3, 5 and 12 times the original frequency showed that the periodogram was capable of finding the approximately correct fundamental frequencies for those sinusoids even with the uneven sampling. These spurious spikes caused by the length of the monitoring period may create complications, when analyzing the final results. Hovatta et al. (2007) reported that many of the periodograms showed a peak at the length of the timescale or at its harmonic. Potentially, if the periodogram were to show a strong peak at a harmonic of the length of the monitoring period, its identification might be compromised if the monitoring period is not correctly identified by the periodogram.

Since the original Lomb-Scargle periodogram failed to detect the correct fundamental frequencies for a number of sources, other approaches were considered. The generalized Lomb-Scargle periodogram, more commonly known as the floating mean periodogram, was suggested by Zechmeister & Kürster (2009). In this approach a new offset is introduced to the estimator. This ‘floating mean term’ fits a full sine wave to the data.

The same sinusoid analysis was run on the generalized LS periodogram and, unlike the original LS periodogram, it successfully detected all 133 fundamental frequencies correctly both with $\frac{1}{T}$ and $\frac{2}{T}$ frequencies. While the analysis is not conclusive, and the original LS periodogram was able to detect the higher frequency sinusoids, the generalized LS periodogram results are encouraging. These tests further confirmed that the generalized LS periodogram should be the method of choice.

3.2.3 Structure function

The structure function is a time-domain method similar to its frequency-domain counterpart the periodogram. It has been used in AGN variability analysis by e.g., Hughes et al. (1992) and Hovatta et al. (2007). The structure function was first introduced by Simonetti et al. (1985). Only the first-order structure function will be used as in most studies (e.g., Hughes et al., 1992; Hovatta et al., 2007). The first-order structure function is defined as

$$D^1(\tau) = \langle [S(t) - S(t+\tau)]^2 \rangle. \quad (15)$$

Here, $S(t)$ is the source flux density at time t and τ is the time lag between observations.

First, the time difference and corresponding structure function between each observation was calculated. Then, the results were binned to 0.05 dex with a minimum time difference τ of 7 days. The resulting structure function was calculated by taking the average of all individual structure functions within each bin.

According to the ideal structure function, a power-law slope should be visible in the middle preceded by a plateau caused by observational noise and followed by a plateau signifying an intrinsic timescale (Hughes et al.,1992). The plateau should asymptote to $log(2.0)$ when the data is normalized with its variance.

The structure function should show the same timescales as the periodogram. If the underlying process contains an intrinsic variability timescale, it should be imprinted on the structure function as well. Therefore, the structure function and periodogram results can be analyzed in order to find true characteristic timescales.

Known issues

While the structure function has often been considered a great tool to be used in place of PSD analysis due to its ability to handle unevenly sampled data and disregard spectral distortions problematic in the frequency domain, Emmanoulopoulos et al. (2010) question its superiority for both evenly and unevenly

sampled data. According to them, SF is in fact not unproblematic and is affected both by the length of the timeseries as well as sampling. For instance, regardless of the PSD slope value, increasing the observation length shifts the SF break towards higher values. The SF break is at the beginning of a plateau, which is at an amplitude twice the variance of the fluctuation (Hughes et al., 1992). However, Emmanoulopoulos et al. (2010) argue that the maximum variance of the timeseries is increased as the observing length is increased thus altering the position of the SF break. The break is mapped into the SF regardless of whether the PSD contains any characteristic timescales. In fact, Emmanoulopoulos et al. (2010) show with simulations, how meaningless breaks appearing in the SFs can be deduced from the length of the timeseries as well as the underlying PSD.

Another problem is the interpretation of the break position. According to Emmanoulopoulos et al. (2010), physically interesting timescales would be mapped in the SF; however, relating them to the PSD breaks is difficult.

In order to facilitate these issues with the structure function, Monte Carlo simulations were used in order to better understand the behavior of the data. While more profound analysis has been left for future studies, the averaged out structure functions from the simulations should provide some estimates on whether the seen timescales are clearly against the null hypothesis. The null hypothesis throughout the analyses in this thesis is that the observed data has an underlying physical process described by a simple power law.

3.2.4 Discrete correlation function

The discrete correlation function (Edelson & Krolik, 1988) is a method which is intended for measuring correlation functions of unevenly sampled data. In this thesis, the DCF is used as an autocorrelation function, where the data of each source is autocorrelated using the DCF method to reveal timescales. The difference to the classical correlation function is in that the DCF correlation is done in discrete pairs with regard to pairwise lag $\Delta\tau_{ij}$ instead of global lag $\Delta\tau$. Therefore, interpolation to even sampling is not initially required.

First, the unbinned discrete correlation is calculated for all pairs as:

$$UDCF_{ij} = \frac{(a_i - \overline{a})(b_j - \overline{b})}{\sqrt{\sigma_a^2 \sigma_b^2}}. \tag{16}$$

At this point no interpolation is required. Generating the DCF requires binning by averaging over M points. The DCF is calculated by

$$DCF(\tau) = \frac{1}{M} \sum UDCF_{ij}(\tau)\,. \tag{17}$$

The size of the bin determines the accuracy and resolution of the DCF. Choosing a small bin size gives higher resolution at the expense of generating spurious correlations, and large bin size smooths the results possibly disregarding some correlations due to lost information. Hovatta et al. (2007) used a bin size of 50 days and noticed no significant difference between that and a smaller bin size of 25 days. The DCF analysis in this thesis was made with a bin size of 50 days; however, bin size of 25 days was also tested to confirm no significant correlations were lost.

No normalization was done at this stage, but some type of normalization procedure may need to be used in order to get more accurate results.

Confidence levels

Because the DCF method gives no proper error estimates for the correlations, EMM13 simulations were used to generate confidence levels. Max-Moerbeck et al. (2014) use the TK95 method to simulate artificial light curves in order to estimate the significance of cross-band correlations. Their idea was to cross-correlate the simulated light curves in order to estimate the frequency of spurious correlations. Because the aim of this thesis was to analyze the variability properties of each source in the sample, significance levels were generated by autocorrelating $N = 1000$ simulated light curves. Because the source sampling and timeseries length is included in the simulations, peaks attributable to these effects, or simply to the length of the timeseries, should be visible in the simulations. In order to generate significance estimates, the average of the autocorrelations was taken, and their sigma-limits were calculated.

The uncertainty of the binned DCF is given by:

$$\sigma_{DCF}(\tau) = \frac{1}{M-1}\left\{\sum\left[UDCF_{ij} - DCF(\tau)\right]^2\right\}^{\frac{1}{2}}. \quad (18)$$

Relationship with power spectral density

The autocorrelation function is the Fourier transform pair of the periodogram. Therefore, using the DCF for autocorrelation and then taking its Fourier transform should give an approximation of the power spectrum of the light curve. Estimating the PSD should technically be possible from the DCF and therefore it will be used as a method for further examination of the underlying power spectrum. While all of the four methods have a strong link, they all take a slightly different approach to the power spectrum estimation and therefore should give a good approximation on the true behavior of the observed data.

4 Results and discussion

The behavior of 123 sources was analyzed. This was the first time the Metsähovi 37 GHz dataset has been analyzed for the current up to 40 years of data. The long timeseries allowed comparing the results across different monitoring epochs and understanding the evolution of the behavior of each source.

4.1 Power spectral density

The PSD analysis was able to find best-fit PSD-slope values for 115 sources. The average PSD slope resulting from the PSD-fitting procedure was $\beta = 1.55$. Figure 8 shows the fitted normal distribution corresponding to $\mu = 1.55$ and $\sigma = 0.27$. As the fit shows, there were some sources, which would have required the fitting interval to start from below $\beta = 1$.

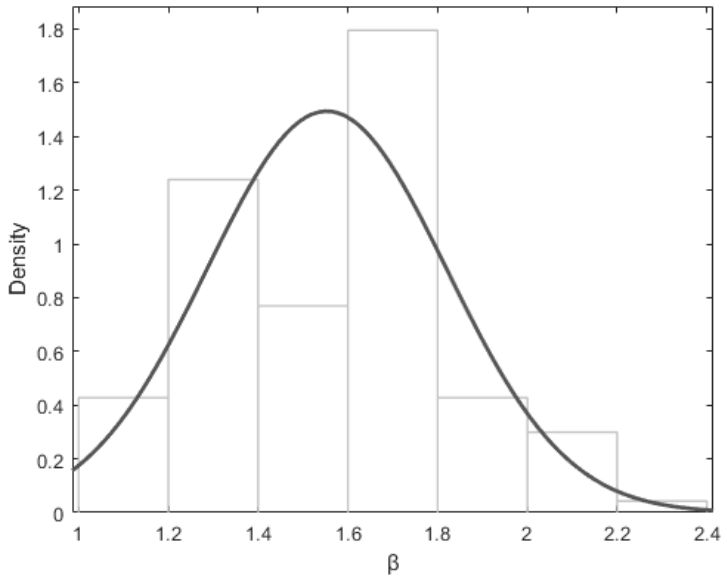

Figure 8: Normal probability distribution fit made to the best-fit slope values obtained from the PSD fitting procedure.

The mean slope value $\beta = 1.55$ is low compared to the results gained by earlier research (e.g., Max-Moerbeck Astudillo, 2013; Ramakrishnan et al., 2015). The average radio slope index in these studies has been reported to be around $2 \leq \beta \leq 2.3$; a slope index $\beta = 2$ would be consistent with the random walk noise process. The similar noise process DRW, briefly discussed in Chapter 2, is a combination of the random walk process in high frequencies and a white noise process in low frequencies.

While different decisions, such as bin size, method of interpolation, segmenting the light curves, as well as simply differences in the sample may have a significant effect on the results, there may also be a physical explanation. As discussed in Chapter 2, a real physical process should contain a break at some lower frequency. A simple power law is expected to be a good approximation for data, which has only been sampled for shorter monitoring periods; however, it is to be expected that at longer monitoring periods a break/bend in the power spectrum would become visible. As was explained, this is a necessary phenomenon, because otherwise the power would not converge. Naturally, approximating the data with a simple power law would eventually cause the fit to shift into flatter indices as the low-frequency part would introduce a flatter portion to the spectrum.

The effect can be visually looked for in the Lomb-Scargle periodograms. Because the used data is unevenly sampled, it is always more difficult to differentiate real physical breaks from the effects of sampling and spectral distortions. However, Monte Carlo simulations should be able to mimic many of these effects enabling better discrimination between real physical phenomena and other fluctuations.

4.1.1 PSD slopes over different monitoring period lengths

To test the effect of analyzing shorter timeseries, the fitting algorithm was run on shorter segments taken from the data: 5, 10, and 20 years. Because the Metsähovi sample has better cadency after the year 2000 due to the increased number of observations in the 37 GHz frequency (as opposed to 22 GHz), the segments were chosen from between 2000 and 2020. For the 5-year segment 2008-2013 was chosen, for the 10-year segment 2010-2020, and for the 20-year segment 2000-2020. The justification for the 5-year segment comes from the studies by Max-Moerbeck Astudillo (2013) and Kiehlmann (2015), which both used radio data observed around the chosen time period. Only the sources which had a minimum of $N = 100$ data points in the 5-year segment were included in the plots in Figure 9, which shows the time evolution of the PSD slopes. Because some of the sources have been observed for a shorter period than 40 years, in some cases the 20-year segment and the entire timeseries may be of equal length. This can be checked from Appendix A, where the first and last observations used in this thesis have been listed for each source. The obtained PSD values over the 4 different monitoring periods for each source have been listed in Appendix B.

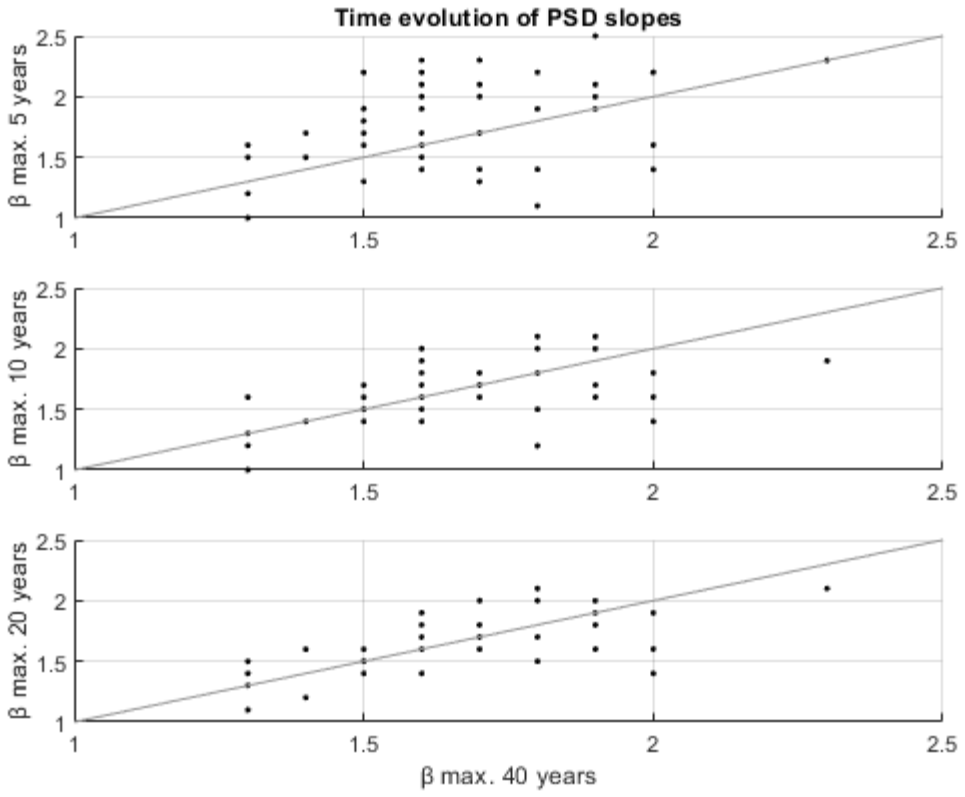

Figure 9: The figure shows three plots where the different shorter monitoring segments are compared to the entire timeseries.

The plots in Figure 9 show clear variations with some of the sources and the length of the timeseries appears to play a significant role in the results. Especially in the 5-year segment, the PSD slope indices are quite heavily distributed to the top half of the plot indicating that for some sources the values are steeper with shorter monitoring periods. This is expected because with longer timeseries also the flatter part of the spectrum in the low frequencies may be sampled. As more data is collected on longer time periods, one should expect the PSD-slope values to eventually remain the same given the underlying power law is chosen correctly. Naturally, this assumes that the timeseries is sufficiently stationary, and it is also a requirement for the PSD analysis to be meaningful. It must also be considered that the sampling density differs between sources and its effect is enhanced with shorter monitoring periods.

The results imply that a 10-year monitoring period may sometimes be long enough to reveal a characteristic timescale in the 37 GHz frequency. However, this is probably not the case for all sources, whose behavior seem to have considerably changed between the 20- and 40-year segments. **PKS0735+17** has an estimated index $\beta = 2.0^{+0.1}_{-0.1}$ for the entire monitoring period but only an index $\beta = 1.4 - 1.5$ for all three other periods. This is due to the large flare between 1985 and 1995, which

is outside the analyzed shorter epochs but dominates the entire timeseries in the lack of presence of any other flares. Had the analysis been made on the segment starting from 1985-1990, the slope values would have been steeper in the shorter segments. Figure 10 shows the entire flux density curve of PKS0735+17.

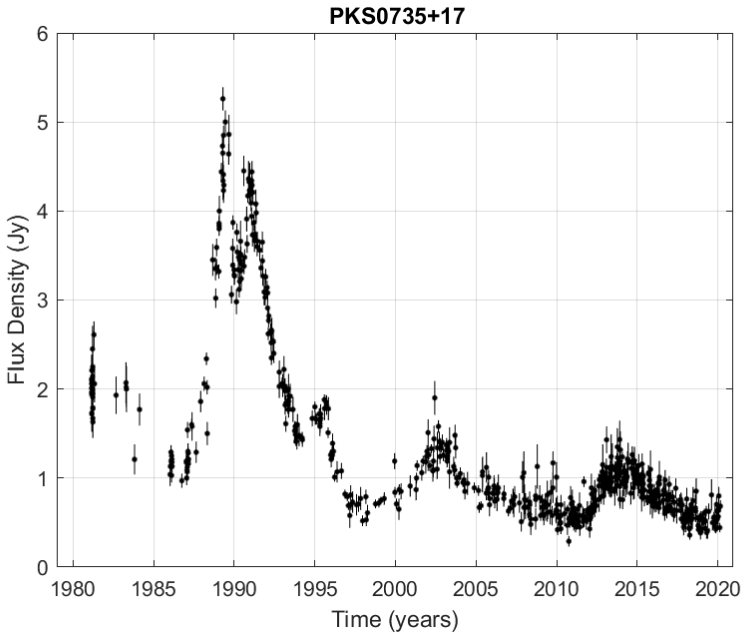

Figure 10: The flux density curve of PKS0735+17 shows a large dominant flare lasting almost 10 years during 1987-1995.

PKS0735+17 shows well why long monitoring periods are needed; the behavior of the source is clearly different before and after the year 2000. While this type of change in the light curve seems to argue against the stationarity requirement, a stationary process may generate non-stationary timeseries as was explained by Vaughan et al. (2003) and discussed in Chapter 2. Therefore, the stationarity cannot be directly evaluated from these results without further analyses and it seems likely that an even longer monitoring period is required to reveal any characteristic timescales.

Some other sources show similar phenomena as well. **0552+398** has a large flare at the beginning of the timeseries displaying the same effects in the PSD values as PKS0735+17. With **4C38.41** the chosen 5-year segment occurs during a relatively featureless period in the light curve, but all the longer segments display steeper PSD slopes due to a number of strong flares.

3C454.3 is an example of a source, whose behavior has clearly changed upon visual examination. The change in the behavior started in 2005 and continues to be different from the monitoring segment before it. Figure 11 shows the flux density curve of 3C454.3.

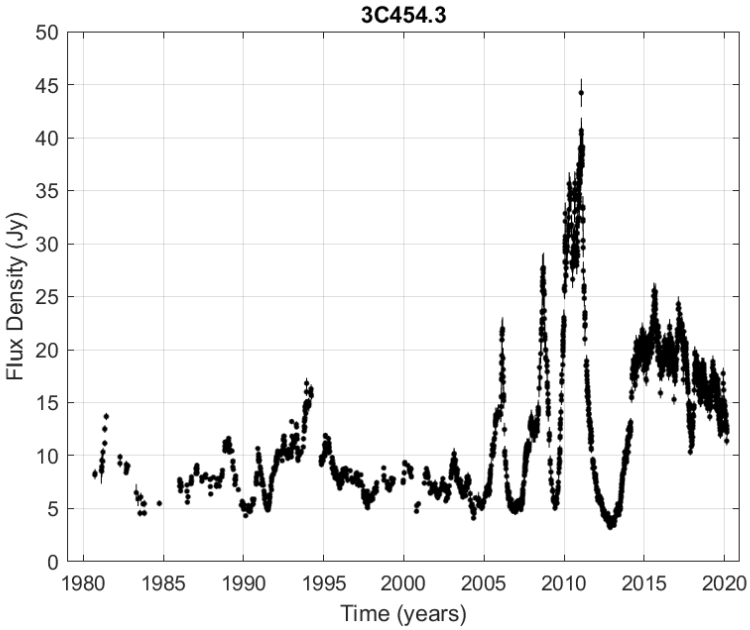

Figure 11: The flux density curve of 3C454.3 clearly shows, how the behavior of the source has changed starting from three large consecutive flares.

It is possible that only some of the sources are adequately stationary to have PSD analysis performed on their entire light curve. A flattening of the PSD slope index β, when compared to shorter monitoring periods (sometimes possibly shorter than 5 years), may indicate that a break frequency exists within the observing period. Sources which exhibit clear changes in behavior, and as such unexpected results in the PSD slope indices, may need to be analyzed in a different manner but at least their monitoring period needs to be longer before any conclusions can be made. In future studies, the stationarity of long-term AGN data should be analyzed further.

4.1.2 Hann window

Apart from clear statistics-related reasons, the difference in the results may be caused by the use of the Hann window. The benefits of the Hann window were introduced by Max-Moerbeck et al. (2014) as they demonstrated the difficulty in obtaining an upper confidence level for their PSD values, when using a simple rectangular window. While both Max-Moerbeck et al. (2014) and Kiehlmann (2015) used the Hann window, e.g., Chatterjee et al. (2008) did not. To test, how the periodogram of 3C279 radio data may have been affected by the Hann window, a segment of 3C279 data was taken from the same time period 1996-2007 as in their study. Although the Chatterjee et al. (2008) data was observed in the 14 GHz

frequency, it should be adequately similar to 37 GHz data for the sake of this demonstration.

After running N = 1000 simulations without the Hann window, 3C279 had a best-fit slope value of $\beta = 2.1$ with an undefined upper limit. With the Hann window, the corresponding slope value was $\beta = 1.9$ with well-defined upper and lower limits. Chatterjee et al. reported $\beta = 2.3^{-0.5}_{+0.5}$. While both slope values are within the estimated confidence bounds, clearly the use of the Hann window gives a flatter slope estimate. This test was repeated for the whole sample in order to see how significantly the Hann window affects the results.

For most sources, using a simple rectangular window caused the upper confidence limit to be undefined and the overall slope estimate to be steeper. Mostly, the Hann windowed results were within the lower confidence limit given by the non-Hann windowed result as may be expected. Figure 12 shows an example when Hann window is and is not used. The plots show very clearly the flattening effect caused by the rectangular window when no side-lobe minimization is done.

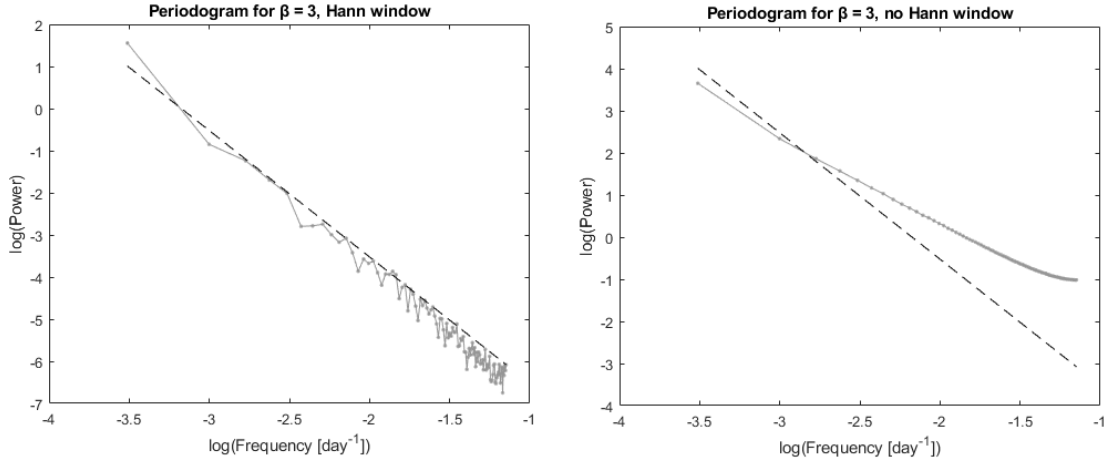

Figure 12: The periodograms for simulated data with even sampling and red-noise leakage. On the right the periodogram of the data and on the left the periodogram of the data multiplied with a Hann window. The black dashed line shows the expected slope of the periodogram.

4.1.3 Comparison with earlier estimates

The sample was also tested for data until 03.08.2013, which is the same sample as Ramakrishnan et al. (2015) used. For unknown reasons, most of the slope values were quite different; however, some were more similar. During e-mail exchange (Ramakrishnan 2020, private communication), it was discussed that finding the same slope values would be very difficult and different interpolation methods and bin sizes would have to be trialed. For this reason, cubic spline interpolation was

tried alongside linear interpolation. However, no major differences in the slope values were found between the two interpolation methods. Subtracting the mean from the data as well as applying detrending did not seem to affect the results.

While the results differed for unknown, possibly method-related reasons, some similar results were found from literature. Park & Trippe (2014) analyzed radio data for the sources 3C279, 3C345, 3C446, and BLLAC. Their best-fit slope values for the 14.5 GHz data were very similar to the results in this thesis, though the index for 3C345 deviated more. Their data was also from a very long time period of 32 years. The results are shown side-by-side with the results from this thesis in Table 2.

Table 2: β_{PT} shows the results by Park & Trippe (2014) and β the results from the analyses of this thesis with their 68.3% confidence levels.

Source	$\boldsymbol{\beta_{PT}}$	$\boldsymbol{\beta}$
3C279	1.45	$1.6^{-0.1}_{+0.1}$
3C345	2.54	$1.9^{-0.1}_{+0.1}$
3C446	1.79	$1.8^{-0.0}_{+0.0}$
BLLAC	1.62	$1.7^{-0.1}_{+0.1}$

The results were also compared to the results in Max-Moerbeck Astudillo (2013). For the same monitoring period, the results for the common sources were quite similar although the frequency in the analyses were 15 GHz (OVRO) and 14.5 GHz (UMRAO). There were some larger deviations as well, but upon inspecting the light curves of both data, they seemed to be well explained by the nature of the observed light curves, i.e., smoother variations in case of a steeper slope indices.

The estimation of the PSD is a volatile process especially when unevenly sampled light curves are analyzed. Small errors or simple differences in e.g., normalization may result in different slope values. While the written code was tested rigorously and different additional methods such as the effects of detrending were analyzed, the results should be confirmed through further analysis including investigation on the effects of heavy interpolation. During testing it became clear that differences of e.g., +-0.4 in the slope values can occur simply due to the uncertain nature of the periodogram and possibly heavy interpolation. One such example with the sampling of 0234+285 is plotted in Figure 13. Gaussian-distributed data was generated with the TK95 method based on the sampling of 0234+285. The generated light curve was then used as the observed light curve and the PSD fit procedure was run based on that data with a known $\beta = 2.1$. The results showed that occasionally the periodogram was further away from the actual PSD slope and sometimes it was fitted perfectly.

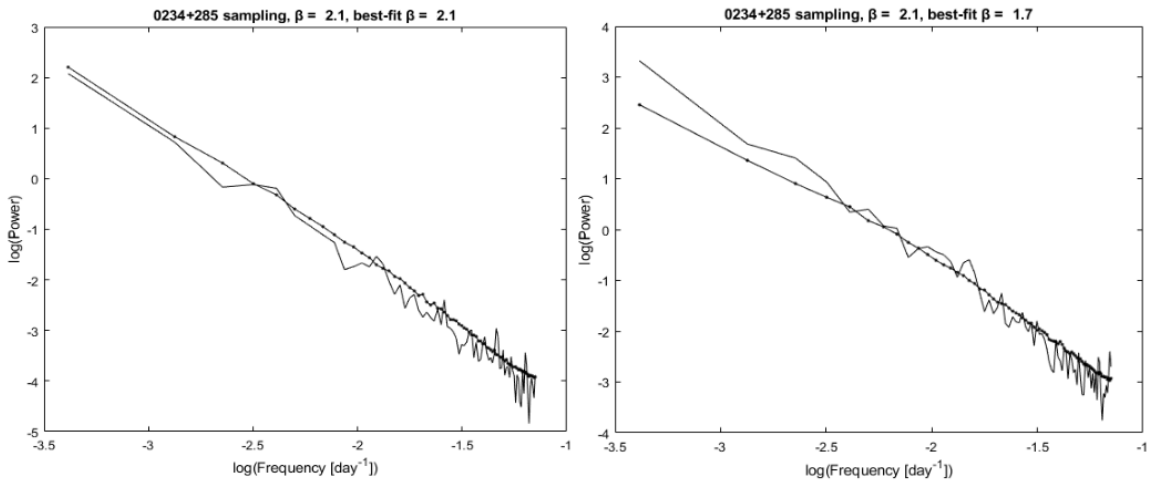

Figure 13: Examples of the periodograms of randomly simulated Gaussian light curves with the sampling of 0234+285.

However, even if there were a method-related inconsistency compared to previous work, the method is consistent in comparing the results between sources and between different epochs. The comparison between epochs showed that often-times short-term data is only weakly stationary, and the correct underlying noise process can not yet be defined. Even in situations where it can later be confirmed that the behavior has remained the same throughout the observing epochs, long monitoring periods are needed to verify it.

Because the PSD estimation requires care and any features may be smoothed out in the binned and windowed periodogram, other methods are required to assess the underlying reasons for the results.

4.2 Lomb-Scargle periodogram

The LS-periodogram analysis revealed that 64 sources deviated from the null hypothesis. The null hypothesis was that the observed data originates from an approximately red-noise process with a simple power law. If a clear deviation occurs when compared to the 3σ-confidence level given by the Monte Carlo simulations, then there is a chance that the null hypothesis can be rejected. A deviation may signify a periodicity or a quasiperiodicity in the light curve, but it can also be an indication that the simple power law used is not an adequate approximation of the underlying noise process. The LS periodogram should be able to give some indications on whether the observed light curve may have a break at some frequency, though care must be taken when analyzing noisy periodograms.

Table 3 lists all the sources, whose LS periodogram had deviations exceeding the 3σ-levels in their estimated spectrums. The table also lists the maximum timescales of these deviations i.e., the most low-frequency peak exceeding the significance level.

If the deviations only occurred in the noisy most high-frequency part of the spectrum, they were not considered to definitively be against the null hypothesis and such sources are not listed in the table. The reasons for this will be explained later in this section.

Table 3: The table lists the sources, whose LS periodograms had at least one peak against the null hypothesis at the 3σ-level. The maximum timescale T_{max} is given in years. The column 'S/M' tells, whether the peak had 1-2 peaks (singular, S) or over 2 peaks (multiple, M).

Source	T_{max}	S/M		Source	T_{max}	S/M
PG0007+106	5.39	M		ON231	0.8	S
0048-097	1.98	S		PKS1222+216	3.89	S
0059+581	3.17	M		3C273	0.85	S
0106+013	5.78	S		3C345	1.75	M
S20109+22	2.53	M		1308+326	9.75	S
0133+476	3.91	M		1324+224	1.46	S
0212+735	1.25	S		OQ530	8.64	M
0224+671	1.92	S		PKS1502+106	3.20	M
0234+285	3.25	M		PKS1510-089	3.69	M
0235+164	2.3	M		4C14.60	1.42	S
0238-084	5.06	S		1546+027	3.01	S
3C84	0.53	M		DA406	9.79	S
0333+321	6.98	S		4C38.41	4.0	M
CTA026	4.87	S		1637+574	2.73	S
0415+379	3.13	M		1642+690	3.64	S
0420-014	9.01	M		PKS1725+044	1.2	S
3C120	3.12	M		1730-130	1.0	S
PKS0446+112	2.08	S		S41739+52	1.13	S
NRAO190	1.57	S		1741-038	8.0	S
0528+134	2.77	S		PKS1749+096	2.29	M
0552+398	1.0	S		1828+487	2.3	S
0716+714	1.0	M		PKS2022-077	2.09	S
0736+017	2.73	M		PKS2032+107	1.75	S
0754+100	6.2	M		2037+511	6.2	S
0814+425	11.56	S		2131-021	4.54	S
OJ248	2.51	M		2134+004	1.0	S
0836+710	4.89	S		2144+092	2.93	S
OJ287	1.77	M		BLLAC	8.5	M
0953+254	5.5	M		2201+315	3.0	S
1055+018	2.44	S		2216-038	3.44	S
1150+497	1.41	S		2230+114	3.9	M
4C29.45	3.88	M		3C454.3	5.44	M

A total of 64 sources had at least 1 peak in the lower frequency part of the spectrum exceeding the 3σ-level of the null hypothesis. Such sources, that have 'M' listed in the third column, had especially clear multiple deviations from the simulated spectrum. Some of the sources marked 'S' had quite significant spikes exceeding the confidence level, and some only by a small margin. The mean timescale was $T_{max} =$ 3.7 years.

Figure 14 shows the plots for some of the sources, which had significant-looking LS periodograms supporting a break/bend in the spectrum. As was hypothesized already when analyzing the PSD slopes and their differences between different epochs, the LS periodograms of these sources give further indications that a simple power law may not be a sufficient estimation for their underlying noise processes.

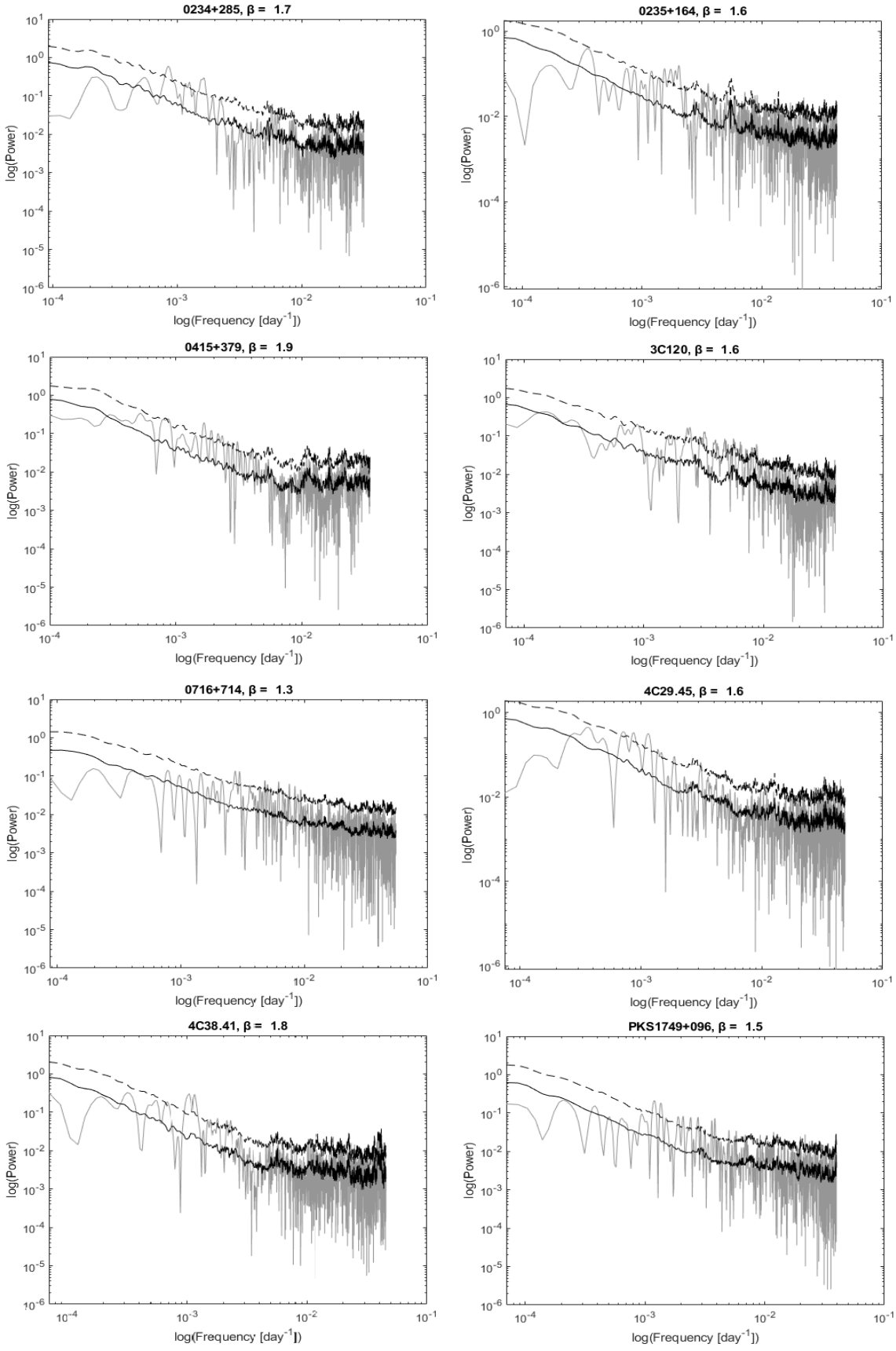
0234+285, β = 1.7
0235+164, β = 1.6
0415+379, β = 1.9
3C120, β = 1.6
0716+714, β = 1.3
4C29.45, β = 1.6
4C38.41, β = 1.8
PKS1749+096, β = 1.5
log(Power)
log(Frequency [day^{-1}])

Figure 14: The LS periodograms for some of the sources, which clearly deviated from the null hypothesis of a simple power law.

In Figure 14 it can be seen how the Monte Carlo simulations are able to mimic the effects and spurious peaks caused by uneven sampling and spectral distortions. While the results have not been binned resulting in somewhat erratic plots, the overall shapes can be fairly well estimated from the data. The LS periodograms of the observed data do not follow the simulations well indicating that the null hypothesis can be rejected at high confidence level.

The results indicate that the simple power law is not a good estimator of the underlying power spectral model for many of the sources. Especially the well-sampled sources with multiple deviations should be good candidates for breaks/bends in the power spectrum and many of the LS periodograms display such behavior. While individual spikes can be statistical fluctuations caused by the spurious window transform of the LS periodogram, if they are visible also in the DCF, they can be considered to give further confidence for the rejection of the null hypothesis.

PKS0735+17 was discussed in the previous section as a source, whose characteristic timescale most likely requires a longer monitoring period to be revealed. This is also suggested by the LS periodogram, which well follows the null hypothesis of a simple power-law. **3C454.3** on the other hand had some deviations from the null hypothesis, but given the clearly peculiar behavior of the source, it may also indicate that sufficient stationarity is not achieved for valid power spectral analysis. The LS periodograms of both sources are shown in Figure 15.

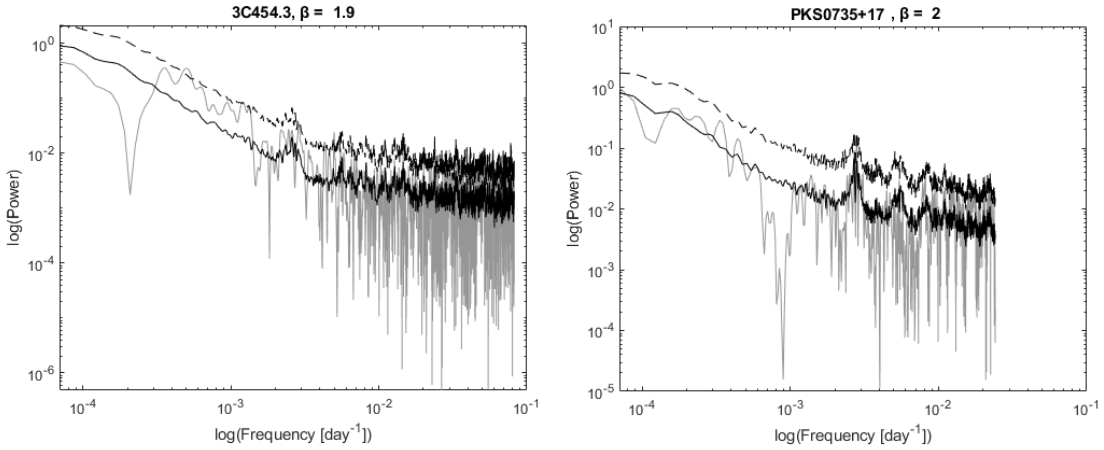

Figure 15: The LS periodograms of 3C454.3 and PKS0735+17. 3C454.3 has some deviations from the null hypothesis, but PKS0735+17 gives a fairly good fit to the simple power law.

Periodicities and quasiperiodicities

Because the underlying noise process does not appear to be adequately described by the power law, detecting any periodicities and quasiperiodicities from the data is very difficult. Visually, **PG0007+106** was the only candidate for a periodicity or a quasiperiodicity with a 5.5 year interval and a 3σ confidence. This behavior is visible in the light curve of the source with flares occurring throughout the monitoring period with an apparent similar interval. From other sources such behavior was very difficult to estimate without first characterizing the underlying noise process correctly and thus allowing proper simulations for the confidence intervals. The light curve of PG0007+106 is plotted in Figure 16.

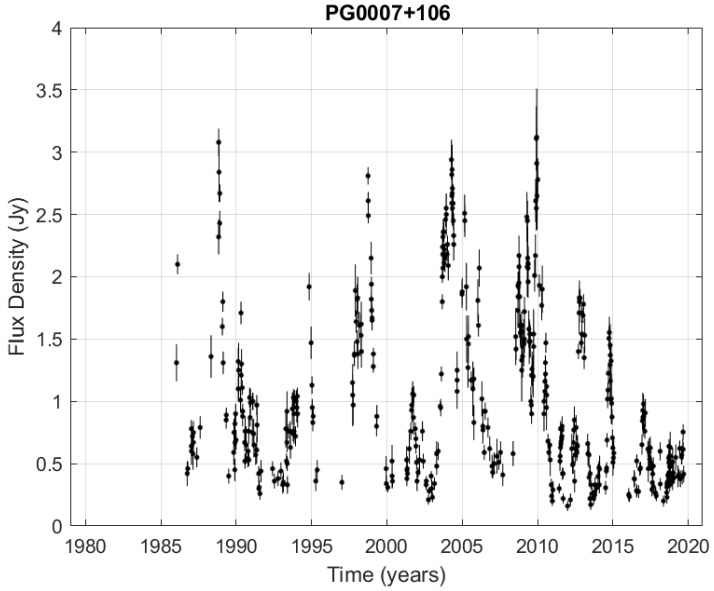

Figure 16: The light curve of PG007+106 shows apparent near-periodic flaring,

4.2.1 Comparison with shorter monitoring period lengths

To see if the simple power law seemed to be a good fit for shorter monitoring periods, LS periodograms were generated for 5 years of data between 2008-2013 with the estimated PSD slope for that monitoring period.

The results showed the hypothesized phenomenon well; for multiple sources the simple power law appeared to be a decent fit for the 5-year segments, but after longer monitoring periods the observations started to deviate. Figures 17, 18, and 19 show the LS periodograms of **0234+285**, **0235+164**, and **OJ248** with both 5 and 25-40 years of data.

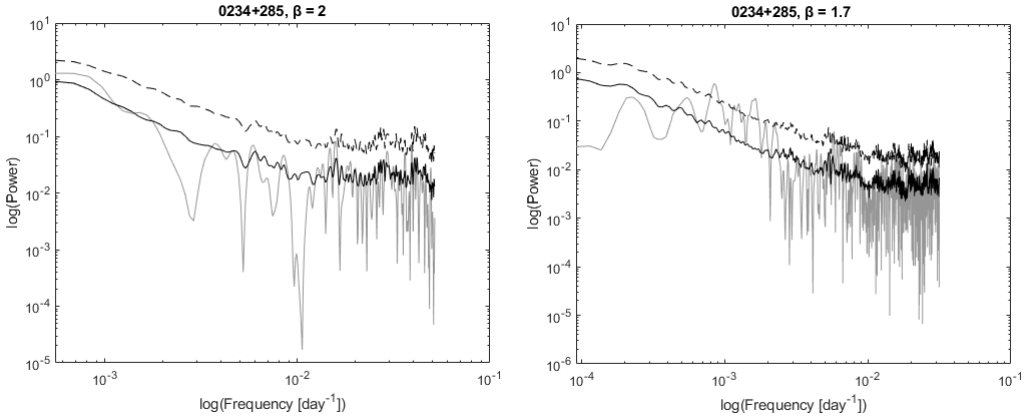

Figure 17: The LS periodograms for 0234+285 with the 5-year segment on the left side and the entire monitoring period of 30 years on the right side.

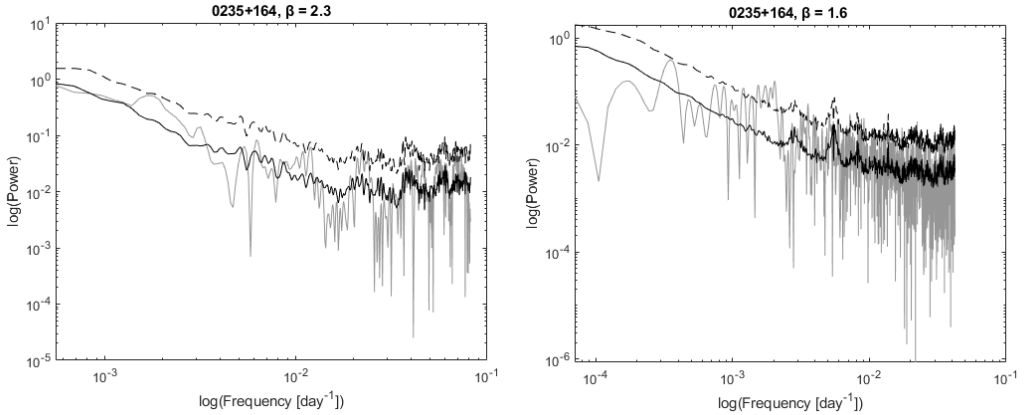

Figure 18: The LS periodograms for 0235+164 with the 5-year segment on the left side and the entire monitoring period of 40 years on the right side.

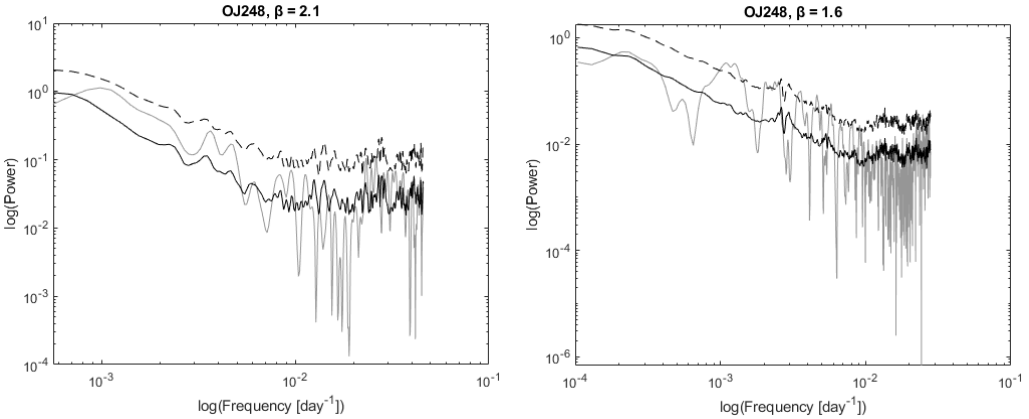

Figure 19: The LS periodograms for OJ248 with the 5-year segment on the left side and the entire monitoring period of 25 years on the right side.

There were also sources, such as PKS0735+17, that showed a decent fit with the simple power law for all monitoring periods (5, 10, 20, and 40 years) even when the shorter segments were chosen from varying temporal locations.

While many sources showed a decent fit with the simple power law for short monitoring periods, the LS periodograms of some sources deviated from the null hypothesis. Figure 20 shows the LS periodograms of **0716+714** for both the 5-year segment and the entire monitoring period of 30 years. Already the 5-year period shows small deviations at 3σ significance. A potential reason could be e.g., a break in the power spectrum at a higher frequency than for some of the other sources. Again, this is something that needs to be simulated further before making any definitive conclusions.

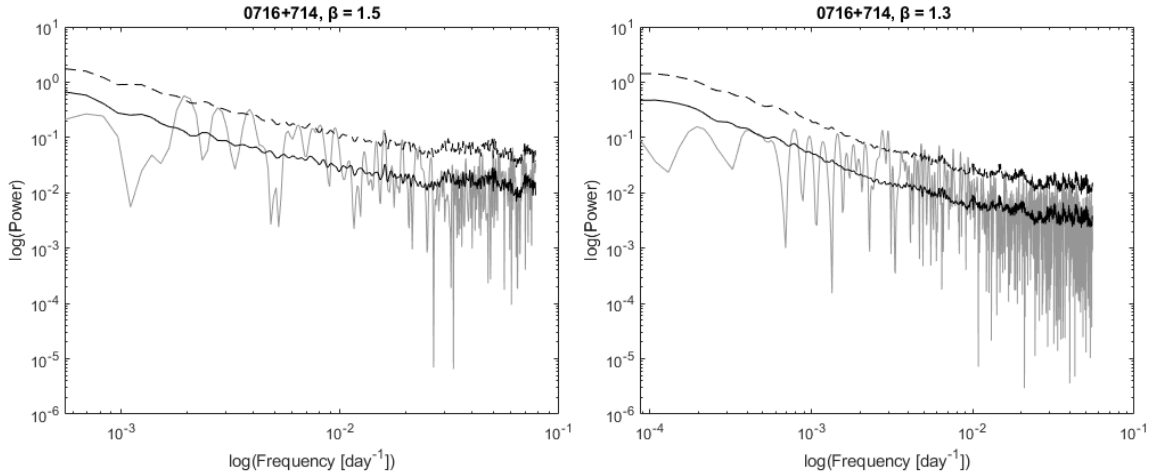

Figure 20: The LS periodograms for 0716+714 with the 5-year segment on the left side and the entire monitoring period of 30 years on the right side.

4.2.2 Encountered difficulties

The initial results from the Lomb-Scargle periodograms were very noisy. This is a known issue with the LS periodogram (e.g., VanderPlas, 2018) due to the fact that the window function is unpredictable as discussed in Chapter 2. From the noisy periodograms it was difficult to determine all timescales as especially the higher frequencies clearly suffered from these effects. While Monte Carlo simulations are able to mimic the effects of sampling, red-noise leak, and aliasing, averaging the simulations seemed to cause their noisiness to flatten out. Therefore, many very high frequencies surpassed the 3σ-limit with a small margin.

To alleviate this issue, monthly averaging of the observed data was attempted as it should help in smoothing out the noisiness and aliasing effects; monthly averaging was also used by Park & Trippe (2014). Binning the periodogram is another possibility and it is usually done with the original periodogram; however, during

tests it appeared to smoothen the spectrum too much and it did not seem suitable for determining timescales, especially periodicities and quasiperiodicities, from the data.

Although monthly averaging gave some help to the noisy high-frequency part, it did not completely eliminate the issue. Also, the binning of the periodogram needs to be studied further for unevenly sampled data as it may be necessary for proper estimations. For the analyses in this thesis, the light curves or the periodograms were not binned, but instead the high frequency part was considered unreliable in estimating the goodness-of-fit. A possibly similar effect was seen in the structure functions discussed in the next chapter. Hughes et al. (1992) deemed this high-frequency plateau to be caused by observational noise and this noisiness was visible in some of the individual structure functions, but smoothened out in the averaged structure function. In future studies this issue should be better considered; however, because in this thesis the overall shape of the power spectrum was of more interest, and the high frequencies are in any case flattened due to aliasing and red-noise leak, the noisy high-frequency part of the spectrum was not considered in the analyses.

4.3 Structure function

From the sample, 55 sources were sampled well-enough with long-enough timeseries to reveal apparent timescales in the structure functions. To best see which features in the structure functions were caused by the length of the timeseries and uneven sampling, Monte Carlo simulations were used to estimate an average structure function for the best-fit PSD and PDF. $N = 100$ light curves were simulated for each source with the EMM13 algorithm and their SFs were generated. From the results, the mean SF and corresponding 1σ-, 2σ -, and 3σ -limits were calculated. These were then plotted with the structure function of the observed data to see how the data fit the simulations.

Because the SFs from the simulations were averaged, the possibly noisy data points were smoothed out much like in the case of the LS periodogram. Therefore, mostly the power-law portion of the SF and the plateau following it were of interest similarly to Hughes et al. (1992). Particularly, it was analyzed how well the power-law portions matched the averaged simulated SFs.

The manually fitted SF slope parameters and timescales are listed in Table 4 for the 55 sources, which had a decently structured structure function. The average values were $\alpha = 1.03$ and $T_{min} = 1.56$ years. The average SF slope is consistent with a red noise process.

Table 4: The obtained timescales, SF slopes and timescale significances for 55 sources. The light curves were not detrended.

Source	α	$T_{min}\,(years)$		Source	α	$T_{min}\,(years)$
NRAO5	–	2.41		1055+018	$0.94^{-0.05}_{+0.05}$	0.96
PG0007+106	$1.28^{-0.07}_{+0.07}$	0.34		4C29.45	$1.09^{-0.06}_{+0.06}$	1.21
0059+581	$1.15^{-0.12}_{+0.12}$	0.68		3C273	$1.22^{-0.04}_{+0.04.}$	1.36
0106+013	$0.86^{-0.05}_{+0.05}$	2.71		3C279	$0.98^{-0.03}_{+0.03}$	2.71
S20109+22	$0.95^{-0.11}_{+0.11}$	0.86		PKS1222+216	$0.85^{-0.04}_{+0.04}$	1.92
0133+476	$0.88^{-0.04}_{+0.04}$	1.52		1308+326	$0.97^{-0.07}_{+0.07}$	3.41
0149+218	$0.95^{-0.09}_{+0.09}$	1.71		1324+224	$0.82^{-0.19}_{+0.19}$	0.76
0224+671	$0.41^{-0.16}_{+0.16}$	1.36		1334-127	$0.84^{-0.08}_{+0.08}$	1.36
0234+285	$1.13^{-0.11}_{+0.11}$	0.76		PKS1413+135	$0.85^{-0.1}_{+0.1}$	2.41
0235+164	$1.4^{-0.16}_{+0.16}$	0.76		OQ530	$1.32^{-0.47}_{+0.47}$	0.68
0238-084	$0.79^{-0.14}_{+0.14}$	2.41		PKS1502+106	$0.99^{-0.07}_{+0.07}$	3.04
0333+321	$1.02^{-0.05}_{+0.05}$	2.15		PKS1510-089	$1.28^{-0.09}_{+0.09}$	0.54
CTA026	$1.06^{-0.07}_{+0.07}$	0.68		1546+027	$1.26^{-0.15}_{+0.15}$	1.71
0355+508	$1.19^{-0.04}_{+0.04}$	1.52		DA406	$0.93^{-0.03}_{+0.03}$	3.41
0415+379	$1.23^{-0.19}_{+0.19}$	0.54		1637+574	$0.84^{-0.09}_{+0.09}$	1.21
0420-014	$1.19^{-0.07}_{+0.07}$	1.52		4C38.41	$1.2^{-0.05}_{+0.05}$	0.96
3C120	$0.98^{-0.21}_{+0.21}$	0.24		3C345	$1.21^{-0.06}_{+0.06}$	1.92
0528+134	$1.0^{-0.05}_{+0.05}$	2.15		1642+690	$1.03^{-0.24}_{+0.24}$	1.08
PKS0605-085	$1.45^{-0.26}_{+0.26}$	2.45		1741-038	$0.93^{-0.04}_{+0.04}$	1.71
0716+714	–	0.48		PKS1749+096	$1.3^{-0.11}_{+0.11}$	0.68
0736+017	$0.86^{-0.12}_{+0.12}$	0.48		2005+403	$1.2^{-0.06}_{+0.06}$	3.41
0754+100	$0.71^{-0.16}_{+0.16}$	1.08		2037+511	$1.05^{-0.13}_{+0.13}$	2.41
0804+499	$0.92^{-0.21}_{+0.21}$	0.43		2131-021	$0.51^{-0.14}_{+0.14}$	1.71
OJ248	$1.13^{-0.12}_{+0.12}$	0.48		2201+171	$0.79^{-0.23}_{+0.23}$	1.21
OJ287	$1.12^{-0.07}_{+0.07}$	0.34		BLLAC	$0.86^{-0.11}_{+0.11}$	3.41
0836+710	$0.61^{-0.07}_{+0.07}$	1.21		3C446	$1.2^{-0.04}_{+0.04}$	3.41
0917+449	$1.66^{-0.27}_{+0.27}$	2.15		3C454.3	$1.12^{-0.07}_{+0.07}$	1.71
0953+254	$1.09^{-0.28}_{+0.28}$	1.52				

The confidence level determination was not as straight-forward as it was with the LS periodogram. Because the structure function of the observed data may vary quite significantly from the simulated data, it is possible that the fit is good for part of the structure function and in such cases the significance levels may show a good fit for the apparent timescale even if it at some point moves towards a negative confidence level. For this reason, also sources which had a clear apparent break within the confidence levels have been listed. If the entire structure function showed a good fit, apart from the noisy high-frequency section and/or only an insignificant break appeared within the confidence levels, then no results have been listed. Figure 21 shows an example of a source, **PKS1413+135**, which initially follows the simulations well but then starts to deviate while the apparent break-timescale is still within the confidence level. Detrending the data shifted the break to log(2.0) and made the deviation significant; however, the timescale location remained the same. The light curve of PKS1413+135 does show a linear trend as the timeseries begins

with a large flare and gradually shifts towards lower overall flux. However, since the data is unevenly sampled, the used intrinsic Matlab function 'detrend' was not optimal and therefore was not used here.

Figure 22 shows the structure function of **3C345**. A clear slope is visible at a timescale of $T = 1.91$ years approximately at the 2σ-confidence limit. Figure 23 shows the structure function of **1741-038**, which shows only a 1σ deviation from the simulations.

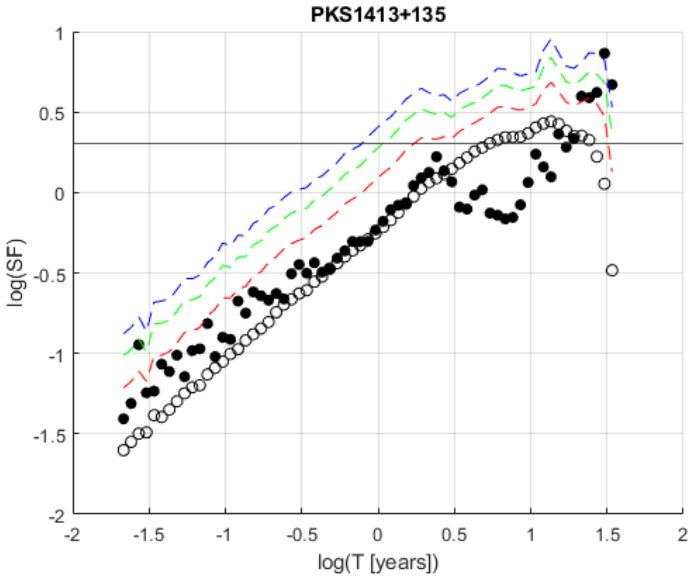

Figure 21: The structure function of PKS1413+135 (filled) with the simulated SF plotted as non-filled circles and the positive confidence levels as 3σ = blue, 2σ = green, and 1σ = red.

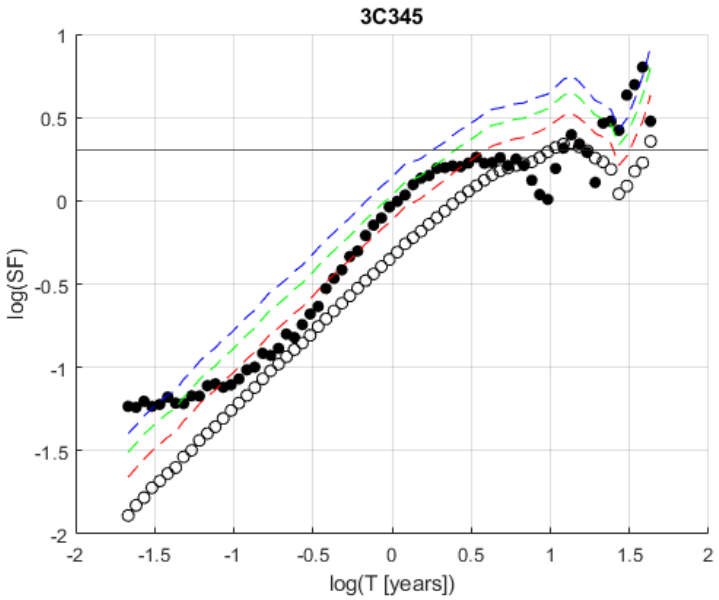

Figure 22: The structure function of 3C345 (filled) with the simulated SF plotted as non-filled circles and the positive confidence levels as 3σ = blue, 2σ = green, and 1σ = red.

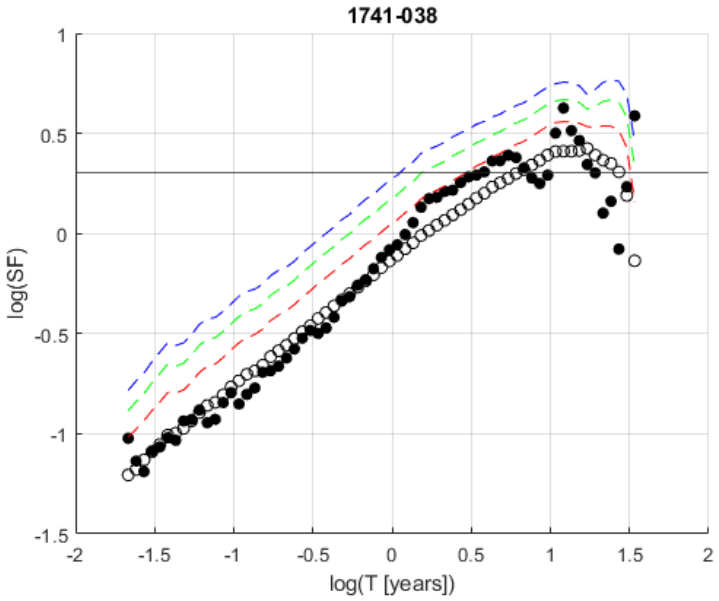

Figure 23: The structure function of 1741-038 (filled) with the simulated SF plotted as non-filled circles and the positive confidence levels as 3σ = blue, 2σ = green, and 1σ = red.

Some of the SFs were fairly well approximated by the simulations; however, many of them deviated significantly. The deviations may be caused by different types of timescales including a periodicity or a quasiperiodicity. Significant consecutive flares may be seen as timescales both in the SF as well as in the LS periodogram, and DCF. Also, a poorly sampled light curve has a very erratic SF, which makes its analysis very difficult. The characteristic timescale caused by a break/bend in the power spectrum would be also seen as a plateau in the structure function. Hughes et al. (1992) consider this to be the point at which correlated behavior shifts to uncorrelated behavior.

A strong linear trend may be visible in the structure functions as T^2 (Hughes et al., 1992), which is likely the reason for some of the shifts making some clear plateaus seemingly insignificant. Although it should usually not be of great concern in long-term data, this naturally depends on whether the data can actually be considered long-term. Because Table 4 lists such cases also, using no detrending in the simulations should not have greatly affected the overall results. In future studies the effects of detrending should be explored further.

4.3.1 Comparison with the PSD best-fit values

According to Emmanoulopoulos et al. (2010) PSD and SF values have a relation of

$$\beta = \alpha + 1 \tag{11}$$

when the following requirements are fulfilled:

i) Stationarity
ii) Zero-mean dataset
iii) Frequency range $0\ to\ \infty$
iv) PSD is given from a power-law form with index $1 < \beta < 3$

To ensure approximately zero-mean datasets, the mean of the light curves were subtracted from the data. Because the frequency range is limited by the length of the monitoring period, the assumption was made that the lengths of these timeseries were long enough to mimic the entire frequency range. This is also in relation to the stationarity requirement, which states that the observed data must be a good representation of the true behavior of the source. Since the data is over a long monitoring period and it has showed some signs of flattening in the PSD analysis, requirement iv) may not be fulfilled unless only the power-law portion of the structure function is considered. Emmanoulopoulos et al. (2010) state that trying to relate the PSD and SF slopes originating from a broken power-law process may lead

to misconceptions about the true underlying process. This must be considered when analyzing the results.

First, to test how the SF slopes and PSD slopes compare, linear least-squares fitting was applied to the averaged structure function from $N = 50$ Monte Carlo simulated light curves with the best-fit PSD. The test was done to five different sources to see how the relation (11) holds. Table 5 shows the results of the test.

Table 5: The table shows the best-fit values for the simulated SF slopes with 95% fit-confidences. The second column lists the values when the fitting was stopped at log(2.0) and the third column the values when the entire structure function was considered. The fourth column shows the corresponding PSD-slope values and their estimated 68.3% confidence intervals.

Source	$\alpha_{\log(2.0)}$	α_{all}	β
PG0007+106	$0.33^{-0.01}_{+0.01}$	$0.29^{-0.02}_{+0.02}$	$1.3^{-0.0}_{+0.0}$
0059+581	$0.73^{-0.02}_{+0.02}$	$0.61^{-0.04}_{+0.04}$	$1.7^{-0.1}_{+0.1}$
0235+164	$0.61^{-0.01}_{+0.01}$	$0.5^{-0.04}_{+0.04}$	$1.6^{-0.0}_{+0.0}$
3C273	$0.91^{-0.01}_{+0.01}$	$0.77^{-0.04}_{+0.04}$	$1.9^{-0.1}_{+0.1}$
3C279	$0.61^{-0.01}_{+0.01}$	$0.51^{-0.04}_{+0.04}$	$1.6^{-0.1}_{+0.1}$
1741-038	$0.61^{-0.01}_{+0.01}$	$0.50^{-0.04}_{+0.04}$	$1.6^{-0.0}_{+0.1}$
BLLAC	$0.72^{-0.01}_{+0.01}$	$0.55^{-0.09}_{+0.09}$	$1.7^{-0.1}_{+0.1}$

If the slope is calculated for the whole structure function, the slope values are slightly flatter than the estimated PSD best-fit indices would suggest. If the estimate is only made for the slope until log(2.0), the slope estimate is very accurate. This is most likely due to an apparent plateau described by Emmanoulopoulos et al. (2010), which is simply related to the length of the timeseries. The results give good support to the expected relation (11) in the case of a simple power law despite the low number of simulations.

To see how the relation holds with the observed data, some of the estimated SF slopes and PSD slopes were compared. It needs to be emphasized that since some of the PSD slope indices clearly change between the observing epochs, the stationarity requirement may not hold, but rather they are at best weakly stationary especially in the short monitoring segments (Vaughan et al., 2003). Thus, while the data was analyzed through different epochs, the PSD and SF slope relation may not be completely accurate. In addition, if the noise process is not of the simple power-law type, the requirements are not fulfilled.

The SF slopes were often steeper than the best-fit PSD slopes. An interesting phenomenon is that some of the estimated SF slopes were close to the PSD best-fit slopes gained from the analysis with 5-year data. The start and end points of the estimated SF slopes were chosen visually according to Hughes et al. (1992), which could hint to an explanation causing the differences between the results. In Figure 24 (**0059+581**) there is a clear slope visible after which a plateau asymptotes to

log(2.0). The slope value $\alpha = 1.11$ would convert to a PSD slope of $\beta = 2.16$. This value would be in accordance with the best-fit value of $\beta = 2.1^{-0.2}_{+0.2}$ for the 2008-2013 data. However, the value is unexpectedly steep compared to the value $\beta = 1.7^{-0.1}_{+0.1}$ for the entire timeseries. A similar effect was seen with some of the sources in Table 6.

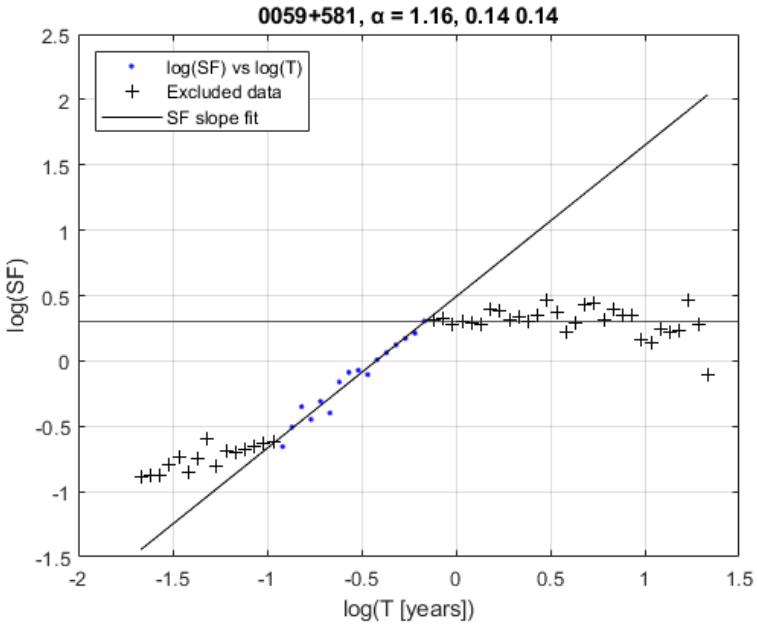

Figure 24: The structure function of 0059+581 with the best-fit slope $\alpha = 1.16$.

Table 6: The values for the SF slope α have their linear least-squares fit 95% confidence intervals included. The PSD-slope values β have their 68.3% confidence levels included. The confidence intervals for the SF slopes are only for the manually chosen power-law portions of the SFs. This means that the bias from manually selecting the most likely power-law part from the structure function exists independently and should be considered when these values are evaluated.

Source	α (2008-2013)	α	β (2008-2013)	β
PG0007+106	$1.44^{-0.21}_{+0.21}$	$1.28^{-0.07}_{+0.07}$	$1.6^{-0.1}_{+0.2}$	$1.3^{-0.0}_{+0.0}$
0059+581	$0.92^{-0.04}_{+0.04}$	$1.16^{-0.14}_{+0.14}$	$2.1^{-0.2}_{+0.2}$	$1.7^{-0.1}_{+0.1}$
0133+476	$0.89^{-0.06}_{+0.06}$	$0.88^{-0.04}_{+0.04}$	$1.9^{-0.1}_{+0.3}$	$1.6^{-0.0}_{+0.1}$
0234+285	$1.14^{-0.1}_{+0.1}$	$1.13^{-0.11}_{+0.11}$	$2.0^{-0.1}_{+0.2}$	$1.7^{-0.0}_{+0.1}$
0235+164	$1.18^{-0.12}_{+0.12}$	$1.4^{-0.16}_{+0.16}$	$2.3^{-0.2}_{+0.3}$	$1.6^{-0.0}_{+0.0}$
CTA026	$1.1^{-0.11}_{+0.11}$	$1.06^{-0.07}_{+0.07}$	$1.8^{-0.2}_{+0.3}$	$1.5^{-0.1}_{+0.2}$
0355+508	$1.29^{-0.05}_{+0.05}$	$1.27^{-0.04}_{+0.04}$	$2.3^{-0.2}_{+0.2}$	$1.7^{-0.1}_{+0.1}$
0415+379	$1.17^{-0.17}_{+0.17}$	$1.23^{-0.19}_{+0.19}$	$2.4^{-0.2}_{+0.3}$	$1.9^{-0.0}_{+0.0}$
0528+134	$1.43^{-0.09}_{+0.09}$	$1.0^{-0.05}_{+0.05}$	$2.2^{-0.1}_{+0.1}$	$2.0^{-0.1}_{+0.1}$

Source	α (2008-2013)	α	β (2008-2013)	β
OJ248	$1.52^{-0.19}_{+0.19}$	$1.13^{-0.12}_{+0.12}$	$2.1^{-0.0}_{+0.1}$	$1.6^{-0.1}_{+0.2}$
3C273	$1.11^{-0.07}_{+0.07}$	$1.24^{-0.05}_{+0.05}$	$2.1^{-0.0}_{+0.1}$	$1.9^{-0.1}_{+0.1}$
3C279	$1.25^{-0.05}_{+0.05}$	$0.98^{-0.03}_{+0.03}$	$2.2^{-0.1}_{+0.1}$	$1.6^{-0.1}_{+0.0}$
PKS1510-089	$1.51^{-0.16}_{+0.16}$	$1.28^{-0.09}_{+0.09}$	$1.7^{-0.2}_{+0.2}$	$1.5^{-0.1}_{+0.1}$
DA406	$1.24^{-0.11}_{+0.11}$	$0.93^{-0.03}_{+0.03}$	$2.1^{-0.1}_{+0.1}$	$1.6^{-0.1}_{+0.2}$
1741-038	$1.13^{-0.13}_{+0.13}$	$0.94^{-0.04}_{+0.04}$	$1.9^{-0.2}_{+0.2}$	$1.6^{-0.0}_{+0.1}$
PKS1749+096	$1.4^{-0.14}_{+0.14}$	$1.3^{-0.11}_{+0.11}$	$1.9^{-0.2}_{+0.2}$	$1.5^{-0.0}_{+0.0}$
2230+114	$1.37^{-0.17}_{+0.17}$	$0.75^{-0.05}_{+0.05}$	$2.2^{-0.3}_{+0.2}$	$1.5^{-0.0}_{+0.0}$
3C446	$1.54^{-0.1}_{+0.1}$	$1.2^{-0.06}_{+0.06}$	$2.2^{-0.1}_{+0.2}$	$1.8^{-0.0}_{+0.0}$

A logical explanation would be a frequency bend/break as has been discussed. Because the SF-slope values were gained from manually fitting a line to the power law-like portion of the plots, a timescale caused by a physical break in the frequency could explain the effects seen with some sources. A 5-year period of radio data may only sample the steep part of the spectrum, which would be seen as a steeper best-fit value for the PSD-slope values. Because the plateau is not considered in the calculation of the SF slope, such flattening might not be visible in the SF-slope value. This type of timescale only visible in the longer monitoring period data would be similar to what Hughes et al. (1992) describe as a shift from correlated behavior to uncorrelated behavior.

3C273: In the structure functions of 3C273 (Figure 25) the slopes have remained similar between the 5-year and 40-year segments. Noteworthy is the clear flattening of the slope towards an index of $\alpha \approx 0$ after the linear least-squares fit in the right-side figure. The PSD indices of 3C273 have shifted from $\beta = 2.1^{-0.0}_{+0.1}$ (2008-2013) to the current $\beta = 1.9^{-0.1}_{+0.1}$. While the difference between the indices is small and the confidence-limit determination was less than ideal, there is a clear structural change in the structure function indicating the existence of a timescale. The nonconformity of the break was further tested via Monte Carlo simulations which show that the break is not consistent with the best-fit $\beta = 1.9^{-0.1}_{+0.1}$ simple power-law within the 2σ confidence level.

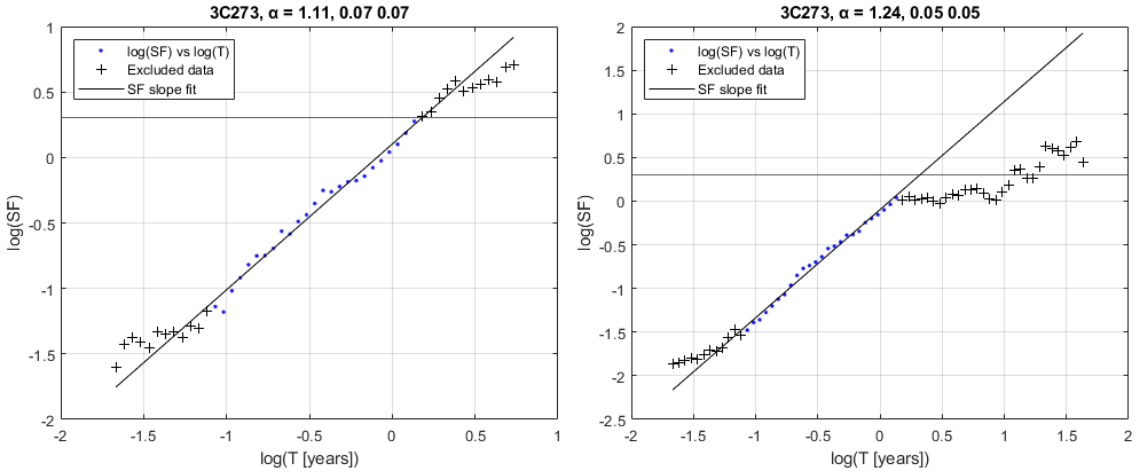

Figure 25: On the left side the structure function of 3C273 with data between 2008-2013 and on the right side with the entire timeseries 1979-2020.

0355+508: In 0355+508 the results show a similar effect as in 3C273 and support the hypothesis of a break/bend in the power spectrum (Figure 26). The manually fitted SF-slope values for the entire timeseries are $\alpha = 1.27^{-0.04}_{+0.04}$ and for the 2008-2013 segment $\alpha = 1.29^{-0.05}_{+0.05}$. The best-fit PSD index for the entire timeseries is $\beta = 1.7^{-0.1}_{+0.1}$ and for the 5-year period $\beta = 2.3^{-0.2}_{+0.2}$. These β-values have a more significant difference than in the case of 3C273 and the PSD slope value for the 5-year segment is clearly more consistent with the SF-slope results. Similarly to 3C273, there is a clear flattening of the slope after the linear least-squares fit on the right-side plot, which indicates an intrinsic timescale.

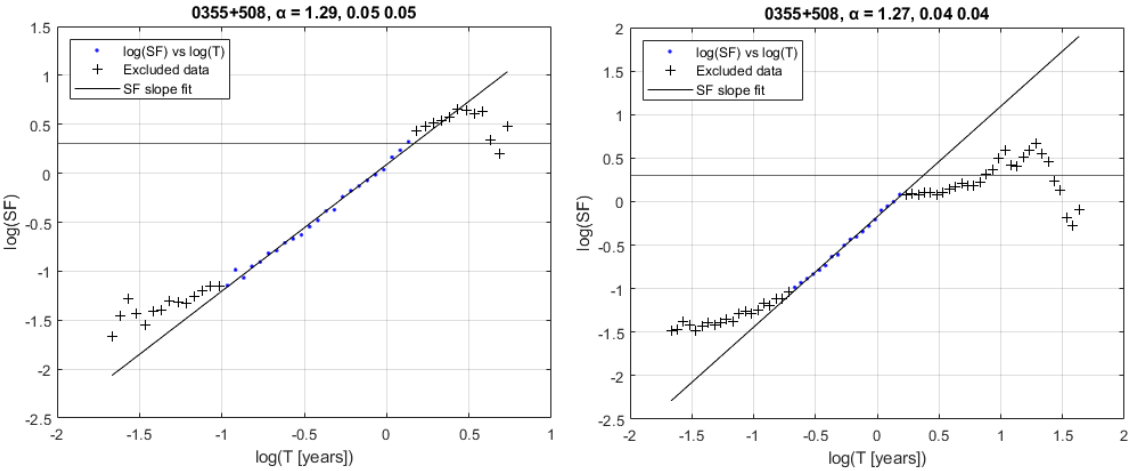

Figure 26: On the left side the structure function of 0355+508 with data between 2008-2013 and on the right side the structure function of 0355+508 with the entire timeseries 1979-2020.

4C38.41: This source was not included in the list of flattening PSD values, but it shows a phenomenon which needs to be discussed. The source has an apparent break both with the 5-year and 40-year segments though their positions are different. If such a timescale cannot be related to a break in the power spectrum, it may be related to e.g., flare duration, which was discussed in Hovatta et al. (2007). This is something, that needs to be studied further with simulations, but such a timescale is also referenced in Hughes et al. (1992) as the minimum timescale in the distribution of response times. It is noteworthy that the LS periodogram of the source during 2008-2013 shows a singular deviation at 1.25 years, which may be related to the separation time between two flares. Figure 27 shows the structure functions of 4C38.41 for both the 5-year and 40-year segments.

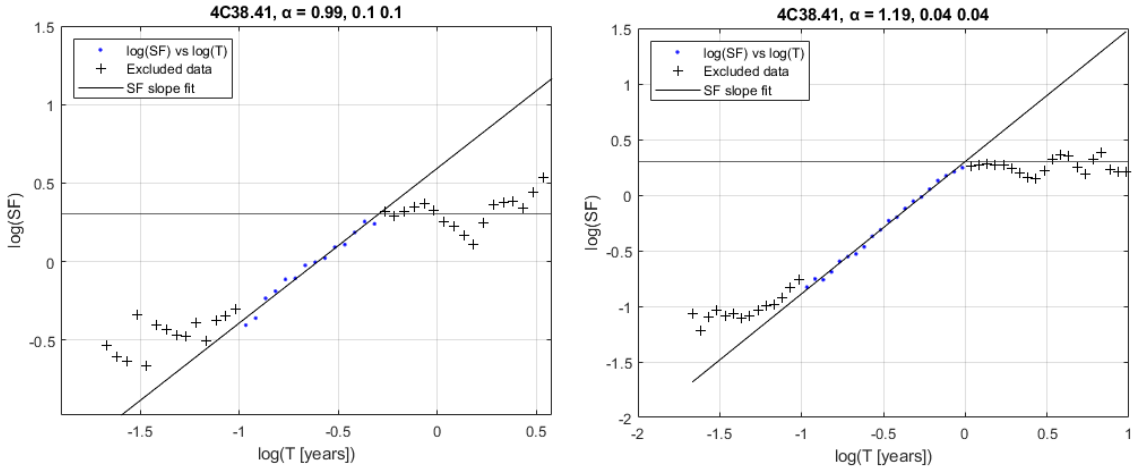

Figure 27: On the left side the structure function of 4C38.41 with data between 2008-2013 and on the right side the structure function of 4C38.41 with the entire timeseries 1979-2020. The timescale of the 5-year period is 0.54 years and the timescale of the 40-year period is 0.96 years.The timescale visible in the 5-year segments is no longer visible in the 40-year segment.

There are also some sources listed in Table 6, that showed a flattening of both the PSD and SF slope. While some of the steeper SF slopes may be caused by linear trends in the short-term data, e.g., **2230+114** showed a clear flattening of the power-law part of the structure function and no evident linear trend in the short-term light curve. This is another effect, which needs to be investigated before any direct conclusions can be made.

A further complication is that the separation of meaningful timescales from statistical fluctuations is not an easy task. A featureless power law can generate a convincing break in the structure function. Figure 28 shows, how despite looking like a real definite timescale, simulated data can create very similar looking structure functions. In fact, upon comparing the data from 0355+508 with the average structure function from Monte Carlo simulations, the break does not exceed the 1σ-

confidence level. The significance level is slightly vague though, because as was discussed, e.g., detrending needs to be tested further before being able to generate as reliable confidence levels as possible.

This effect was tested for various sources and the same apparent breaks were often seen after simulating sufficiently many light curves and taking their structure functions.

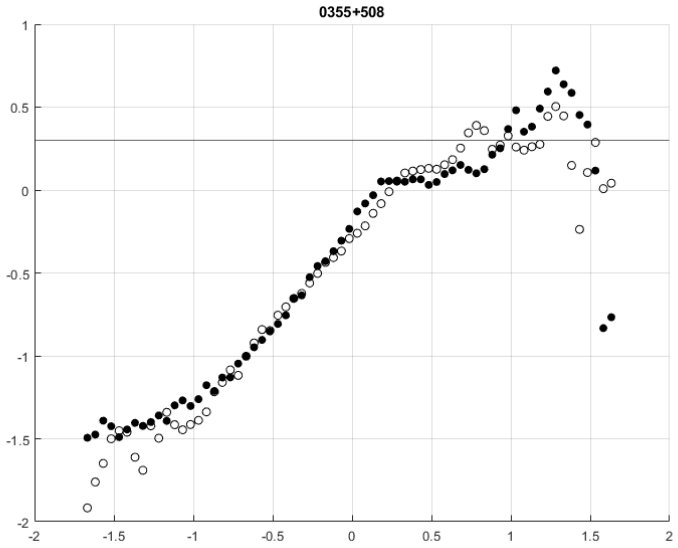

Figure 28: Simulating a light curve with the statistical properties of 0355+508 sometimes resulted in a similar looking structure function with an almost corresponding apparent timescale.

Clearly, the structure function suffers from great uncertainty with its results. While the initial tests were promising, the seen breaks in structure functions cannot be easily differentiated for whether they are the result of statistical fluctuations or true timescales. Monte Carlo simulations should be helpful in giving estimates on how reliable the results are; however, the effects of e.g., sampling should be analyzed further. The PSD analysis of 0355+508 gives indications of a break in the spectrum; however, the structure function cannot definitively confirm this. A seemingly matching break is visible in the analysis, but the simple power spectrum still gives a fairly good fit to it.

To understand, if the structure function results would stabilize similarly as with the flattened PSD results, the structure functions were plotted for all four monitoring periods. Figure 29 shows the structure functions of 0355+508 through the epochs of 5, 10, 20, and 40 years.

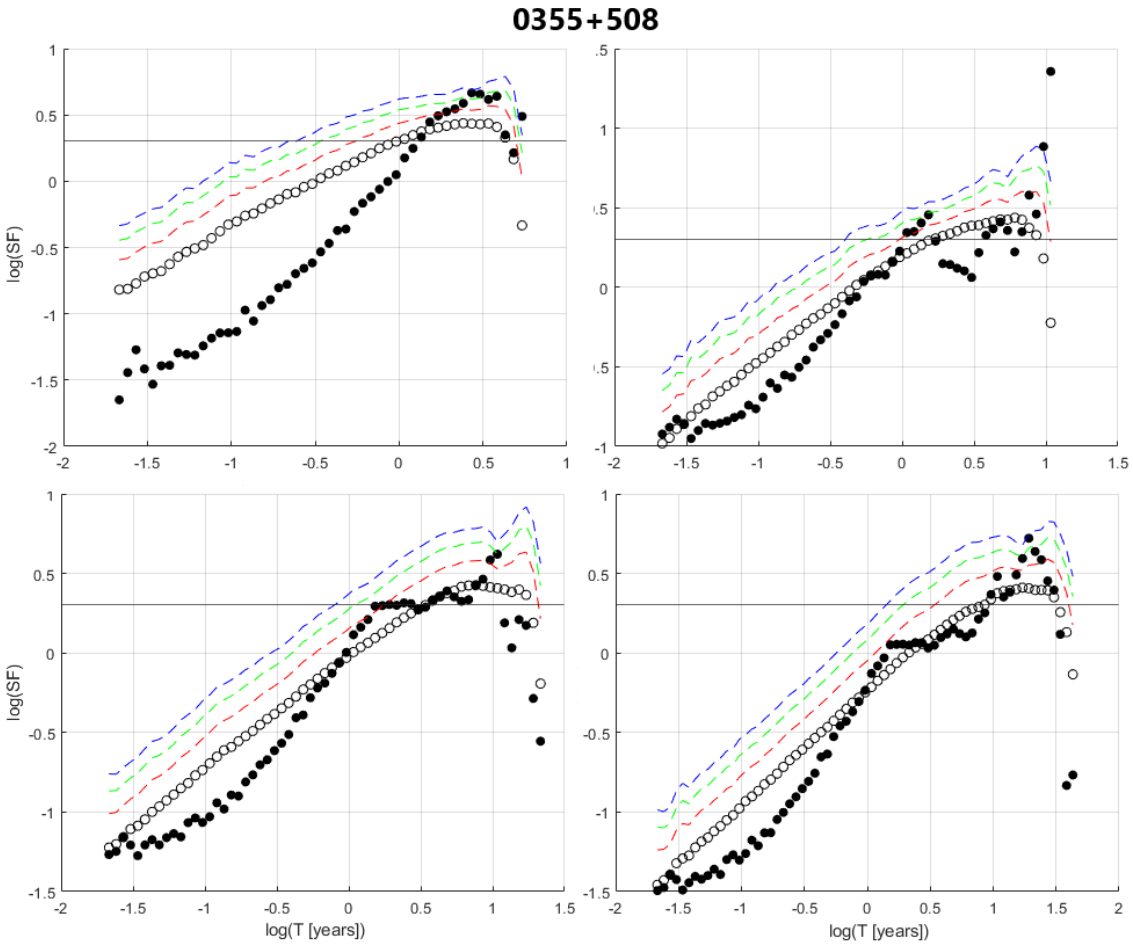

Figure 29: Top left shows the structure function of 0355+508 for 5 years, top right for 10 years, bottom left for 20 years, and bottom right for 40 years. The simulations with the best-fit PSD for the entire timeseries are plotted alongside the positive confidence intervals for reference.

The plots show that the 5-year segment appears as a steep simple power law and the 10-year segment is starting to show some effects of an appearing characteristic timescale. A peculiar phenomenon is seen, where the plateau shifts away from the $log(2.0)$ expected asymptote even as the timescale remains the same between the 20- and 40-year segments. The cross-section where the simulated structure function meets the $log(2.0)$-line shifts to higher values as was expected from Emmanoulopoulos et al. (2010). The same plots for 3C273 are in Figure 30.

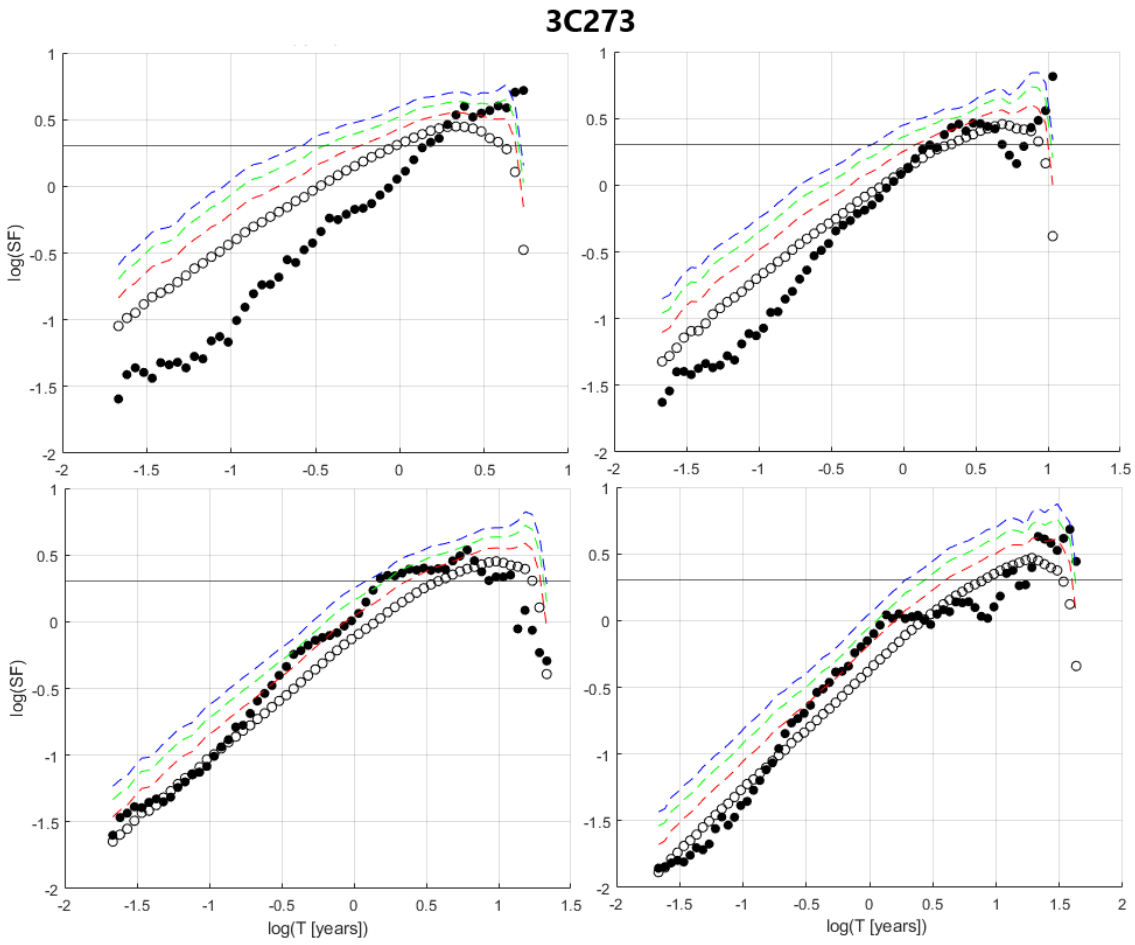

Figure 30: Top left shows the structure function of 3C273 for 5 years, top right for 10 years, bottom left for 20 years, and bottom right for 40 years. The simulations with the best-fit PSD for the entire timeseries are plotted alongside the positive confidence intervals for reference.

The results for 0355+508 and 3C273 are very similar. They would indicate that at least a 20-year monitoring period is required for a break to be visible. It is unclear why the timescale is moving away from the asymptote and whether it will remain stable: With both 0355+508 and 3C273 the break timescale has asymptoted to about 1 with 40 years of data. This shift may be related to the increase in maximum variance discussed by Emmanoulopoulos et al. (2010). With 3C273, the use of detrending shifts the break closer towards log(2.0), but with 0355+508 there is no effect. However, the timescale remains the same between the 20- and 40-year segments for both sources. Seeing the timescale remain the same both between the 20- and 40-year segments gives confidence that the timescale may be real. These types of results were seen with some of the other tested sources as well.

Given the uncertainties in the tests, no definite conclusions could be drawn about the underlying noise process simply from the structure functions. Before better methods are developed, it may be beneficial to generate the structure functions for shorter and longer segments to estimate if a persistent timescale can be seen in a similar manner to Figures 29&30. Additionally, detrending may likely need to be applied depending on the source.

The structure function would be a helpful method if the uncertainties and timescale locations could be modelled correctly because both with the periodogram and the LS periodogram, it is difficult to assess the effects of sampling and spectral distortions on the power spectrum shape even when using Monte Carlo simulations. Especially the LS periodogram generates a very distorted power spectrum due to red-noise leak, aliasing, and the unstructured window transform. Finding the best-fit power spectral model requires iterating over many different models and model parameters, which is very time-consuming. At least with the simple and bending power-law models, some hints on their suitability might be seen from the structure function. Unfortunately, the uncertain nature of the positions of the breaks make it difficult to compare the results reliably. As Emmanoulopoulos et al. (2010) state, the structure function reliability should be developed further by similar tools employed with the PSD estimation.

4.3.2 Encountered difficulties

The most critical problems with the structure function are the fitting procedure and the locations of apparent timescales.

As expected, while for some sources defining a slope and the smallest timescale was not possible, some structure functions required a decision to be made on how uncertain situations would be handled. Hughes et al. (1992) state that normalizing the structure function with the light curve variance should cause its plateau to asymptote to log(2.0). For uncertain reasons, some sources had their plateau at either a higher or lower value than what the structure function asymptoted to. Practically, there were two choices on how to handle the situation: Either the cross-section of the slope and plateau could be used as T_{min}, or simply, the point where the plateau in some situations clearly started (visually). Naturally, in some sources the plateau start was not easy to determine. Nevertheless, if there was a significant peak after log(2.0), T_{min} was chosen to be at the cross-section of log (2.0) and the structure function. If a clear plateau occurred before log (2.0), this turnover timescale was chosen as T_{min}.

In some cases, initial small-sample tests with detrending seemed to move the plateau closer to the expected plateau; however, detrending was not ideal as the used Matlab function is intended for evenly sampled data. It should not be a serious issue for long-term data, but as has been shown, the definition of long-term data can vary.

For this reason, it is a good idea to test detrending to see how it affects the structure function of individual sources.

Another interesting phenomenon was that only some of the structure functions showed a clear initial plateau usually attributed to observational noise (Hughes et al., 1992). This is also something that should be investigated further e.g., how it depends on the distribution of the data points.

To better understand how the structure function works, it would be beneficial to simulate data with a chosen PSD and PDF with imposed periodicity and flare durations and then do Monte Carlo simulations based on the artificial data. This would help in determining, how the maximum timescale can best be defined and how the simulations relate to the underlying data. Simulations would also aid in assigning errors to the structure function points as well as help define the uncertainties in the timescale locations. With simulations, also the effect of detrending could be better analyzed.

4.4 Discrete correlation function

In the DCF analysis, 22 sources had a peak exceeding the 3σ-confidence limit. These sources are listed in Table 7. The average timescale was $T = 7.03$ years. The light curves were not detrended.

Table 7: The table lists all the timescales and corresponding sources, which exceeded the 3σ significance.

Source	$\boldsymbol{T(years)}$
PG0007+106	5.55
0212+735	15.14
0235+164	16.1
PKS0446+112	8.15
3C120	3.49
0716+714	6.1
0754+100	6.51
0804+499	0.89
0814+425	13.49
OJ248	2.4
0836+710	5.14
0953+254	4.04
1036+054	4.86
ON231	8.7
4C29.45	11.58
3C345	8.97
1638+398	3.22
1642+690	3.36

Source	$T(years)$
PKS2022-077	4.04
2131-021	4.32
2201+171	5.41
2216-038	13.36

In all of the listed cases, the timescale was linked to the separation time between large flares. The flaring did not have to be recurring, but only two stronger flares were enough to show a significant timescale in the DCF corresponding to the time between the flares. This shows that the DCF can well isolate such occurrences; however, since the significance levels are based on the null hypothesis of a simple power-law, their actual significance is unclear. In future studies, it needs to be clarified whether such strong flares are actually against other underlying noise processes or whether the significance estimation needs to be done differently for the DCF. Naturally, if the flares are periodic or quasiperiodic, then the significance should be high. Figure 31 shows the flux density curve of 3C120. There are two large flares between 2015-2020 which seem to correspond to the obtained timescale. There are also some smaller flares, two of which occur between 2003-2008 and appear to have a similar timescale. Figure 32 shows the DCF of 3C120 for reference.

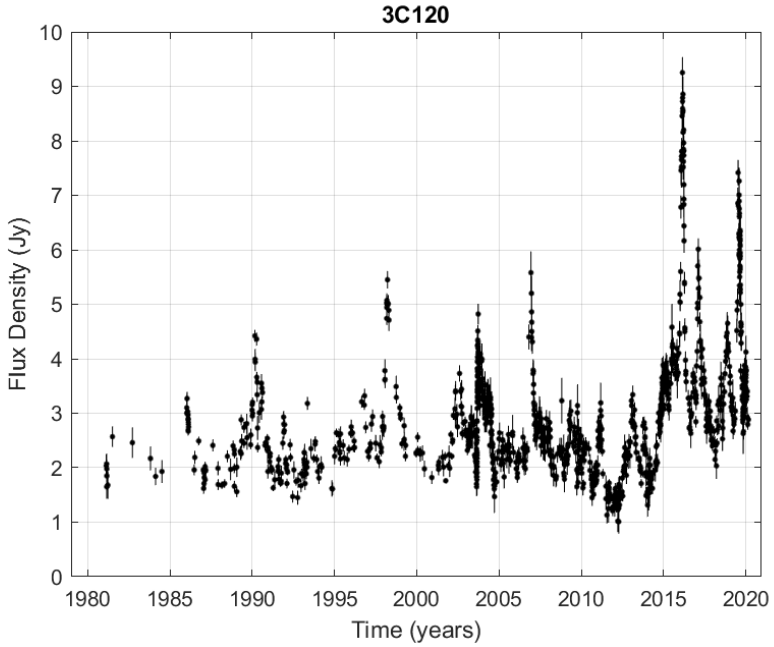

Figure 31: The flux density curve of 3C120 shows two pairs of flares appearing to correspond to the obtained timescale.

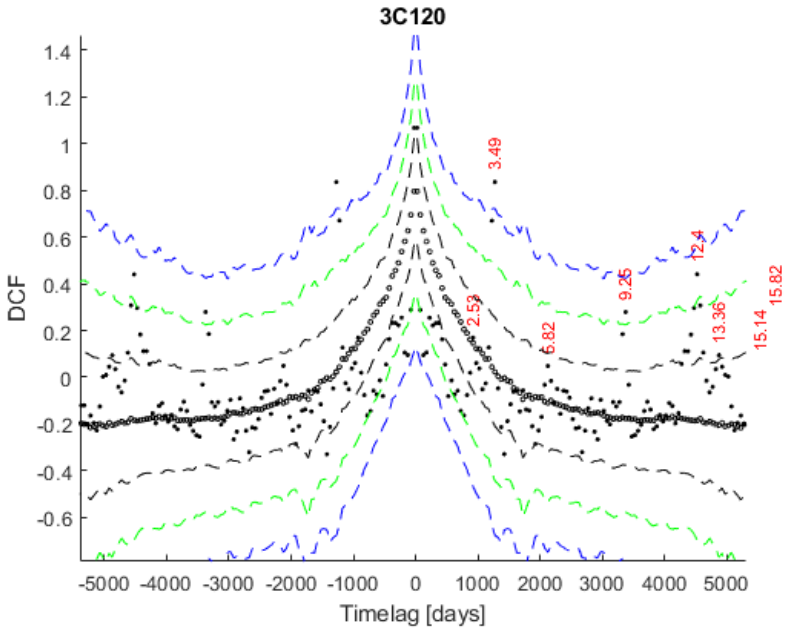

Figure 32: The DCF of 3C120.

While there were few timescales exceeding the 3σ-limit, there were often multiple timescales exceeding the 1σ-limit and at least some timescales exceeding the 2σ-limit. A timescale was also considered significant, if before a positive peak, it dropped below the negative σ-limits.

Monte Carlo simulations also showed well the typical problem of unrealistically long apparent timescales encountered e.g., by Hovatta et al. (2007) when analyzing their DCF results. Figure 33 is the DCF of 0202+149 and it illustrates how the DCF significance levels sharply rise when reaching longer timescales. As shown by the simulations, these are only related to the length of the timeseries.

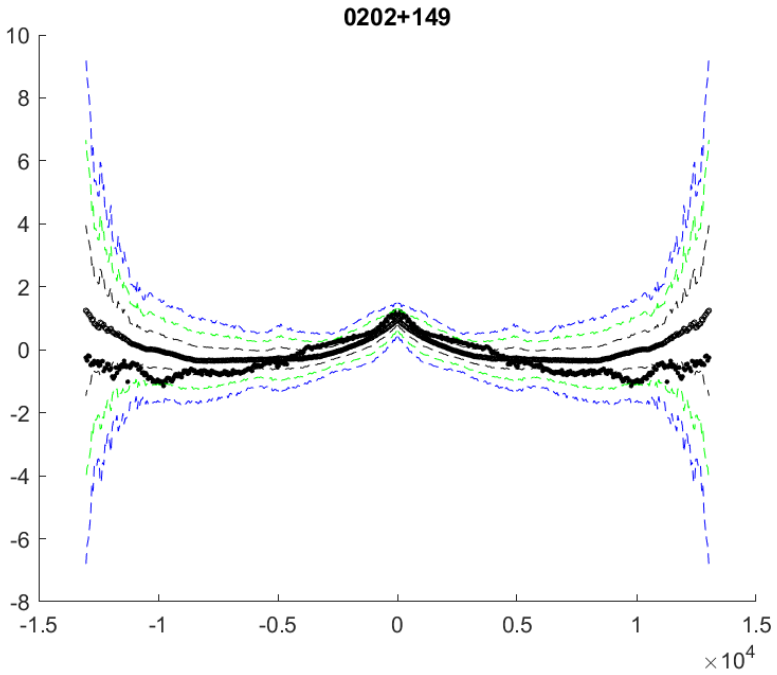

Figure 33: The DCF of 0202+149 shows well how the correlation confidence levels rise as longer timescales are probed.

4.4.1 Fourier transformations of the DCFs

As was explained in Chapter 4, the autocorrelation function and power spectral density are Fourier transform pairs. This means that the estimated power spectrum of a source can be retrieved by taking the Fourier transform of the DCF.

In order to test this relation, $N = 100$ simulations were generated, and the Fourier transform of each simulated DCF was taken alongside the DCF of the observed data. The estimated PSD was then plotted in log-space in order to see the behavior between the observed and simulated data.

There were 27 sources, which clearly deviated from the simulations. Because no goodness-of-fit test was performed between the observed and simulated data, the chosen sources were biased by subjective evaluation of the PSD shape between the observed and simulated data. For this reason, only very well sampled and clear deviations were assessed.

4C29.45 is a source with data spanning 37 years. The DCF of the source shows a timescale of $T = 2.8$ years. Figure 34 shows the PSD estimates of both the observed and simulated data. As was already seen with the LS periodogram and SF, the data does not appear consistent with a simple power law. While uneven sampling is capable of producing PSDs, which appear to have features, the simulations show no such features. The PSD of the observed data shows a flat slope until around 2-3 years after which it clearly steepens.

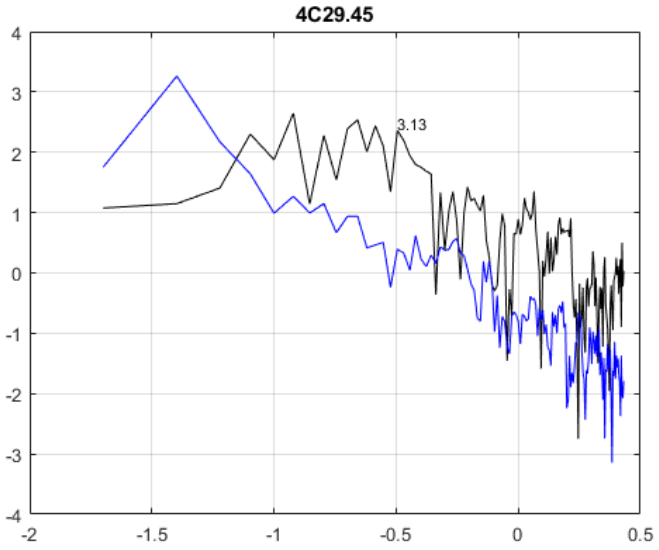

Figure 34: The PSD estimate of the simulated data (blue) and the PSD estimate of the observed data (black) of 4C29.45 seem to clearly deviate in shape, though no confidence intervals were plotted to definitively prove this.

0235+164 is another example of a source, which had an apparent deviation from the simulations. The monitoring period for 0235+165 is 39 years. The DCF timescale 1.58 years corresponds to a peak of 1.67 years in the PSD estimate. Similar timescales were also seen in the LS periodogram as expected. Figure 35 shows the PSD estimate of the source.

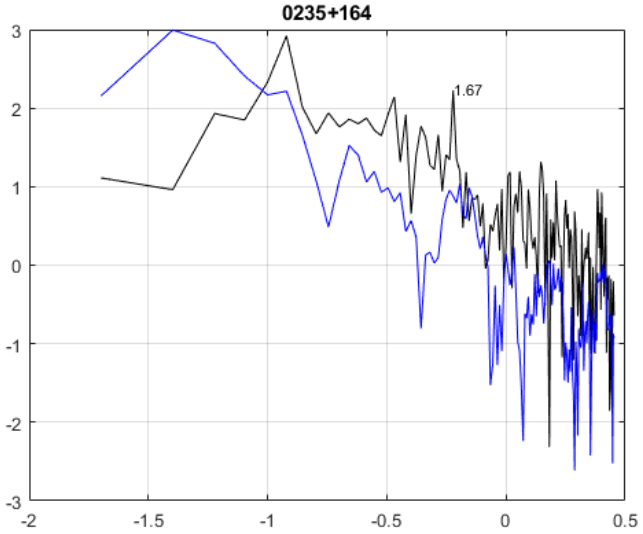

Figure 35: The PSD estimate of 0235+164 (black) shows apparent deviations from the simulated data (blue).

While estimating the PSD from the autocorrelation function was done purely for testing purposes and no true effects can be assessed without generating some confidence limits and using correct normalization, many of the results were clearly similar to the LS periodogram results. It may be worth studying further, how this method compares to the periodogram analysis and if there are some benefits to it. Merrifield & McHardy (1994) have done work on analyzing the autocorrelation method as a mean to assess the source PSD and it could be further compared to the other methods used in this thesis.

4.4.2 Encountered difficulties

Finding significant correlations is somewhat ambiguous with the DCF. While Monte Carlo simulations were used for confidence intervals, deciding the most significant correlations was difficult. For example, if the autocorrelation went from negative 3σ-correlation to positive $< 1\sigma$-correlation, its actual significance was difficult to determine. Hovatta et al. (2007) considered the most significant correlation as the data point, before which the DCF went to under zero and then reached an apparently large value in comparison to the other peaks in the DCF. Because simulations were used in the analyses of this thesis, also apparent peaks caused by sampling could be fairly well identified.

As with the structure function, simulations with known PSD and PDF should be made in order to estimate, how the DCF correlations can best be identified. The errors in peak locations were not estimated in this thesis; however, this should be done in future studies, when the characteristic timescales and correct power spectral models are estimated in an exact manner. Also different normalization procedures will probably need to be used in order to make the most accurate estimates on the timescales.

4.5 Discussion

The structure function gives either the minimum timescale of uncorrelated behavior or the minimum timescale in the distribution of response times (Hughes et al. 1992). According to Hughes et al. (1992), it is difficult to differentiate between the two underlying reasons. Looking at the Lomb-Scargle periodograms of the long-term data for those sources with deviations from the null hypothesis, the SF timescale may be linked to the possible break frequency. Because the LS periodograms have a problem with noise in the high frequencies, it was difficult to determine any high frequency timescales from them. Nevertheless, in some cases a similar timescale as to what the SF suggests could be found in the LS periodogram before an apparent steepening of the spectrum. This is only a visual estimation, which should be

analyzed further. Any apparent correlations should always be analyzed with statistical methods before making any definitive conclusions. Table 8 lists the average timescales from the analyses.

Table 8: The average timescales from the LS periodogram, DCF and SF analyses. The DCF minimum timescales were calculated from the shortest apparently significant timescale at minimum at the 1σ significance.

T_{max} LS (years)	T_{min} DCF (years)	T_{min} SF(years)
3.67	3.64	1.56

The LS periodogram and DCF average timescales are near identical. For almost all sources, the maximum timescale of the LS periodogram was also visible in the DCF. Some of the shorter timescales were sometimes not well identifiable in the DCF, but in some situations the minimum DCF timescales were shorter than the maximum timescale of the LS periodogram. The inability of the DCF to identify some of the smaller timescales may be due to e.g., the bin size. As was expected (Hovatta et al., 2007), the structure functions gave shorter timescales than the other two methods, the SF average being a little less than half of the LS periodogram and DCF averages.

The similarities in the LS periodogram and DCF results give confidence that the obtained timescales are real deviations from the null hypothesis as opposed to statistical fluctuations. While the PSD and autocorrelation function are Fourier transform pairs and should give similar results, the methods of obtaining the results are different.

An important matter is, how relevant are the maximum timescales of the LS periodograms and minimum and most significant timescales of the DCFs. The analyses in this thesis indicate that a simple power law is not an adequately good estimate for the underlying noise process of long-term AGN radio data. This was shown with the violation of the null hypothesis across different sources. However, since the null hypothesis was only that the underlying noise process be of simple power-law type, no significance about individual timescales can be made before a good estimation for the underlying power spectral model can be decided. In this thesis, the LS periodogram and DCF timescales were thus mostly of interest in comparing how the methods identify timescales.

The structure function and LS periodogram results may be of interest when searching for a break frequency; however, as explained by Emmanoulopoulos et al. (2010), care needs to be taken when comparing these results with each other. If the null hypothesis is not violated in the LS periodograms, the broken or bending power-law model might still need to be used in future studies. Morris et al. (2019) note, that in the case of weak stationarity, the PSD and PDF are interlinked; This means that the PDF may change across the timeseries unless the data is somehow made stationary e.g., with the broken power-law model.

Because no straight comparisons between the sources and source types were made, redshift corrections were not calculated in this thesis. In future work, the power spectral models will be properly characterized after which the redshift corrections and comparisons will be made in order to reveal any physical conditions possibly attributing to the differences in the results between sources and source types.

4.5.1 Importance of comparing results across methods

As was shown, the methods can be unreliable when used alone. The periodogram smoothens out any periodic and quasiperiodic behavior, and it is also difficult to see any clear features in the power spectrum.

The LS periodogram is better suited for seeking such features and other timescales, but it is troubled by red-noise leakage, aliasing and noise from the unstructured window transform. While Monte Carlo simulations help in defining significance limits to the data, spurious spikes are still difficult to isolate.

The structure function shows the features of the power spectral model well; however, simple statistical fluctuations may appear as if they were features, and there is no simple way of discriminating between those and real phenomena other than using Monte Carlo simulations. The sampling and length of the timeseries seem to play a significant role on how erratic the structure function is.

The discrete correlation function shows the autocorrelation peaks well and Monte Carlo simulations help in discriminating any peaks caused by sampling. However, it can be difficult to isolate the most important peaks unless some sort of normalization procedure is employed.

Even with these issues, all of the approaches proved helpful in analyzing the characteristics of the observed data. Especially when the methods are used together, their drawbacks are not as severe because the results can be compared and estimated for reliability. One method can show a statistical fluctuation appearing to be a real characteristic timescale; however, if the other methods show the same timescale, it is a lot more likely to be a real phenomenon.

4.5.2 Underlying noise process

The analyses of this thesis showed that the common PSD estimation using the TK95 method, the LS periodogram and the structure function may be of help when trying to identify the underlying physical noise process and characteristic timescales. The flat PSD-slope values were initially of concern because they were clearly flatter than earlier radio analyses had estimated. Although the frequency break eventually became a clear candidate as an explanation, a mistake in the code was thoroughly looked for. However, because similar effects were seen in the LS periodograms and structure functions as well as the power spectrums generated from the DCF

autocorrelations, the results can be considered more reliable. Naturally, an error in the simulation procedure may generate unreliable confidence levels.

Despite the PSD estimation via the periodogram being a common analysis tool, the structure function could be surprisingly helpful in assessing the PSD slope value results given the uncertainties can be modelled correctly. While a simple power law should be easily fitted to the periodogram, if the underlying noise process is not featureless, the procedure becomes more complex. The structure function would provide a simple way of visually assessing whether the data looks like it might contain features not explained by the simple power law.

While the analyses in this thesis were able to give some support to the expectation that 40 years of monitoring would be enough in the radio to reveal information about the characteristic timescales of some of the sources, no definite timescales were yet defined. In future work, the methods will be analyzed further in order to be able to extract the correct information by evaluating the uncertainties in the timescale locations. The broken and smoothly bending power laws will be used and fitted to the data, because it seems clear that the simple power law is not an adequate estimation for long-term data. The statistical nature of the data must also be scrutinized i.e., its stationarity must be analyzed. While some sources seemed to be good candidates for breaks/bends in the power spectrum, there were sources, which did not display such behavior. This may indicate that even longer observation periods are sometimes needed.

5 Conclusions

The aim of this thesis was to characterize timescales for AGN radio variability and specifically to identify how the monitoring period length affects the results. Of special interest was to understand, whether the simple power law can adequately describe the underlying noise process of radio AGNs especially for long monitoring periods.

The results from the PSD and SF analyses gave indications that some of the observed data have reached a monitoring period length adequate to show a break in the power spectrum. The LS periodograms showed an apparent flattening of the spectrum in lower frequencies for multiple sources. While further analyses are required due to the uncertainties in the tests, the results from this thesis were that the simple power law is usually not an adequate description of the underlying noise process of AGNs in the radio domain when data has been gathered for 40 years.

The periodogram analysis suggested that sometimes a monitoring period of 10 years might be enough to show a characteristic timescale in the data. However, the structure function analysis showed that a timescale in such a situation may require e.g., 20 years of monitoring before being properly identifiable. Of course, there were also multiple sources, which did not seem to have a stable PSD nor a clear SF timescale and thus were either too poorly sampled, only sampled for the steep part of their spectrum, or otherwise lacked the required stationarity.

Because the underlying physical process for many of the sources seemed to not be adequately described by the simple power law, only the timescales possibly representing the characteristic break in the power spectrum should be considered as significant timescales, though their locations are uncertain. No periodicities or quasiperiodicities could be reliably estimated from the data; however, as the simulations were inadequate due to the used power spectral model, this result does not mean the sample could not contain a source exhibiting this type of behavior.

Future studies using data from long monitoring periods should focus on trying different broken or bending power-law models when analyzing the behavior of AGNs in the radio frequencies and defining better estimates for when a break can be expected to occur. With a more accurate power spectral model the results could then be compared between sources and source types based on the characteristic timescales. This type of analysis could reveal if the source types have differences attributable to e.g., black hole mass or other physical parameters. With an accurate estimate of the PSD, any periodicities and quasiperiodicities would become possible to identify as well. While these types of timescales are expected to be rare within the AGN population, it would be an important aspect to study in order to reveal possible binary black hole systems.

References

Aller, M. F., Aller, H., D., Hughes, P. A., 1991. In Variability of Active Galactic Nuclei, ed. H. R. Miller & P. J. Wiita, Cambridge University Press (England), 184, ISBN: 978-0521412957

Böttcher M. & Reimer A., 2012. In Relativistic Jets from Active Galactic Nuclei, ed. Böttcher, M. Harris, D. E., Krawczynski, H.. Wiley (Germany), 406, ISBN: 978-3-527-41037-8

Böttcher, M. Harris, D. E., Krawczynski, H., 2012. In Relativistic Jets from Active Galactic Nuclei, ed. Böttcher, M. Harris, D. E., Krawczynski, H., Wiley (Germany), 406, ISBN: 978-3-527-41037-8

Krawczynski, H., Böttcher M., Reimer A., 2012. In Relativistic Jets from Active Galactic Nuclei, ed. Böttcher, M. Harris, D. E., Krawczynski, H., Wiley (Germany), 406, ISBN: 978-3-527-41037-8

Bloomfield P., 2000. Fourier Analysis of Time Series. An Introduction, Wiley (United States), ISBN: 0-471-88948-2

Chatterjee, R., Jorstad, S. G., Marscher, A. P..; Oh, H., McHardy, I. M., Aller, M. F., Aller, H. D., Balonek, T. J., Miller, H. R., Ryle, W. T., Tosti, G., Kurtanidze, O., Nikolashvili, M., Larionov, V.M., Hagen-Thorn, V. A., 2008. Correlated Multi-Wave Band Variability in the Blazar 3C 279 from 1996 to 2007 , *The Astrophysical Journal,* Volume 689, Issue 1, December 2008, Pages 79-94, DOI: 10.1086/592598

Chatterjee, K., Younsi, Z., Liska, M., Tchekhovskoy, A., Markoff, S. B., Yoon, D., van Eijnatten, D., Hesp, C., Ingram, A., van der Klis, M. B. M., 2020. Observational signatures of disc and jet misalignment in images of accreting black holes, *Monthly Notices of the Royal Astronomical Society*, Volume 499, Issue 1, November 2020, Pages 362–378, DOI: 10.1093/mnras/staa2718

Do, T., Ghez, A. M., Morris, M. R., Yelda, S., Meyer, L., Lu J. R., Hornstein, S. D., Matthews, K., 2009. A near-infrared variability study of the galactic black hole: a red noise source with no detected periodicity, *The Astrophysical Journal,* Volume 691, Number 2, February 2009, Pages 1021-1034, DOI: 10.1088/0004-637X/691/2/1021

Edelson, R. A. and Krolik, J. H., 1988. The Discrete Correlation Function: A New Method for Analyzing Unevenly Sampled Variability Data, *Astrophysical Journal,* Volume 333, p. 646, DOI: 10.1086/166773

Emmanoulopoulos, D., McHardy, I. M, Uttley, P., 2010. On the use of structure functions to study blazar variability: caveats and problems, *Monthly Notices of the Royal Astronomical Society,* Volume 404, Issue 2, May 2010, Pages 931-946, DOI: 10.1111/j.1365-2966.2010.16328.x

Emmanoulopoulos, D., McHardy, I. M., Papadakis, I. E., 2013. Generating artificial light curves: Revisited and updated, *Monthly Notices of the Royal Astronomical Society*, Volume 443, Issue 2, August 2013, Pages 907-927, DOI: 10.1093/mnras/stt764

Graham, M. J., Djorgovski, S. G., Stern, D., Glikman, E.; Drake, A. J., Mahabal, A. A., Donalek, C., Larson, S., Christensen, E., 2015. A possible close supermassive black-hole binary in a quasar with optical periodicity, *Nature*, Volume 518, Issue 7537, February 2015, Pages 74-76, DOI: 10.1038/nature14143

Hovatta, T., Tornikoski, M., Lainela, M., Lehto, H. J. , Valtaoja, E., Torniainen, I., Aller, M. F., and Aller, H. D. 2007. Statistical analyses of long-term variability of AGN at high radio frequencies. *Astronomy & Astrophysics*, volume 469, number 3, pages 899-912, DOI: 10.1051/0004-6361:20077529

Hovatta, T., Nieppola, E., Tornikoski, M., Valtaoja, E., Aller, M. F., Aller, H. D., 2008. Long-term radio variability of AGN: flare characteristics. *Astronomy & Astrophysics,* Volume 485, Pages 51-61, DOI: 10.1051/0004-6361:200809806

Hovatta, T. & Lindfors, E., 2020. Relativistic Jets of Blazars, *New Astronomy Reviews,* Volume 87, December 2019, DOI: 1016/j.newar.2020.101541

Hughes, P. A., Aller, H. D., Aller, M. F., 1992. The University of Michigan Radio Astronomy Data Base. I. Structure Function Analysis and the Relation between BL Lacertae Objects and Quasi-stellar Objects, *Astrophysical Journal,* Volume 396, September 1992, Page 469-486, DOI: 10.1086/171734

Kiehlmann, S., 2015. Origin of the gamma-ray emission in AGN jets - A multi-wavelength photometry and polarimetry data analysis of the quasar 3C 279. PhD thesis, Universität zu Köln. P. 185. Available: http://kups.ub.uni-koeln.de/id/eprint/6231

Lainela, M. & Valtaoja, E., 1993. Structure function analysis of high radio frequency variability in the Metsähovi monitoring sample of active galactic nuclei, *The Astrophysical Journal,* Volume 416, October 1993, Pages 485-495, DOI: 10.1086/173252

Lomb, N. R., 1976. Least-Squares Frequency Analysis of Unequally Spaced Data, *Astrophysics and Space Science*, Volume 39, Issue 2, February 1976, Pages 447-462, DOI: 10.1007/BF00648343

Mandelbrot, B. B., Wallis, J. R., 1969. Computer experiments with fractional Gaussian noises. Part 1: Sample graphs, averages, and variances. *Water Resources Research 5*, Pages 228-241, DOI: 10.1029/WR005i001p00228

Marscher, A. P. & Gear, W. K., 1985. Models for high-frequency radio outbursts in extragalactic sources with application to the early 1983 millimeter-to-infrared flare of 3C 273, *The Astrophysical Journal,* Volume 298, November 1985, Pages 114-127, Bibcode: 1985ApJ...298..114M

Max-Moerbeck, W., Richards, J. L., Hovatta, T., Pavlidou, V., Pearson, T. J., Readhead, A., C., S., 2014. A method for the estimation of the significance of cross-correlations in unevenly sampled red-noise time series, *Monthly Notices of the Royal Astronomical Society*, Volume 445, Issue 1, November 2014, Pages 437-459, DOI: 10.1093/mnras/stu1707

Max-Moerbeck Astudillo, W. K., 2013. The Relationship Between the Radio and Gamma-Ray Emission of Blazars. Dissertation (Ph.D.), California Institute of Technology, DOI: 10.7907/ZX5X-V114.

Markowitz, A., Edelson, R., Vaughan, S., Uttley, P., George, I. M., Griffiths, R. E., Kaspi, S., Lawrence, A., McHardy, I., Nandra, K., Pounds, K., Reeves, J., Schurch, N., Warwick, R., 2003. X-Ray Fluctuation Power Spectral Densities of Seyfert 1 Galaxies, *The Astrophysical Journal*, Volume 593, Issue 1, August 2003, Pages 96-114, DOI: 10.1086/375330

Merrifield, M. R. & McHardy, I. M., 1994. Monthly Notices of the Royal Astronomical Society, Volume 271, Issue 4, December 1994, Pages 899–909, DOI: 10.1093/mnras/271.4.899

Morris, P. J., Chakraborty, N., Garret, C., 2019. Monthly Notices of the Royal Astronomical Society, Volume 489, Issue 2, October 2019, Pages 2117-2129. DOI: 10.1093/mnras/stz2259

Nandra, K., George, I. M., Mushotzky, R. F., Turner, T. J., Yaqoob, T. 1997. ASCA observations of Seyfert 1 galaxies. I. Data analysis, imaging, and timing. *The Astrophysical Journal.* Volume 476, February 10, Pages 70-82, DOI: 10.1086/313053

Netzer, H., 2013. The Physics and Evolution of Active Galactic Nuclei, Cambridge University Press (the United Kingdom), ISBN: 9781107306554

Papadakis, E., 2004. The scaling of the X-ray variability with black hole mass in active galactic nuclei, Monthly Notices of the Royal Astronomical Society, Volume 348, Issue 1, February 2004, Pages 207–213, DOI: 10.1111/j.1365-2966.2004.07351.x

Papadakis, I., E., 2004. The scaling of the X-ray variability with black hole mass in active galactic nuclei, *Monthly Notices of the Royal Astronomical Society,* Volume 348, Issue 1, Pages 207-213, DOI: 10.1111/j.1365-2966.2004.07351.x

Papadakis, I. E. & Lawrence, A., 1992. Improved methods for power spectrum modelling of red noise, *Monthly Notices of the Royal Astronomical Society,* Volume 261, 1993, Pages 612-624, Bibcode: 1993MNRAS.261..612P

Park, J-H. and Trippe, S., 2014. Radio variability and random walk noise properties of four blazars, *The Astrophysical Journal,* Volume 785, Issue 1, April 2014, Page 76 (8pp), DOI: 10.1088/0004-637X/785/1/76

Press, W. H., 1978. Flicker noises in astronomy and elsewhere, Comments on Modern Physics, Part C - Comments on Astrophysics, Volume 7, Number 4, Pages 103-119, Bibcode: 1978ComAp...7..103P

Press W.H., Rybicki G.B., 1997. Desperately Seeking Non-Gaussianity. In: Maoz D., Sternberg A., Leibowitz E.M. (eds) *Astronomical Time Series. Astrophysics and Space Science Library*, Volume 218. Springer, Dordrecht. DOI: 10.1007/978-94-015-8941-3_6

Priestley, M. B., 1981. Spectral Analysis and Time Series, *Journal of Forecasting*, Volume 1, October/December 1982, Issue 4, Academic Press, London, 1981, DOI: 10.1002/for.3980010411

Raiteri, C.M., Villata, M., Acosta-Pulido, J. *et al.,* 2017. Blazar spectral variability as explained by a twisted inhomogeneous jet, *Nature* 552, December 2017, Pages 374-377, DOI: 10.1038/nature24623

Ramakrishnan, V., Hovatta, T., Nieppola, E., Tornikoski, M., Lähteenmäki, A., Valtaoja, E., 2015. Locating the γ-ray emission site in Fermi/LAT blazars from correlation analysis between 37 GHz radio and γ-ray light curves, *Monthly Notices of the Royal Astronomical Society*, Volume 452, Issue 2, September 2015, Pages 1280–1294, DOI: 10.1093/mnras/stv321

Scargle, J. D., 1982. Studies in astronomical time series analysis. II - Statistical aspects of spectral analysis of unevenly spaced data, *Astrophysical Journal,* Part 1, vol. 263, December 1982, p.835-853, DOI: 10.1086/160554

Schuster, A., 1987. On lunar and solar periodicities of earthquakes. *Proceedings of the Royal Society of London*, Volume 61, Pages 455–465, Bibcode: 1897RSPS...61..455S

Simonetti, J. H., Cordes, J. M., Heeschen, D. S., 1985. Flicker of extragalactic radio sources at two frequencies, *The Astrophysical Journal,* Volume 296, September 1985, Pages 45-59, DOI: 10.1086/163418

Springford A., Eadie, G. M., Thomson, D. J., 2020. Improving the Lomb-Scargle periodogram with the Thomson Multitaper, *The Astronomical Journal,* Volume 159, May 2020, Number 5, Pages 205-217, DOI: 10.3847/1538-3881/ab7fa1

Timmer, J., König, M., 1995. On generating power law noise, *Astronomy and Astrophysics*, Volume 300, August 1995, Pages 707-710, Bibcode: 1995A&A...300..707T

Schreiber, T. & Schmitz, A., 1996. Improved Surrogate Data for Nonlinearity Tests, *Physical Review Letters,* Volume 77, July 1996, Issue 4, Pages 635-638, DOI: 10.1103/PhysRevLett.77.635

Uttley, P., McHardy, I. M., Papadakis I.E. 2002. Measuring the broad-band power spectra of active galactic nuclei with *RXTE, Monthly Notices of the Royal Astronomical Society*, Volume 332, Issue 1, May 2002, Pages 231–250, DOI: 10.1046/j.1365-8711.2002.05298.x

Uttley P., McHardy, I. M., Vaughan, S., 2005. Non-linear X-ray variability in X-ray binaries and active galaxies, *Monthly Notices of the Royal Astronomical Society*, Volume 359, Issue 1, May 2005, Pages 345–362, DOI: 10.1111/j.1365-2966.2005.08886.x

Van der Klis, M., 1997. In Statistical Challenges in Modern Astronomy II,
ed. G.J. Babu, E.D. Feigelson, Springer-Verlag (New York), Page 321, ISBN 978-1-4612-1968-2

VanderPlas, J. T., 2018. Understanding the Lomb-Scargle Periodogram, *The Astrophysical Journal Supplement Series,* Volume 236, Number 1, May 2018, Pages 16(28pp), DOI: 10.3847/1538-4365/aab766

Vaughan, S., Edelson, R., Warwick, R. S., Uttley, P., 2003. On characterizing the variability properties of X-ray light curves from active galaxies, *Monthly Notices of the Royal Astronomical Society*, Volume 345, Issue 4, November 2003, Pages 1271–1284, DOI: 10.1046/j.1365-2966.2003.07042.x

Vaughan, S., Uttley, P., Markowitz, A. G., Huppenkothen, D., Middleton, M. J., Alston, W. N., Scargle, J. D., Farr, W. M., 2016, False periodicities in quasar time-domain surveys, *Monthly Notices of the Royal Astronomical Society*, Volume 461, Issue 3, 21 September 2016, Pages 3145–3152, DOI: 10.1093/mnras/stw1412

Zechmeister, M., Kürster, M., 2009, The generalised Lomb-Scargle periodogram. A new formalism for the floating-mean and Keplerian periodograms, *Astronomy & Astrophysics,* Volume 496, Number 2, March 2009, Pages 577-584, DOI: 10.1051/0004-6361:200811296

Zechmeister M., 2018. GLS (Generalised Lomb-Scargle periodogram). Matlab code. Available: https://github.com/mzechmeister/GLS/tree/master/matlab

Appendix A

Table A1: The Metsähovi name and IERS designation of the sources are in columns 1 and 2. Column 3 states the source type and columns 4 and 5 the first and last observations used in this thesis. The last column states the number of data points (detections).

Source (Metsähovi name)	Source	Type	First obs.	Last obs.	Detections
NRAO5	0003-066	BLO	26.10.1992	24.2.2020	164
PG0007+106	0007+106	GAL	16.1.1986	24.2.2020	470
0016+731	0016+731	LPQ	7.7.1988	27.2.2020	213
0048-097	0048-097	BLO	30.10.1992	27.2.2020	111
0059+581	0059+581	QSO	2.10.1998	24.2.2020	405
0106+013	0106+013	HPQ	28.2.1981	24.2.2020	430
S20109+22	0109+224	BLO	8.7.1984	28.2.2020	437
0133+476	0133+476	HPQ	20.1.1981	27.2.2020	892
0149+218	0149+218	LPQ	1.7.1988	25.2.2020	272
0202+149	0202+149	HPQ	8.7.1984	27.2.2020	357
0212+735	0212+735	HPQ	6.7.1988	27.2.2020	282
0218+357	0218+357	QSO	1.7.1992	28.2.2020	189
3C66A	0219+428	BLO	25.1.1989	28.2.2020	604
0224+671	0224+671	QSO	9.5.1990	25.2.2020	308
0229+131	0229+131	QSO	4.6.1992	14.2.2020	156
0234+285	0234+285	HPQ	21.2.1990	25.2.2020	738
0235+164	0235+164	BLO	19.2.1981	24.2.2020	1321
0238-084	0238-084	GAL	19.1.1991	25.2.2020	213
0248+430	0248+430	QSO	10.7.1984	28.2.2020	186
4C47.08	0300+470	BLO	20.1.1989	24.2.2020	116
0306+102	0306+102	QSO	20.1.1989	25.2.2020	198
3C84	0316+413	GAL	24.10.1979	28.2.2020	8049
0333+321	0333+321	LPQ	24.10.1979	28.2.2020	654
CTA026	0336-019	QSO	12.7.1988	24.2.2020	630
0355+508	0355+508	QSO	24.10.1979	26.2.2020	1027
0415+379	0415+379	GAL	12.10.1992	25.2.2020	729
0420-014	0420-014	HPQ	19.2.1984	27.2.2020	945
PKS0422+0036	0422+004	BLO	11.1.1986	27.2.2020	260
3C120	0430+052	GAL	18.2.1981	27.2.2020	1211
NRAO190	0440-003	QSO	22.12.1994	21.2.2020	200
PKS0446+112	0446+112	GAL	1.7.1988	26.2.2020	207
PKS0458-020	0458-020	HPQ	26.2.1988	25.2.2020	303

Source (Metsähovi name)	Source	Type	First obs.	Last obs.	Detections
0507+179	0507+179	QSO	18.11.2005	27.2.2020	154
0528+134	0528+134	LPQ	3.5.1988	25.2.2020	931
0552+398	0552+398	LPQ	11.4.1990	24.2.2020	791
PKS0605-085	0605-085	QSO	13.2.1993	25.2.2020	233
0642+449	0642+449	QSO	19.2.1981	28.2.2020	713
0716+714	0716+714	BLO	29.6.1988	28.2.2020	1681
PKS0723-008	0723-008	BLO	28.10.1993	13.2.2020	155
PKS0735+17	0735+178	BLO	27.2.1981	27.2.2020	710
0736+017	0736+017	HPQ	15.4.1983	27.2.2020	519
0748+126	0748+126	QSO	27.12.2001	13.2.2020	155
0754+100	0754+100	BLO	25.10.1979	25.2.2020	336
0804+499	0804+499	HPQ	28.6.1988	28.2.2020	438
0805-077	0805-077	QSO	10.7.2002	4.2.2020	103
0814+425	0814+425	BLO	13.5.1988	20.2.2020	260
0823+033	0823+033	BLO	2.6.1992	25.2.2020	102
OJ248	0827+243	LPQ	28.10.1993	24.2.2020	549
0829+046	0829+046	BLO	11.2.1995	24.2.2020	145
0836+710	0836+710	LPQ	15.5.1988	24.2.2020	1138
OJ287	0851+202	BLO	13.6.1980	28.2.2020	2523
0859+470	0859+470	QSO	10.10.1992	23.2.2020	115
0906+430	0906+430	GAL	23.4.1983	28.2.2020	224
0917+449	0917+449	QSO	17.9.2001	8.1.2020	134
4C39.25	0923+392	LPQ	13.6.1980	27.2.2020	1269
0945+408	0945+408	LPQ	28.6.1988	28.2.2020	225
0953+254	0953+254	LPQ	28.6.1988	8.2.2020	319
S40954+556	0954+556	HPQ	29.6.1988	17.2.2020	199
S40954+65	0954+658	BLO	23.4.1983	28.2.2020	467
1036+054	1036+054	QSO	11.10.2005	28.2.2020	110
1049+215	1049+215	QSO	29.6.1988	25.2.2020	127
1055+018	1055+018	BLO	18.2.1981	24.2.2020	840
MARK421	1101+384	BLO	12.2.1986	23.2.2020	831
1150+497	1150+497	QSO	29.1.1989	27.2.2020	173
4C29.45	1156+295	HPQ	23.4.1983	25.2.2020	1433
ON231	1219+285	BLO	19.2.1981	14.2.2020	376
PKS1222+216	1222+216	QSO	6.12.1993	29.2.2020	794
3C273	1226+023	LPQ	21.12.1979	29.2.2020	2086
3C279	1253-055	LPQ	21.12.1979	29.2.2020	2119
1308+326	1308+326	BLO	7.3.1981	23.2.2020	796
1324+224	1324+224	QSO	25.10.1996	7.2.2020	273

Source (Metsähovi name)	Source	Type	First obs.	Last obs.	Detections
1334-127	1334-127	QSO	7.5.2001	25.2.2020	382
PKS1406-076	1406-076	QSO	3.12.1988	14.2.2020	230
PKS1413+135	1413+135	BLO	14.2.1989	29.2.2020	519
OQ530	1418+546	BLO	13.4.1983	20.2.2020	420
PKS1502+106	1502+106	HPQ	22.9.1981	26.2.2020	694
PKS1510-089	1510-089	HPQ	16.4.1983	25.2.2020	1171
4C14.60	1538+149	BLO	15.4.1983	26.2.2020	343
1546+027	1546+027	QSO	18.4.1992	27.2.2020	167
1606+106	1606+106	LPQ	24.2.1993	26.2.2020	480
DA406	1611+343	LPQ	14.5.1988	29.2.2020	832
4C38.41	1633+382	LPQ	28.2.1981	26.2.2020	1354
1637+574	1637+574	LPQ	23.4.1983	27.2.2020	614
1638+398	1638+398	QSO	20.5.1996	28.2.2020	207
3C345	1641+399	HPQ	12.6.1980	28.2.2020	1872
1642+690	1642+690	QSO	16.10.1993	25.2.2020	193
MARK501	1652+398	BLO	4.5.1988	28.2.2020	1522
PKS1725+044	1725+044	QSO	26.8.1991	26.2.2020	225
1730-130	1730-130	QSO	14.4.1995	25.2.2020	495
S41739+52	1739+522	HPQ	12.5.1988	24.2.2020	291
1741-038	1741-038	HPQ	14.4.1988	25.2.2020	855
PKS1749+096	1749+096	BLO	27.9.1980	26.2.2020	1154
S51803+784	1803+784	BLO	29.6.1988	23.2.2020	313
3C371.0	1807+698	BLO	14.4.1983	27.2.2020	323
4C56.27	1823+568	BLO	30.6.1988	26.2.2020	207
1828+487	1828+487	LPQ	27.12.1992	19.2.2020	294
3C390.3	1845+797	GAL	1.2.1989	26.1.2020	152
1901+319	1901+319	QSO	16.10.1993	26.2.2020	216
1928+738	1928+738	LPQ	8.5.1988	26.2.2020	364
1954+513	1954+513	QSO	30.6.1988	28.2.2020	308
2005+403	2005+403	QSO	28.2.1981	28.2.2020	930
S52007+77	2007+777	LPQ	14.5.1988	23.2.2020	225
2021+614	2021+614	GAL	24.4.1983	28.2.2020	330
2022+171	2022+171	QSO	16.4.1995	27.2.2020	249
PKS2022-077	2022-077	BLO	4.12.2001	21.8.2019	116
2037+511	2037+511	QSO	25.10.1993	28.2.2020	269
2121+053	2121+053	QSO	12.10.1992	23.2.2020	219
2131-021	2131-021	BLO	12.10.1992	10.1.2020	190
2134+004	2134+004	LPQ	24.10.1979	3.2.2020	659
2136+141	2136+141	LPQ	17.1.1987	26.2.2020	315

Source (Metsähovi name)	Source	Type	First obs.	Last obs.	Detections
2144+092	2144+092	QSO	30.6.1988	5.1.2020	148
2145+067	2145+067	LPQ	2.2.1986	14.2.2020	983
BLLAC	2200+420	BLO	24.10.1979	29.2.2020	3073
2201+171	2201+171	BLO	29.4.2001	14.2.2020	168
2201+315	2201+315	BLO	16.9.1982	29.2.2020	934
2216-038	2216-038	QSO	1.12.1988	3.11.2019	115
3C446	2223-052	BLO	11.1.1986	19.1.2020	667
2227-088	2227-088	QSO	1.12.1988	5.1.2020	217
2230+114	2230+114	HPQ	16.1.1986	23.2.2020	1071
2234+282	2234+282	BLO	29.6.1988	26.2.2020	257
3C454.3	2251+158	HPQ	23.9.1980	28.2.2020	2654
2344+092	2344+092	GAL	30.6.1988	26.2.2020	124
4C45.51	2351+456	QSO	8.3.2002	23.1.2020	172

Appendix B

The values in Table B1 include the estimated PSD slopes for monitoring segments 2008-2013, 2010-2020, 2000-2020, and 1980-2020. The confidence levels are the 68.3% estimations; however, the method for estimating them has been shown to be somewhat lacking in reliability (Max-Moerbeck et al., 2014) and as such the confidence levels should only be considered as broad guidelines on the goodness of the fits. If the confidence level has been marked u, the confidence level was undefined, i.e., at the borders of the probed frequencies, or the PSD slope had a p-value of less than 0.317.

Table B1: The PSD slope estimates and their 68.3% confidence intervals for those sources, that had a defined slope estimate during the 5-year segment.

Source	All	2008-2013	2010-2020	2000-2020
PG0007+106	1.3^{-u}_{+u}	$1.6^{-0.1}_{+0.1}$	1.6^{-u}_{+u}	1.5^{-u}_{+u}
0059+581	$1.7^{-0.1}_{+0.1}$	$2.1^{-0.2}_{+0.2}$	$1.7^{-0.1}_{+0.2}$	$1.6^{-0.0}_{+0.7}$
0133+476	$1.6^{-0.1}_{+0.0}$	$1.9^{-0.1}_{+0.3}$	$1.7^{-0.0}_{+0.0}$	$1.7^{-0.1}_{+0.1}$
3C66A	$1.3^{-0.2}_{+0.1}$	$\leq 1.0^{-u}_{+0.2}$	$\leq 1.0^{-u}_{+u}$	1.1^{-u}_{+u}
0234+285	$1.7^{-0.1}_{+0.1}$	$2.0^{-0,1}_{+0.2}$	$1.7^{-0.1}_{+0.0}$	$1.7^{-0.2}_{+0.1}$
0235+164	1.6^{-u}_{+u}	$2.3^{-0.2}_{+0.3}$	1.7^{-u}_{+u}	1.7^{-u}_{+u}
3C84	$2.3^{-0.2}_{+0.2}$	$2.3^{-0.1}_{+0.1}$	$1.9^{-0.1}_{+0.0}$	$2.1^{-0.0}_{+0.0}$
0333+321	$1.6^{-0.1}_{+0.2}$	$1.9^{-0.2}_{+0.3}$	$2.0^{-0.1}_{+0.0}$	$2.0^{-0.2}_{+0.2}$
CTA026	$1.5^{-0.1}_{+0.2}$	$1.8^{-0.2}_{+0.3}$	$1.6^{-0.0}_{+0.0}$	$1.6^{-0.1}_{+0.2}$
0355+508	$1.7^{-0.1}_{+0.1}$	$2.3^{-0.2}_{+0.2}$	$1.8^{-0.1}_{+0.1}$	$1.8^{-0.1}_{+0.1}$
0415+379	$1.9^{-0.0}_{+0.0}$	$2.4^{-0,2}_{+0.3}$	$1.7^{-0.1}_{+0.1}$	$1.9^{-0.1}_{+0.0}$
0420-014	$1.9^{-0.1}_{+0.0}$	1.9^{-u}_{+u}	$2.1^{-0.0}_{+0.1}$	$2.1^{-0.1}_{+0.0}$
3C120	$1.6^{-0.0}_{+0.1}$	1.5^{-u}_{+u}	1.9^{-u}_{+u}	$1.7^{-0.0}_{+0.1}$
0528+134	$2.0^{-0,1}_{+0.1}$	$2.2^{-0.1}_{+0.1}$	$1.9^{-0.2}_{+0.1}$	$1.9^{-0.0}_{+0.1}$
0552+398	1.8^{-u}_{+u}	$1.1^{-u}_{+0.3}$	$1.3^{-0.2}_{+0.0}$	1.5^{-u}_{+u}
0642+449	$1.5^{-0.1}_{+0.2}$	$1.3^{-u}_{+0.2}$	1.5^{-u}_{+u}	$1.6^{-0.0}_{+0.0}$
0716+714	1.3^{-u}_{+u}	$1.5^{-0.1}_{+0.1}$	1.3^{-u}_{+u}	1.3^{-u}_{+u}
PKS0735+17	$2.0^{-0.1}_{+0.1}$	$1.4^{-0.2}_{+0.3}$	1.4^{-u}_{+u}	1.5^{-u}_{+u}
0736+017	$1.3^{-0.0}_{+0.0}$	$1.2^{-u}_{+0.2}$	$1.3^{-0.1}_{+0.2}$	$1.5^{-0.2}_{+0.2}$
OJ248	$1.6^{-0.1}_{+0.2}$	$2.1^{-0.0}_{+0.1}$	$1.9^{-0.2}_{+0.1}$	$1.7^{-0.1}_{+0.1}$
0836+710	$1.4^{-0.1}_{+0.1}$	$1.4^{-0.0}_{+0.2}$	1.4^{-u}_{+u}	1.2^{-u}_{+u}
OJ287	$1.6^{-0.0}_{+0.1}$	$1.7^{-0.1}_{+0.1}$	$1.6^{-0.0}_{+0.1}$	$1.6^{-0.0}_{+0.0}$
1055+018	$1.5^{-0.0}_{+0.1}$	$1.6^{-0.2}_{+0.2}$	$1.8^{-0.1}_{+0.1}$	$1.7^{-0.1}_{+0.1}$
4C29.45	$1.6^{-0.1}_{+0.0}$	$1.9^{-0.2}_{+0.2}$	$1.8^{-0.1}_{+0.1}$	$1.7^{-0.1}_{+0.1}$
PKS1222+216	$1.5^{-0.0}_{+0.1}$	$1.6^{-0.1}_{+0.3}$	$1.6^{-0.1}_{+0.1}$	$1.5^{-0.1}_{+0.2}$
3C273	$1.9^{-0.1}_{+0.1}$	$2.1^{-0.0}_{+0.1}$	$2.0^{-0.1}_{+0.1}$	$1.9^{-0.1}_{+0.0}$
3C279	$1.6^{-0.1}_{+0.0}$	$2.2^{-0.1}_{+0.2}$	$1.9^{-0.1}_{+0.1}$	$1.7^{-0.0}_{+0.0}$
1308+326	$1.7^{-0.1}_{+0.1}$	$1.3^{-0.2}_{+0.1}$	$1.8^{-0.1}_{+0.2}$	$1.6^{-0.1}_{+0.1}$
1324+224	1.5^{-u}_{+u}	$1.6^{-0.2}_{+0.4}$	$1.5^{-0.1}_{+0.0}$	$1.4^{-0.2}_{+0.3}$

Source	All	2008-2013	2010-2020	2000-2020
1334-127	$1.6^{-0.1}_{+0.2}$	$1.7^{-0.2}_{+0.3}$	1.6^{-u}_{+u}	$1.6^{-0.1}_{+0.2}$
PKS1502+105	$1.9^{-0.2}_{+0.6}$	$2.0^{-0.0}_{+0.2}$	$2.1^{-0.2}_{+0.1}$	$2.0^{-0.1}_{+0.2}$
PKS1510-089	$1.5^{-0.1}_{+0.1}$	$1.7^{-0.2}_{+0.2}$	$1.6^{-0.1}_{+0.0}$	$1.5^{-0.1}_{+0.1}$
1606+106	$1.7^{-0.2}_{+0.2}$	$1.7^{-0.3}_{+0.3}$	$1.6^{-0.2}_{+0.2}$	$2.0^{-0.2}_{+0.2}$
DA406	$1.6^{-0.01}_{+0.1}$	$2.1^{-0.1}_{+0.1}$	$1.6^{-0.1}_{+0.1}$	$1.7^{-0.1}_{+0.1}$
4C38.41	$1.8^{-0.1}_{+0.1}$	$1.4^{-0.0}_{+0.1}$	$1.8^{-0.1}_{+0.1}$	$1.7^{-0.1}_{+0.1}$
1637+574	$1.4^{-0.1}_{+0.1}$	$1.6^{-0.2}_{+0.3}$	1.5^{-u}_{+u}	$1.6^{-0.1}_{+0.2}$
3C345	$1.9^{-0.1}_{+0.1}$	$1.9^{-0.0}_{+0.1}$	$1.6^{-0.1}_{+0.1}$	$1.6^{-0.0}_{+0.1}$
1730-130	$2.0^{-0.2}_{+0.2}$	$1.6^{-0.1}_{+0.2}$	$1.6^{-0.2}_{+0.2}$	$1.6^{-0.1}_{+0.1}$
1741-038	$1.6^{-0.0}_{+0.1}$	$1.9^{-0.2}_{+0.3}$	$1.7^{-0.1}_{+0.2}$	$1.8^{-0.1}_{+0.2}$
PKS1749+096	1.5^{-u}_{+u}	$1.9^{-0.2}_{+0.2}$	$1.6^{-0.1}_{+0.2}$	1.5^{-u}_{+u}
2005+403	$1.7^{-0.1}_{+0.0}$	1.4^{-u}_{+u}	1.8^{-u}_{+u}	$1.8^{-0.0}_{+0.1}$
2145+067	$1.8^{-0.0}_{+0.1}$	$1.9^{-0.1}_{+0.3}$	$1.5^{-0.2}_{+0.1}$	$2.1^{-0.1}_{+0.1}$
BLLAC	$1.7^{-0.1}_{+0.1}$	$2.0^{-0.0}_{+0.1}$	$1.8^{-0.1}_{+0.1}$	$1.6^{-0.0}_{+0.1}$
2201+315	1.5^{-u}_{+u}	1.4^{-u}_{+u}	$1.4^{-0.1}_{+0.2}$	$1.4^{-0.0}_{+0.1}$
2230+114	$1.5^{-0.0}_{+0.0}$	$2.2^{-0.3}_{+0.2}$	$1.7^{-0.0}_{+0.1}$	$1.6^{-0.0}_{+0.0}$
3C446	$1.8^{-0.0}_{+0.0}$	$2.2^{-0.1}_{+0.1}$	$2.0^{-0.1}_{+0.1}$	$2.0^{-0.1}_{+0.1}$
3C454.3	$1.9^{-0.1}_{+0.1}$	$2.0^{-0.1}_{+0.2}$	$2.0^{-0.1}_{+0.0}$	$1.8^{-0.0}_{+0.0}$